JOURNAL OF THE AERONAUTICAL SCIENCES

UNI
OF MICHIGAN
JAN 21 1953
ENGINEERING
LIBRARY

VOLUME 20 JANUARY, 1953 NUMBER 1

CONTENTS

Similarity Laws for Stressing Heated Wings ..... H. S. TSIEN 1

The Effect of the Torsional Rigidity of a Single Stiffener on the Buckling Characteristics of a Panel Subjected to Axial Compression with Large Deflections ..... T. K. STEELE AND C. T. WANG 12

Boundary-Layer Stability and Transition in Subsonic and Supersonic Flow ..... CARL GAZLEY, JR. 19

Equilibrium Temperature of an Unheated Icing Surface as a Function of Air Speed ..... BERNARD L. MESSINGER 29

Blade Adjustment in Axial-Flow Compressor Stages ..... ALLAN W. MCCOY AND ALTON V. HOOPER 43

Generalized Theory of Convective Heat Transfer in a Free-Molecule Flow ..... A. K. OPPENHEIM 49

Readers' Forum: "A Rational Discussion of the Hydraulic Analogy," by E. V. Laitone; "A Heat Cycle Low Reynolds Number Transonic Tunnel," by Raymond L. Chuan; "On Second-Order Supersonic Flow Past a Slowly Oscillating Airfoil," by Milton D. Van Dyke; "A Method for Location of Detached Shock Waves Ahead of Plane Bodies," by Robert Wesley Truitt; "A Note on Tabular Methods for Flexural Vibrations," by William T. Thomson; "On Linearized Theory," by John W. Miles, "Interaction Between Stalled and Unstalled Flow," by Peter F. Jordan; "Physical Explanation of Singular Integrals at Supersonic Speeds," by Lee S. Wasserman; "Frequency Response and the Transfer Functions of the Human Pilot Measured in Flight," by G. M. Andrew; "Compressible Laminar Boundary Layer on a Heat-Insulated Body," by N. Rott; "Potential Limit in Transonic Flow," by Pei Chi Chou; "Note on the Dynamic Stability of a Missile in Rolling Flight," by Arthur E. Bryson, Jr. 59–71

Published by the

INSTITUTE OF THE AERONAUTICAL SCIENCES, INC.

JOURNAL OF THE AERONAUTICAL SCIENCES

Editor: HUGH L. DRYDEN, *Director, N.A.C.A.*

Associate Editor: ROBERT R. DEXTER *Managing Editor:* BERNEICE H. JARCK

Editorial Committee

Aerodynamics

Francis Clauser
Howard Emmons
Alexander Flax
R. Paul Harrington
R. T. Jones
Carl Kaplan
H. W. Liepmann
C. C. Lin
H. F. Ludloff
Harold Luskin
John R. Markham
Clark B. Millikan
Shatswell Ober
W. Bailey Oswald
Allen E. Puckett
Elliott G. Reid
H. J. E. Reid
Russell Robinson
G. B. Schubauer
W. R. Sears
John Stack
Theodore von Kármán
Richard von Mises

Air Transport

Charles Froesch
J. A. Herlihy
R. D. Kelly
Otto E. Kirchner
Jerome Lederer
John C. Leslie
R. Dixon Speas

Flight Testing

W. K. Ebel
R. R. Gilruth
Melvin N. Gough
E. G. Stout

Structures and Materials

W. B. Bleakney
E. W. Conlon
L. H. Donnell
E. C. Hartmann
N. J. Hoff
Samuel Levy
E. E. Lundquist
Alfred S. Niles
W. Ramberg
E. Reissner
F. R. Shanley
H. W. Sibert
C. R. Strang
S. Timoshenko
H. S. Tsien
Chi-Teh Wang

Rotating Wing Aircraft

F. B. Gustafson
K. H. Hohenemser
Bartram Kelley
R. B. Maloy
Ralph McClarren
R. H. Miller
R. H. Prewitt
Igor I. Sikorsky

Vibration and Flutter

Lee Arnold
M. A. Biot
R. L. Bisplinghoff
William Bollay
Chieh-Chien Chang
I. E. Garrick
Martin Goland
J. P. Den Hartog

Aircraft Design

W. E. Beall
W. K. Ebel
Hall L. Hibbard
Richard Hutton
C. L. Johnson
A. A. Kartveli
C. J. McCarthy
Fred E. Weick
Robert J. Woods

Electronics in Aviation

K. C. Black
E. F. Herzog
David S. Little
D. K. Martin
George Rappaport
Paul Rosenberg
L. M. Sherer

Physiologic Problems

H. G. Armstrong
Louis H. Bauer
Robert J. Benford
Eugene Du Bois
W. Randolph Lovelace, II
Ross A. MacFarland

Fuels and Oils

D. P. Barnard
J. H. Doolittle
Graham Edgar
R. T. Goodwin
S. D. Heron
A. M. Rothrock

Flight Propulsion

George W. Brady
Frank W. Caldwell
L. S. Hobbs
E. E. Johnson
Joseph Keenan
R. P. Kroon
Hans Reissner
Abe Silverstein
C. Fayette Taylor
E. S. Taylor
P. Taylor
E. S. Thompson
H. S. Tsien

Instruments

Allan G. Binnie
J. R. Bradburn
Charles H. Colvin
C. S. Draper
S. G. Eskin
O. E. Esval
H. W. Holzapfel
W. L. Howland
George H. Purcell
C. F. Savage
O. Hugo Schuck
C. L. Seward, Jr.
L. D. Statham
R. C. Sylvander
D. K. Warner

Meteorology

C. F. Brooks
D. M. Little
E. J. Minser
F. W. Reichelderfer
H. C. Willett

SUBSCRIPTION RATES

JOURNAL OF THE AERONAUTICAL SCIENCES, Published Monthly.—United States and Possessions: 1 Year, $12.00; Single Copies, $1.50. Foreign Countries Including Canada (American Currency Rates): 1 Year, $13.00; Single Copies, $1.50.

AERONAUTICAL ENGINEERING REVIEW, Published Monthly.—United States and Possessions: 1 Year, $3.00; Single Copies, $0.50. Foreign Countries Including Canada (American Currency Rates): 1 Year, $3.50; Single Copies, $0.50.

Notices of change of address should be sent to the Institute at least 30 days prior to actual change of address.

Manuscripts for publication, proofs, and all correspondence should be addressed to the Editorial Office of the JOURNAL.

Correspondence regarding subscriptions may be addressed to Publication Office, 20th and Northampton Sts., Easton, Pa., or to the Editorial Office of the JOURNAL OF THE AERONAUTICAL SCIENCES, 2 East 64th Street, New York 21, New York.

Copyright, 1953, by the Institute of the Aeronautical Sciences, Inc.

Entered as Second Class Matter at the Post Office, Easton, Pa., May 1, 1937. Acceptance for mailing at a special rate of Postage provided for in the Act of August 24, 1912. Authorized April 20, 1937.

ENGINEERING
LIBRARY
TL
501
.J86

JOURNAL OF THE AERONAUTICAL SCIENCES

VOLUME 20 JANUARY, 1953 NUMBER 1

Similarity Laws for Stressing Heated Wings

H. S. TSIEN*

California Institute of Technology

SUMMARY

It will be shown that the differential equations for a heated plate with large temperature gradient and for a similar plate at constant temperature can be made the same by a proper modification of the thickness and the loading for the isothermal plate. This fact leads to the result that the stresses in the heated plate can be *calculated* from *measured* strains on the unheated plate by a series of relations, called the "similarity laws." The application of this analog theory to solid wings under aerodynamic heating is discussed in detail. The loading on the unheated analog wing is, however, complicated and involves the novel concept of feedback and "body force" loading. The problem of stressing a heated box-wing structure can be solved by the same analog method and is briefly discussed.

INTRODUCTION

THE HIGH STAGNATION TEMPERATURE for flight of aircraft at supersonic speeds results in severe aerodynamic heating of the surfaces of aircraft. For instance, in a recent paper by Kaye,[1] the transient temperature distribution in a wedge-shaped solid wing was calculated for accelerated flight and was found to be rapidly varying both with respect to the space points in the wing and with respect to time instants. When there are large temperature gradients in the material, there are generally large thermal stresses due to the uneven thermal expansion of the material. Therefore, concurrent with the severe aerodynamic heating, there is the problem of determining the thermal stresses in the wing. The purpose of this paper is to suggest a method of stressing such heated wings.

The starting point of the stress analysis is the temperature distribution in the wing. Because the rate of change of temperature is small in comparison to the speed of sound propagation in the material, the stress calculation can be considered as a quasi-steady problem. That is, the stress in the wing at each time instant can be calculated from the temperature distribution at that time instant without the inertia effects from the time variation of the material displacements required by the changing stresses and the thermal expansions. This problem in general theory of elasticity is greatly simplified by the fact that the wing is thin, and therefore the Kirchhoff hypothesis for bending of thin plates holds. In fact, the problem of thermal stresses in an elastic plate has been treated some time ago by Nádai.[2] The present study generalizes the earlier theory in two directions: Nádai's assumption of linear temperature profile across the plate is no longer necessary. The temperature profile is now arbitrary. Secondly, Young's modulus E of the material is now allowed to vary as a function of temperature. Thus, the effects of decrease in Young's modulus with increase in temperature can be taken into account in the present theory.

However, the main purpose of the present paper is not just to construct a theory for heated plates. The main purpose is to utilize the theory to formulate a law of similarity, whereby the problem of stressing a heated wing can be solved by performing a set of experiments on a properly proportioned and properly loaded wing at room temperature without heating. This concept of similarity law has been explored before by the present author[3] for thin-walled cylinders. It is believed that this approach to the problem of stressing a heated wing has many practical advantages over a pure analytical solution, as will be discussed later in the paper.

BASIC EQUATIONS FOR HEATED PLATE

Let the plane of the plate be the x-y plane, and its variable thickness be $b(x,y)$. The z-axis is normal to the plate and pointing downward. The temperature above the ambient is specified by $T(x,y;\ z)$. Actually, the distance z is measured from the "median surface," the position of which will be specified presently. Therefore, it is implied here that the median surface, although not exactly coinciding with the x-y plane, is

Received June 10, 1952.

* Robert H. Goddard Professor of Jet Propulsion, Daniel and Florence Guggenheim Jet Propulsion Center.

nevertheless sufficiently flat to be considered as the x-y plane. Let u, v, and w be the displacement of a point (x,y) on the median surface in the x, y, and z directions, respectively, due to elastic strain and thermal expansion. Then, according to Kirchhoff's bending hypothesis, the total strains of a point (x, y, z) in the plate are given by

$$\left.\begin{aligned} \epsilon_x &= (\partial u/\partial x) - z(\partial^2 w/\partial x^2) \\ \epsilon_y &= (\partial v/\partial y) - z(\partial^2 w/\partial y^2) \\ \gamma_{xy} &= (\partial u/\partial y) + (\partial v/\partial x) - 2z(\partial^2 w/\partial x \partial y) \end{aligned}\right\} \quad (1)$$

where ϵ_x is the direct strain in x, ϵ_y is the direct strain in y, and γ_{xy} is the shear strain in the x-y plane. All other strains are small and negligible for thin plates.

Let $E(T) = E(x,y; z)$ be the variable Young's modulus, ν the constant Poisson's ratio, and σ_x, σ_y, τ_{xy} the significant components of stresses. Then the strains can be computed from these quantities as follows:

$$\left.\begin{aligned} \epsilon_x &= [(\sigma_x - \nu\sigma_y)/E(x,y; z)] + aT(x,y; z) \\ \epsilon_y &= [(\sigma_y - \nu\sigma_x)/E(x,y; z)] + aT(x,y; z) \\ \gamma_{xy} &= 2(1 + \nu)\tau_{xy}/E(x,y; z) \end{aligned}\right\} \quad (2)$$

where a is the coefficient of thermal expansion. By solving Eq. (2) for stresses, one has

$$\left.\begin{aligned} \sigma_x &= \frac{E(x,y; z)}{1 - \nu^2}\,[(\epsilon_x + \nu\epsilon_y) - (1 + \nu)aT(x,y; z)] \\ \sigma_y &= \frac{E(x,y; z)}{1 - \nu^2}\,[(\epsilon_y + \nu\epsilon_x) - (1 + \nu)aT(x,y; z)] \\ \tau_{xy} &= [E(x,y; z)/2(1 + \nu)]\,\gamma_{xy} \end{aligned}\right\} \quad (3)$$

In the theory of thin plates, the important quantities are not the stresses but are rather the sectional forces and the sectional moments derived from the stresses. These sectional quantities are defined as

$$N_x = \int \sigma_x\,dz, \quad N_y = \int dz, \quad N_{xy} = \int \tau_{xy}\,dz \quad (4)$$

$$M_x = \int \sigma_x z\,dz, \quad M_y = \int \sigma_y z\,dz, \quad M_{xy} = -\int \tau_{xy} z\,dz \quad (5)$$

where all integrations extend across the whole thickness of the plate. N_x and N_y are then sectional normal forces, N_{xy} is the sectional shear, M_x and M_y are the sectional bending moments, and M_{xy} is the sectional twisting moment. By substituting Eq. (1) into Eq. (3) and then into Eqs. (4) and (5), one has, for example,

$$N_x = D_0\left(\frac{\partial u}{\partial x} + \nu\frac{\partial v}{\partial y}\right) - D_1\left(\frac{\partial^2 w}{\partial x^2} + \nu\frac{\partial^2 w}{\partial y^2}\right) - N_T$$

$$M_x = D_1\left(\frac{\partial u}{\partial x} + \nu\frac{\partial v}{\partial y}\right) - D_2\left(\frac{\partial^2 w}{\partial x^2} + \nu\frac{\partial^2 w}{\partial y^2}\right) - M_T$$

where

$$D_0(x,y) = \frac{1}{1 - \nu^2}\int E(x,y; z)\,dz \quad (6)$$

$$D_1(x,y) = \frac{1}{1 - \nu^2}\int E(x,y; z)z\,dz \quad (7)$$

$$D_2(x,y) = \frac{1}{1 - \nu^2}\int E(x,y; z)z^2\,dz \quad (8)$$

$$N_T = \frac{a}{1 - \nu}\int E(x,y; z)T(x,y; z)\,dz \quad (9)$$

$$M_T = \frac{a}{1 - \nu}\int E(x,y; z)T(x,y; z)z\,dz \quad (10)$$

N_T and M_T being due to thermal expansion of the material can thus be called thermal sectional normal force and thermal bending moment, respectively. From the above typical expressions for N_x and M_x, it is seen that a simplification results if the median surface is so chosen that

$$D_1 = 0 \quad (11)$$

In fact, this is the condition for fixing the position of the median surface. With the median surface so determined, the sectional quantities can be calculated as

$$\left.\begin{aligned} N_x &= D_0\left(\frac{\partial u}{\partial x} + \nu\frac{\partial v}{\partial y}\right) - N_T \\ N_y &= D_0\left(\frac{\partial v}{\partial y} + \nu\frac{\partial u}{\partial x}\right) - N_T \\ N_{xy} &= \frac{1 - \nu}{2}D_0\left(\frac{\partial v}{\partial y} + \frac{\partial u}{\partial y}\right) \end{aligned}\right\} \quad (12)$$

$$\left.\begin{aligned} M_x &= -D_2\left(\frac{\partial^2 w}{\partial x^2} + \nu\frac{\partial^2 w}{\partial y^2}\right) - M_T \\ M_y &= -D_2\left(\frac{\partial^2 w}{\partial y^2} + \nu\frac{\partial^2 w}{\partial x^2}\right) - M_T \\ M_{xy} &= (1 - \nu)D_2\frac{\partial^2 w}{\partial x \partial y} \end{aligned}\right\} \quad (13)$$

The equilibrium of forces in the medium surface requires

$$\left.\begin{aligned} (\partial N_x/\partial x) + (\partial N_{xy}/\partial y) &= 0 \\ (\partial N_{xy}/\partial x) + (\partial N_y/\partial y) &= 0 \end{aligned}\right\} \quad (14)$$

By substituting Eq. (12) into Eq. (14), the following two equations for u and v are obtained:

$$\left.\begin{aligned} \frac{\partial}{\partial x}\left[D_0\left(\frac{\partial u}{\partial x} + \nu\frac{\partial v}{\partial y}\right)\right] + \frac{1 - \nu}{2}\frac{\partial}{\partial y}\left[D_0\left(\frac{\partial v}{\partial x} + \frac{\partial u}{\partial y}\right)\right] &= \frac{\partial N_T}{\partial x} \\ \frac{1 - \nu}{2}\frac{\partial}{\partial x}\left[D_0\left(\frac{\partial v}{\partial x} + \frac{\partial u}{\partial y}\right)\right] + \frac{\partial}{\partial y}\left[D_0\left(\frac{\partial v}{\partial y} + \nu\frac{\partial u}{\partial x}\right)\right] &= \frac{\partial N_T}{\partial y} \end{aligned}\right\} \quad (15)$$

When the temperature distribution is specified, the right sides of these equations are known. Then Eq. (15) is a set of simultaneous partial differential equations for u and v. If the boundary conditions of the problem are specified in the displacements, Eq. (15) is the proper basis of solution.

If the boundary conditions of the problem are specified in terms of forces instead of displacements, it would be more convenient to use the stress function $\varphi(x,y)$ as the basis of solution. Σ is defined through the following relations and satisfies Eq. (14) automatically:

$$N_x = \frac{\partial^2\varphi}{\partial y^2}, \qquad -N_{xy} = \frac{\partial^2\varphi}{\partial x\partial y}, \qquad N_y = \frac{\partial^2\varphi}{\partial x^2} \tag{16}$$

By substituting these relations into Eq. (12), one has

$$\left.\begin{aligned} \frac{\partial u}{\partial x} &= \frac{1}{(1-\nu^2)D_0}\left[\left(\frac{\partial^2\varphi}{\partial y^2} - \nu\frac{\partial^2\varphi}{\partial x^2}\right) + (1-\nu)N_T\right] \\ \frac{\partial v}{\partial y} &= \frac{1}{(1-\nu^2)D_0}\left[\left(\frac{\partial^2\varphi}{\partial x^2} - \nu\frac{\partial^2\varphi}{\partial y^2}\right) + (1-\nu)N_T\right] \\ -\left(\frac{\partial v}{\partial x} + \frac{\partial u}{\partial y}\right) &= \frac{2}{(1-\nu)D_0}\frac{\partial^2\varphi}{\partial x\partial y} \end{aligned}\right\} \tag{17}$$

When the first equation of Eqs. (17) is differentiated twice with respect to y, the second equation is differentiated twice with respect to x, the third equation is differentiated with respect to x and y, and the results are added, a single equation for φ is obtained:

$$\frac{1}{(1-\nu^2)}\frac{\partial^2}{\partial x^2}\left[\frac{1}{D_0}\left(\frac{\partial^2\varphi}{\partial x^2} - \nu\frac{\partial^2\varphi}{\partial y^2}\right)\right] + \frac{2}{(1-\nu)}\frac{\partial^2}{\partial x\partial y}\left(\frac{1}{D_0}\frac{\partial^2\varphi}{\partial x\partial y}\right) + \frac{1}{1-\nu^2}\frac{\partial^2}{\partial y^2}\left[\frac{1}{D_0}\left(\frac{\partial^2\varphi}{\partial y^2} - \nu\frac{\partial^2\varphi}{\partial x^2}\right)\right] + \frac{1}{1+\nu}\nabla^2\left(\frac{N_T}{D_0}\right) = 0 \tag{18}$$

where ∇^2 is the Laplacian operator. At the boundary of the plate (Fig. 1a), if l, m are the direction cosines of the "outside" normal n to the boundary direction s, then sectional normal force N_n to the boundary and the sectional shearing force N_{ns} along the boundary are given as follows:

$$N_n = \frac{N_x + N_y}{2} + \frac{N_x - N_y}{2}(l^2 - m^2) + N_{xy}(2lm) = \frac{1}{2}\Delta^2\varphi + \frac{1}{2}(l^2 - m^2)\left(\frac{\partial^2\varphi}{\partial y^2} - \frac{\partial^2\varphi}{\partial x^2}\right) - 2lm\frac{\partial^2\varphi}{\partial x\partial y} \tag{19}$$

$$N_{ns} = -(N_x - N_y)lm + (l^2 - m^2)N_{xy} = -lm\left(\frac{\partial^2\varphi}{\partial y^2} - \frac{\partial^2\varphi}{\partial x^2}\right) - (l^2 - m^2)\frac{\partial^2\varphi}{\partial x\partial y} \tag{20}$$

With the boundary described and the boundary forces specified, Eqs. (18), (19), and (20) then give the proper formulation of the problem.

If p is the downward pressure loading on the plate, then the equilibrium of forces normal to the plane of the plate requires

$$\frac{\partial^2 M_x}{\partial x^2} - 2\frac{\partial^2 M_{xy}}{\partial x\partial y} + \frac{\partial^2 M_y}{\partial y^2} = -p - N_x\frac{\partial^2 w}{\partial x^2} - 2N_{xy}\frac{\partial^2 w}{\partial x\partial y} - N_y\frac{\partial^2 w}{\partial y^2}$$

By substituting the sectional moments obtained from Eq. (13) into the above equilibrium equation, an equation for the lateral deflection w results:

$$\frac{\partial^2}{\partial x^2}\left[D_2\left(\frac{\partial^2 w}{\partial x^2} + \nu\frac{\partial^2 w}{\partial y^2}\right)\right] + 2(1-\nu)\frac{\partial^2}{\partial x\partial y}\left(D_2\frac{\partial^2 w}{\partial x\partial y}\right) + \frac{\partial^2}{\partial y^2}\left[D_2\left(\frac{\partial^2 w}{\partial y^2} + \nu\frac{\partial^2 w}{\partial x^2}\right)\right] = -\nabla^2 M_T + p + N_x\frac{\partial^2 w}{\partial x^2} + 2N_{xy}\frac{\partial^2 w}{\partial x\partial y} + N_y\frac{\partial^2 w}{\partial y^2} \tag{21}$$

Part of the boundary conditions will be expressed in terms of w directly. For instance, if the boundary s with outside normal n is a "fixed edge," then on that boundary

$$w = 0, \qquad \partial w/\partial n = 0 \tag{22}$$

The other part of the boundary conditions is described in terms of sectional moments. If l, m are the direction cosines of the outside normal, the sectional bending moments M_n, M_s and the sectional twisting moment M_{ns} on the boundary (Fig. 1b) are, then,

$$\left.\begin{aligned} M_n = \frac{M_x + M_y}{2} + \frac{M_x - M_y}{2}(l^2 - m^2) - M_{xy}(2lm) = -M_T - \frac{1+\nu}{2} D_2\nabla^2 w - \\ \frac{1-\nu}{2} D_2(l^2 - m^2)\left(\frac{\partial^2 w}{\partial x^2} - \frac{\partial^2 w}{\partial y^2}\right) - 2(1-\nu)D_2 lm \frac{\partial^2 w}{\partial x \partial y} \\ M_s = \frac{M_x + M_y}{2} - \frac{M_x - M_y}{2}(l^2 - m^2) + M_{xy}(2lm) = -M_T - \frac{1+\nu}{2} D_2\nabla^2 w + \\ \frac{1-\nu}{2} D_2(l^2 - m^2)\left(\frac{\partial^2 w}{\partial x^2} - \frac{\partial^2 w}{\partial y^2}\right) + 2(1-\nu)D_2 lm \frac{\partial^2 w}{\partial x \partial y} \end{aligned}\right\} \quad (23)$$

$$M_{ns} = (M_x - M_y)lm + (l^2 - m^2)M_{xy} = -(1-\nu)D_2 lm\left(\frac{\partial^2 w}{\partial x^2} - \frac{\partial^2 w}{\partial y^2}\right) + (1-\nu)D_2(l^2 - m^2)\frac{\partial^2 w}{\partial x \partial y} \quad (24)$$

For a "free edge," the Kirchhoff boundary conditions are, then,

$$M_n = 0, \quad \frac{\partial M_n}{\partial n} + \frac{M_n - M_s}{r} + \frac{\partial M_{ns}}{\partial s} = 0 \quad (25)$$

where r is the radius of curvature of the boundary s, or

$$1/r = (1/m)\,(dl/ds) \quad (26)$$

Plate at Constant Temperature

For a plate at the constant reference room temperature, all the temperature terms in the equations developed in the previous section vanish. By using a bar over a quantity to differentiate the present case from the previous case, one has for strains

$$\left.\begin{aligned} \bar{\epsilon}_x &= (\partial\bar{u}/\partial x) - \bar{z}(\partial^2\bar{w}/\partial x^2) \\ \bar{\epsilon}_y &= (\partial\bar{v}/\partial y) - \bar{z}(\partial^2\bar{w}/\partial y^2) \\ \bar{\gamma}_{xy} &= (\partial\bar{v}/\partial x) + (\partial\bar{u}/\partial y) - 2\bar{z}(\partial^2\bar{w}/\partial x\partial y) \end{aligned}\right\} \quad (27)$$

Let $\bar{E}$ be Young's modulus, now a constant, then

$$\left.\begin{aligned} \bar{\sigma}_x &= [\bar{E}/(1-\nu^2)]\,(\bar{\epsilon}_x + \nu\bar{\epsilon}_y) \\ \bar{\sigma}_y &= [\bar{E}/(1-\nu^2)]\,(\bar{\epsilon}_y + \nu\bar{\epsilon}_x) \\ \bar{\tau}_{xy} &= [\bar{E}/2(1+\nu)]\bar{\gamma}_{xy} \end{aligned}\right\} \quad (28)$$

The sectional forces and the sectional moments defined as Eqs. (4) and (5) are

$$\left.\begin{aligned} \bar{N}_x &= \bar{D}_0\left(\frac{\partial\bar{u}}{\partial x} + \nu\frac{\partial\bar{v}}{\partial y}\right) \\ \bar{N}_y &= \bar{D}_0\left(\frac{\partial\bar{v}}{\partial y} + \nu\frac{\partial\bar{u}}{\partial x}\right) \\ \bar{N}_{xy} &= \frac{1-\nu}{2}\bar{D}_0\left(\frac{\partial\bar{v}}{\partial x} + \frac{\partial\bar{u}}{\partial y}\right) \end{aligned}\right\} \quad (29)$$

$$\left.\begin{aligned} \bar{M}_x &= -\bar{D}_2\left(\frac{\partial^2\bar{w}}{\partial x^2} + \nu\frac{\partial^2\bar{w}}{\partial y^2}\right) \\ \bar{M}_y &= -\bar{D}_2\left(\frac{\partial^2\bar{w}}{\partial y^2} + \nu\frac{\partial^2\bar{w}}{\partial x^2}\right) \\ \bar{M}_{xy} &= (1-\nu)\,\bar{D}_2\frac{\partial^2\bar{w}}{\partial x\partial y} \end{aligned}\right\} \quad (30)$$

where, with $\bar{b}(x,y)$ as the thickness of the plate at the point (x,y),

$$\bar{D}_0(x,y) = \frac{\bar{E}}{1-\nu^2}\bar{b}(x,y), \quad \bar{D}_2(x,y) = \frac{\bar{E}}{1-\nu^2}\frac{\bar{b}^3}{12} \quad (31)$$

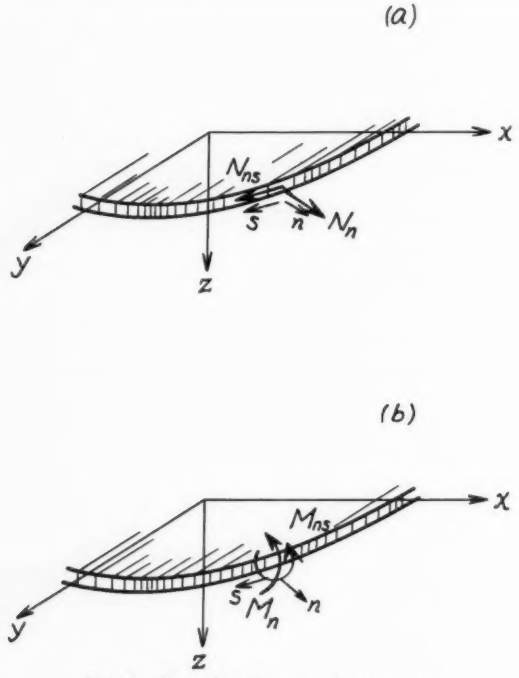

FIG. 1. Boundary forces and moments.

The median surface now lies midway between the upper and the lower surfaces of the plate.

Now introduce a potential $F(x,y)$ for the body forces X and Y, which are the forces per unit area of the median surface in the x and y directions:

$$X = -\partial F/\partial x, \qquad Y = -\partial F/\partial y \tag{32}$$

Then the equations of equilibrium of forces in the medium surface are

$$\left.\begin{aligned}(\partial \bar{N}_x/\partial x) + (\partial \bar{N}_{xy}/\partial y) - (\partial F/\partial x) &= 0\\ (\partial \bar{N}_{xy}/\partial x) + (\partial \bar{N}_y/\partial y) - (\partial F/\partial y) &= 0\end{aligned}\right\} \tag{33}$$

By substituting Eq. (29) into the above equations, a set of equations for $\bar{u}$ and $\bar{v}$ is obtained:

$$\left.\begin{aligned}\frac{\partial}{\partial x}\left[\bar{D}_0\left(\frac{\partial \bar{u}}{\partial x} + \nu\frac{\partial \bar{v}}{\partial y}\right)\right] + \frac{1-\nu}{2}\frac{\partial}{\partial y}\left[\bar{D}_0\left(\frac{\partial \bar{v}}{\partial x} + \frac{\partial \bar{u}}{\partial y}\right)\right] &= \frac{\partial F}{\partial x}\\ \frac{1-\nu}{2}\frac{\partial}{\partial x}\left[\bar{D}_0\left(\frac{\partial \bar{v}}{\partial x} + \frac{\partial \bar{u}}{\partial y}\right)\right] + \frac{\partial}{\partial y}\left[\bar{D}_0\left(\frac{\partial \bar{v}}{\partial y} + \nu\frac{\partial \bar{u}}{\partial x}\right)\right] &= \frac{\partial F}{\partial y}\end{aligned}\right\} \tag{34}$$

Eq. (33) will be automatically satisfied, if a new stress function $\bar{\varphi}(x,y)$ is introduced such that

$$\bar{N}_x = \frac{\partial^2\bar{\varphi}}{\partial y^2} + F, \quad -\bar{N}_{xy} = \frac{\partial^2\bar{\varphi}}{\partial x\partial y}, \quad \bar{N}_y = \frac{\partial^2\bar{\varphi}}{\partial x^2} + F \tag{35}$$

The equation for $\bar{\varphi}$ is now

$$\frac{1}{1-\nu^2}\frac{\partial^2}{\partial x^2}\left[\frac{1}{D_0}\left(\frac{\partial^2\varphi}{\partial x^2} - \nu\frac{\partial^2\bar{\varphi}}{\partial y^2}\right)\right] + \frac{2}{1-\nu}\frac{\partial^2}{\partial x\partial y}\left(\frac{1}{D_0}\frac{\partial^2\bar{\varphi}}{\partial x\partial y}\right) + \frac{1}{1-\nu^2}\frac{\partial^2}{\partial y^2}\left[\frac{1}{D_0}\left(\frac{\partial^2\bar{\varphi}}{\partial y^2} - \nu\frac{\partial^2\bar{\varphi}}{\partial x^2}\right)\right] + \frac{1}{1+\nu}\nabla^2\left(\frac{F}{\bar{D}_0}\right) = 0 \tag{36}$$

At the boundary of the plate,

$$\begin{aligned}\bar{N}_n &= \frac{\bar{N}_x + \bar{N}_y}{2} + \frac{\bar{N}_x - \bar{N}_y}{2}(l^2 - m^2) + \bar{N}_{xy}2lm\\ &= F + \frac{1}{2}\nabla^2\bar{\varphi} + \frac{1}{2}(l^2 - m^2)\left(\frac{\partial^2\bar{\varphi}}{\partial y^2} - \frac{\partial^2\bar{\varphi}}{\partial x^2}\right) - 2lm\frac{\partial^2\bar{\varphi}}{\partial x\partial y}\end{aligned} \tag{37}$$

$$\begin{aligned}\bar{N}_{ns} &= -(\bar{N}_x - \bar{N}_y)lm + (l^2 - m^2)\bar{N}_{xy}\\ &= -lm\left(\frac{\partial^2\bar{\varphi}}{\partial y^2} - \frac{\partial^2\bar{\varphi}}{\partial x^2}\right) - (l^2 - m^2)\frac{\partial^2\bar{\varphi}}{\partial x\partial y}\end{aligned} \tag{38}$$

If $\bar{p}(x,y)$ is the downward pressure loading of the plate at the point (x,y), the equilibrium of lateral forces gives the following equation for $\bar{w}$:

$$\frac{\partial^2}{\partial x^2}\left[\bar{D}_2\left(\frac{\partial^2\bar{w}}{\partial x^2} + \nu\frac{\partial^2\bar{w}}{\partial y^2}\right)\right] + 2(1-\nu)\frac{\partial^2}{\partial x\partial y}\left(\bar{D}_2\frac{\partial^2\bar{w}}{\partial x\partial y}\right) + \frac{\partial^2}{\partial y^2}\left[\bar{D}_2\left(\frac{\partial^2\bar{w}}{\partial y^2} + \nu\frac{\partial^2\bar{w}}{\partial x^2}\right)\right] = \bar{p} + \bar{N}_x\frac{\partial^2\bar{w}}{\partial x^2} + 2\bar{N}_{xy}\frac{\partial^2\bar{w}}{\partial x\partial y} + \bar{N}_y\frac{\partial^2\bar{w}}{\partial y^2} \tag{39}$$

The sectional bending moments $\bar{M}_n$, $\bar{M}_s$ and the sectional twisting moment $\bar{M}_{ns}$ are, then,

$$\left.\begin{aligned}\bar{M}_n &= -\frac{1+\nu}{2}\bar{D}_2\nabla^2\bar{w} - \frac{1-\nu}{2}\bar{D}_2(l^2 - m^2)\left(\frac{\partial^2\bar{w}}{\partial x^2} - \frac{\partial^2\bar{w}}{\partial y^2}\right) - 2(1-\nu)\bar{D}_2lm\frac{\partial^2\bar{w}}{\partial x\partial y}\\ \bar{M}_s &= -\frac{1+\nu}{2}\bar{D}_2\nabla^2\bar{w} + \frac{1-\nu}{2}\bar{D}_2(l^2 - m^2)\left(\frac{\partial^2\bar{w}}{\partial x^2} - \frac{\partial^2\bar{w}}{\partial y^2}\right) + 2(1-\nu)\bar{D}_2lm\frac{\partial^2\bar{w}}{\partial x\partial y}\end{aligned}\right\} \tag{40}$$

$$\bar{M}_{ns} = -(1-\nu)\bar{D}_2lm\left(\frac{\partial^2\bar{w}}{\partial x^2} - \frac{\partial^2 w}{\partial y^2}\right) + (1-\nu)\bar{D}_2(l^2 - m^2)\frac{\partial^2\bar{w}}{\partial x\partial y} \tag{41}$$

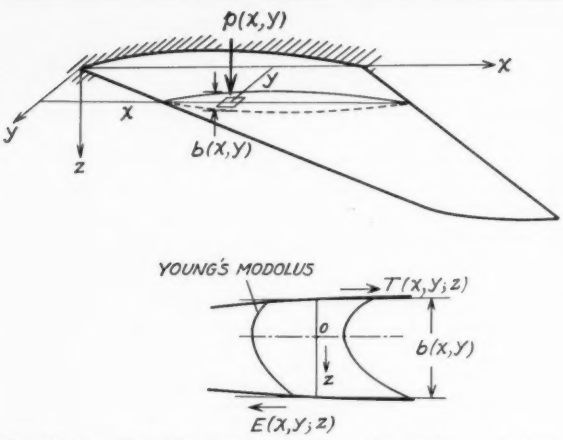

FIG. 2. Loads and boundary conditions of a solid heated wing.

SIMILARITY LAWS FOR SOLID THIN WINGS

By comparing the corresponding equations for the heated plate and for the plate at room temperature, their similarity is evident. The question is then whether it is possible to find a corresponding plate at room temperature such that, with proper loading, the plate will give solutions that are similar to that of the heated plate. To fix ideas, let the heated plate and the unheated plate both have the same plane form. The temperature distribution of the heated plate is specified so that N_T and M_T are known functions of the coordinates (x,y). The heated plate is built in at one end but free at all other edges (Fig. 2). The lateral pressure loading p for the heated plate is also specified. The problem is to find the thickness distribution $\bar{b}(x,y)$ and the loading of the unheated plate, such that $\bar{\varphi}(x,y)$ and $\bar{w}(x,y)$ are the same as $\varphi(x,y)$ and $w(x,y)$, respectively, except a proportionality factor.

Let α and β be two constants; then it is clear that the Eqs. (18) and (36) for $\varphi(x,y)$ and $\bar{\varphi}(x,y)$ will be exactly the same if

$$\bar{D}_0 = \alpha D_0 \tag{42}$$

$$\bar{\varphi} = \beta\varphi \tag{43}$$

$$F = \beta N_T \tag{44}$$

Then, because of Eqs. (16) and (35),

$$\bar{N}_x = \beta(N_x + N_T), \quad \bar{N}_{xy} = \beta N_{xy}, \quad \bar{N}_y = \beta(N_y + N_T) \tag{45}$$

Now, if λ and μ are two additional constants, and

$$\bar{D}_2 = \lambda D_2 \tag{46}$$

$$\bar{w} = \mu w \tag{47}$$

then the equation for $\bar{w}$, Eq. (39), can be rewritten as

$$\frac{\partial^2}{\partial x^2}\left[D_2\left(\frac{\partial^2 w}{\partial x} + \nu\frac{\partial^2 w}{\partial y^2}\right)\right] + 2(1-\nu)\frac{\partial^2}{\partial x\partial y}\left(D_2\frac{\partial^2 w}{\partial x\partial y}\right) + \frac{\partial^2}{\partial y^2}\left[\left(\frac{\partial^2 w}{\partial y^2} + \nu\frac{\partial^2 w}{\partial x^2}\right)\right] =$$

$$\frac{1}{\lambda\mu}p + \frac{\beta}{\lambda\mu}N_T\nabla^2\bar{w} + \frac{\beta}{\lambda}\left(N_x\frac{\partial^2 w}{\partial x^2} + 2N_{xy}\frac{\partial^2 w}{\partial x\partial y} + N_y\frac{\partial^2 w}{\partial y^2}\right)$$

Therefore it can be deduced, by comparing the above equation with Eq. (21), that, in order for w and $\bar{w}$ to satisfy the same equation,

$$\lambda = \beta \tag{48}$$

$$\bar{p} = -\beta N_T\nabla^2\bar{w} - \beta\mu\nabla^2 M_T + \beta\mu p \tag{49}$$

On the boundary of the heated plate, the forces N_n and N_{ns} vanish. By comparing Eqs. (19) and (20) with Eqs. (37) and (38) and by noting Eqs. (43) and (44),

$$\bar{N}_n = \beta N_T, \qquad \bar{N}_{ns} = 0 \tag{50}$$

Similarly, by comparing Eqs. (23) and (24) with Eqs. (37) and (38) and by noting Eqs. (46) and (47), the boundary conditions of Eq. (25) for the free edge of the heated plate reduces to

$$\left.\begin{aligned} \bar{M}_n &= \beta\mu M_T \\ \frac{\partial\bar{M}_n}{\partial n} + \frac{\bar{M}_n - \bar{M}_s}{r} + \frac{\partial\bar{M}_{ns}}{\partial s} &= \beta\mu\frac{\partial\bar{M}_T}{\partial n} \end{aligned}\right\} \tag{51}$$

The boundary conditions for the built-in edge, Eqs. (22), give

$$\bar{w} = 0, \qquad \partial\bar{w}/\partial n = 0 \tag{52}$$

As a first application of the theory developed, consider the simple case of a thin wing of solid section: The purpose is to find the stresses in the heated wing by performing experiments on an unheated "corresponding" or analog wing. The first step is to understand clearly the meaning of Eqs. (42) and (46). These equations, in fact, determine the thickness $\bar{b}$ of the unheated wing. Now let g be ratio $E/\bar{E}$ and η the nondimensional thickness variable measured from the upper surface of the plate such that $\eta = -1$ at upper surface and $\eta = 1$ at the lower surface. Let η_0 be the value of η at the median surface. Then,

$$D_0(x,y) = \frac{\bar{E}b}{2(1-\nu^2)}\int_{-1}^{1} g(x,y;\eta)\,d\eta$$

$$D_1(x,y) = \frac{\bar{E}b^2}{4(1-\nu^2)} \int_{-1}^{1} g(x,y;\eta)\,(\eta-\eta_0)\,d\eta$$

$$D_2(x,y) = \frac{\bar{E}b^3}{8(1-\nu^2)} \int_{-1}^{1} g(x,y;\eta)\,(\eta-\eta_0)^2\,d\eta$$

By using Eq. (31) and the above relations, the conditions of Eqs. (11), (42), and (46) can be written as

$$\int_{-1}^{1} g(x,y;\eta)\,(\eta-\eta_0)\,d\eta = 0 \tag{53}$$

$$\frac{\alpha}{2}\,b(x,y) \int_{-1}^{1} g(x,y;\eta)\,d\eta = \bar{b}(x,y) \tag{54}$$

$$\frac{\lambda}{8}\,b^3(x,y) \int_{-1}^{1} g(x,y;\eta)\,(\eta-\eta_0)^2\,d\eta = \frac{1}{12}\,\bar{b}^3(x,y) \tag{55}$$

By eliminating b, $\bar{b}$, and η_0 from these equations, one obtains

$$\left(\frac{1}{12}\,\frac{\alpha^3}{\lambda}\right)\left(\int_{-1}^{1} g\,d\eta\right)^4 = \left(\int_{-1}^{1} g\cdot\eta^2\,d\eta\right)\times \left(\int_{-1}^{1} g\,d\eta\right) - \left(\int_{-1}^{1} g\cdot\eta\,d\eta\right)^2 \tag{56}$$

Eq. (56) shows that the "Young's modulus profiles" $g(\eta)$ for various points (x,y) of the heated plate are not entirely arbitrary but must satisfy that relation so that the "similarity" between the heated wing and the isothermal analog wing is possible. If g is a fixed function—i.e., the temperature profiles across the plate are similar—or Young's modulus is constant, then Eq. (56) is certainly satisfied.* For any given problem of a heated wing then, the first step is to compute the value of α^3/λ or α^3/β for various points of the wing by Eq. (56). If these values do not differ very much, then, as an approximation, the average of the computed α^3/β can be used. Then the similarity procedure is possible. But in any event, the value of α^3/β is fixed by the problem, not at the free choice of the stress analyst. Thus, if β is chosen, then α is fixed. Furthermore, λ is equal to β according to Eq. (48). Therefore, out of the four constants, α, β, λ, and μ, only two (β and μ) can be chosen arbitrarily. When this is done, Eq. (54) determines the appropriate thickness $\bar{b}(x,y)$ for the unheated analog wing.

* Mathematically speaking, Eq. (56) is a functional equation. The solution of it gives the explicit required character of g. This problem is discussed in the Appendix.

With the geometry of the analog wing determined, the next step is to specify the loads on it. Eq. (50) shows that the unheated wing must be loaded with a sectional tension force βN_T at the boundary but no sectional shearing force. The first of Eqs. (51) shows that, at the free edge, the analog wing should have a bending moment equal to $\beta\mu M_T$. The numerical value of μ is arbitrary and is at the disposal of the experimenter. The second of Eqs. (51) can be interpreted as an upward support force $-\beta\mu(\partial M_T/\partial n)$ per unit length of boundary but no twisting moment at the boundary. Eq. (52) shows that a built-in edge of the heated wing corresponds to a built-in edge of the analog wing.

On the unheated wing, Eqs. (32) and (44) specify a body force

$$X = -\beta\,\frac{\partial N_T}{\partial x},\quad Y = -\beta\,\frac{\partial N_T}{\partial y} \tag{57}$$

These are forces in the x and y direction per unit area of the wing surface and are loads perhaps new to structures testing. The lateral pressure loading $\bar{p}$ on the analog wing is specified by Eq. (49). If $\Delta\bar{\epsilon}_x$ and $\Delta\bar{\epsilon}_y$ denote the differences of x and y components of direct strains measured on the isothermal wing on the top and the bottom surfaces—i.e., according to Eq. (28)

$$\left.\begin{aligned}\Delta\bar{\epsilon}_x(x,y) &= \bar{\epsilon}_x\left(x,y;-\frac{\bar{b}}{2}\right) - \bar{\epsilon}_x\left(x,y;\frac{\bar{b}}{2}\right) = \bar{b}(x,y)\,\frac{\partial^2\bar{w}}{\partial x^2}\\ \Delta\bar{\epsilon}_y(x,y) &= \bar{\epsilon}_y\left(x,y;-\frac{\bar{b}}{2}\right) - \bar{\epsilon}_y\left(x,y;\frac{\bar{b}}{2}\right) = \bar{b}(x,y)\,\frac{\partial^2\bar{w}}{\partial y^2}\end{aligned}\right\} \tag{58}$$

then Eq. (49) can be written as

$$\bar{p} = (-\beta N_T/\bar{b})\,(\Delta\bar{\epsilon}_x + \Delta\bar{\epsilon}_y) - \beta\mu\nabla^2 M_T + \beta\mu p \tag{59}$$

Needless to say, if there are concentrated lateral loads, the ratio of these loads on the test wing and on the original wing is also equal to $\beta\mu$.

The physical significance of Eq. (59) is different from that of Eq. (57) in that the body force loading is completely specified before the test because N_T is a known quantity, while the first term of $\bar{p}$ itself depends upon the experimentally determined $\Delta\bar{\epsilon}_x$ and $\Delta\bar{\epsilon}_y$. Therefore, if the loads are considered as input to the wing structure and the experimentally measured strains as output, then Eq. (57) shows that the output also partly determines the input. In other words, there is a "feedback link" in the experimental setup of the analog wing.

With the loading on the unheated wing so specified, the relation between $\bar{\varphi}$ and φ and between $\bar{w}$ and w are given by Eqs. (43) and (47). The stresses in the original heated wing can then be computed from the measured strains on the test wing. For instance, from Eqs. (1) and (3),

$$\sigma_x(x,y;z) = \frac{E(x,y;z)}{1-\nu^2}\left[\left(\frac{\partial u}{\partial x} + \nu\,\frac{\partial u}{\partial y}\right) - z\left(\frac{\partial^2 w}{\partial x^2} + \nu\,\frac{\partial^2 w}{\partial y^2}\right) - (1+\nu)aT(x,y;z)\right]$$

By using Eq. (17), the above equation is reduced to

$$\sigma_x(x,y;z) = \frac{E(x,y;z)}{1-\nu^2}\left\{\frac{N_T}{D_0} + \frac{1}{D_0}\frac{\partial^2\varphi}{\partial y^2} - z\left(\frac{\partial^2 w}{\partial x^2} + \nu\frac{\partial^2 w}{\partial y^2}\right) - (1+\nu)aT(x,y;z)\right\}$$

But according to Eqs. (42), (43), (29), and (35),

$$\frac{1}{D_0}\frac{\partial^2\varphi}{\partial y^2} = \frac{\alpha}{\beta}\frac{1}{\bar{D}_0}\frac{\partial^2\bar{\varphi}}{\partial y^2} = \frac{\alpha}{\beta}\frac{1}{\bar{D}_0}[\bar{N}_x - \beta N_T] = \frac{\alpha}{\beta}\left(\frac{\partial\bar{u}}{\partial x} + \nu\frac{\partial\bar{v}}{\partial y}\right) - \frac{N_T}{D_0}$$

However,

$$\frac{\partial\bar{u}}{\partial x} = \frac{1}{2}\left[\bar{\epsilon}_x\left(x,y;-\frac{\bar{b}}{2}\right) + \bar{\epsilon}_x\left(x,y;\frac{\bar{b}}{2}\right)\right] = \bar{\epsilon}_x(x,y) \tag{60}$$

$$\frac{\partial\bar{v}}{\partial y} = \frac{1}{2}\left[\bar{\epsilon}y\left(x,y;-\frac{\bar{b}}{2}\right) + \bar{\epsilon}_y\left(x,y;\frac{\bar{b}}{2}\right)\right] = \bar{\epsilon}_y(x,y) \tag{61}$$

where $\bar{\epsilon}_x(x,y)$ is the average of the x-strain at the top and the bottom surfaces of the analog wing at the point (x,y) and $\bar{\epsilon}_y(x,y)$ is the average of the y-strain. Thus, together with Eq. (58), the above expressions give

$$\sigma(x,y;z) = \frac{E(x,y;z)}{1-\nu^2}\left\{\frac{\alpha}{\beta}(\bar{\epsilon}_x + \nu\bar{\epsilon}_y) - \frac{z}{\mu\bar{b}}(\Delta\bar{\epsilon}_x + \nu\Delta\bar{\epsilon}_y) - (1+\nu)aT(x,y;z)\right\} \tag{62}$$

It may be proper to point out again that the quantity z in the above equation and in the subsequent equations is the distance from the median surface, positive if the point is below the median surface. Similar to Eq. (62), one has

$$\sigma_y(x,y;z) = \frac{E(x,y;z)}{1-\nu^2}\left[\frac{\alpha}{\beta}(\bar{\epsilon}_y + \nu_x\bar{\epsilon}) - \frac{z}{\mu\bar{b}}(\Delta\bar{\epsilon}_y + \nu\Delta\bar{\epsilon}_x) - (1+v)\,aT(x,y;z)\right] \tag{63}$$

If the difference $\Delta\bar{\gamma}_{xy}$ of the shear strain and the average shear strain $\bar{\gamma}_{xy}$ are defined as

$$\Delta\bar{\gamma}_{xy}(x,y) = \bar{\gamma}_{xy}\left(x,y;-\frac{\bar{b}}{2}\right) - \bar{\gamma}_{xy}\left(x,y;\frac{\bar{b}}{2}\right) \tag{64}$$

$$\bar{\gamma}_{xy}(x,y) = \frac{1}{2}\left[\bar{\gamma}_{xy}\left(x,y;-\frac{\bar{b}}{2}\right) + \bar{\gamma}_{xy}\left(x,y;\frac{\bar{b}}{2}\right)\right] \tag{65}$$

the shear stress in the original heated wing is calculated as

$$\tau_{xy}(x,y;z) = \frac{E(x,y;z)}{2(1+\nu)}\left[\frac{\alpha}{\beta}\bar{\gamma}_{xy}(x,y) - \frac{z}{\mu\bar{b}}\Delta\bar{\gamma}_{xy}(x,y)\right] \tag{66}$$

Eqs. (62), (63), and (66) allow the calculation of the stresses in the heated wing from test data of the unheated wing. They also show the advantage having the constants (β/α) and μ smaller than unity, so that the strains of the unheated wing are magnified in computing the stresses in the heated wing. Then, for a specified load on the heated wing, the test load on the unheated wing is reduced and the analog wing will not be overstrained. Fig. 3 gives a summary of the loading of the unheated test wing, together with the equation numbers of relations that specify the quantities in terms of the quantities of the original heated wing.

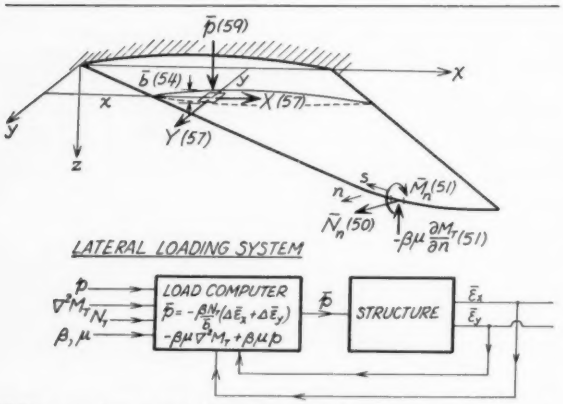

FIG. 3. Loads and boundary conditions of the analog test wing. (Numbers in parentheses correspond to numbered equations in the text where the appropriate relation with quantities of the original heated wing can be found.)

ALTERNATE TEST PROCEDURE FOR THIN SOLID WINGS

In the previous section, the simulated tests on the isothermal wing are proposed with simultaneous loading both in the plane of the median surface and in lateral pressure. This results in a rather complicated load system at the free boundary of the wing. To simplify the load system at the boundary, the loading in the plane of the median surface and the lateral loading can be separated—that is, two separate tests, properly correlated, are made on the analog wing, and the stresses in the heated wing are obtained by a synthesis of the test results.

To determine first the sectional forces N_x, N_y, and N_{xy}, the unheated wing is dimensioned to satisfy Eq. (42). It is then loaded with body forces specified by Eq. (57), but no lateral load is applied. At the "free edge" of the wing, it is loaded according to Eq. (50). Then the magnitude of the sectional forces for the heated wing can be computed from Eq. (45) if $\bar{N}_x$, $\bar{N}_y$, and $\bar{N}_{xy}$ are determined. These sectional forces can be calculated from the measured strains on the wing. Although theoretically there should be no bending of the wing, actually bending will be present because of deviations of the real wing from the idealized wing assumed in the theory. The effects of such spurious bending can be eliminated by taking the average of the strains of the top and the bottom surfaces. Let the superscript 1 denote the quantities induced by this loading in the plane of the median surface. Introduce the following notations for the average strains:

$$\left.\begin{aligned}
\bar{\bar{\epsilon}}_x^{(1)}(x,y) &= \frac{1}{2}\left[\bar{\epsilon}_x^{(1)}\left(x,y;\,-\frac{\bar{b}}{2}\right) + \bar{\epsilon}_x^{(1)}\left(x,y;\,\frac{\bar{b}}{2}\right)\right] \\
\bar{\bar{\epsilon}}_y^{(1)}(x,y) &= \frac{1}{2}\left[\bar{\epsilon}_y^{(1)}\left(x,y;\,-\frac{\bar{b}}{2}\right) + \bar{\epsilon}_y^{(1)}\left(x,y;\,\frac{\bar{b}}{2}\right)\right] \\
\bar{\bar{\gamma}}_{xy}^{(1)}(x,y) &= \frac{1}{2}\left[\bar{\gamma}_{xy}^{(1)}\left(x,y;\,-\frac{\bar{b}}{2}\right) + \bar{\gamma}_{xy}^{(1)}\left(x,y;\,\frac{\bar{b}}{2}\right)\right]
\end{aligned}\right\} \tag{67}$$

Then the sectional forces N_x, N_y, and N_{xy} for the heated wing can be calculated as

$$\left.\begin{aligned}
N_x(x,y) &= \frac{\alpha}{\beta} D_0[\bar{\bar{\epsilon}}_x^{(1)} + \nu\bar{\bar{\epsilon}}_y^{(1)}] - N_T \\
N_y(x,y) &= \frac{\alpha}{\beta} D_0[\bar{\bar{\epsilon}}_y^{(1)} + \nu\bar{\bar{\epsilon}}_x^{(1)}] - N_T \\
N_{xy} &= \frac{\alpha}{\beta}\frac{1-\nu}{2} D_0\,\bar{\bar{\gamma}}_{xy}^{(1)}
\end{aligned}\right\} \tag{68}$$

When the average strains of Eq. (67) are measured, the loading in the plane of the median surface, the body forces, and the boundary forces can be removed. The second step of the test is to load the unheated wing laterally. Let Eqs. (46) and (47) be satisfied. Then, in order that $\bar{w}$ and w satisfy the same differential equation, the lateral loading $\bar{p}$ on the test wing must be specified as

$$\bar{p} = -\lambda\mu\nabla^2 M_T + \lambda\mu p + \lambda\left[N_x\frac{\partial^2\bar{w}}{\partial x^2} + 2N_{xy}\frac{\partial^2\bar{w}}{\partial x\partial y} + N_y\frac{\partial^2\bar{w}}{\partial y^2}\right] \tag{69}$$

On the "free edges" of the wing, there is a bending moment equal to $\lambda\mu M_T$ and an upward support force $-\lambda\mu(\partial M_T/\partial n)$ per unit length of the boundary.

Let the superscript 2 denote the quantities induced by bending; then,

$$\left.\begin{aligned}
\Delta\bar{\epsilon}^{(2)}(x,y) &= \bar{\epsilon}_y^{(2)}\left(x,y;\,-\frac{\bar{b}}{2}\right) - \bar{\epsilon}_x^{(2)}\left(x,y;\,\frac{\bar{b}}{2}\right) = \bar{b}(x,y)\frac{\partial^2\bar{w}}{\partial x^2} \\
\Delta\bar{\epsilon}_y^{(2)}(x,y) &= \bar{\epsilon}_y^{(2)}\left(x,y;\,-\frac{\bar{b}}{2}\right) - \bar{\epsilon}_y^{(2)}\left(x,y;\,\frac{\bar{b}}{2}\right) = \bar{b}(x,y)\frac{\partial^2\bar{w}}{\partial y^2} \\
\Delta\bar{\gamma}_{xy}^{(2)}(x,y) &= \bar{\gamma}_{xy}^{(2)}\left(x,y;\,-\frac{\bar{b}}{2}\right) - \bar{\gamma}_{xy}^{(22)}(x,y;\,\frac{\bar{b}}{2}) = 2\bar{b}(x,y)\frac{\partial^2\bar{w}}{\partial x\partial y}
\end{aligned}\right\} \tag{70}$$

With these strains differences between the top and the bottom surfaces, the loading Eq. (69) can be written as

$$\bar{p}(x,y) = -\lambda\mu\nabla^2 M_T + \lambda\mu p(x,y) + \lambda\left[N_x\frac{\Delta\bar{\epsilon}_x^{(2)}}{\bar{b}} + N_{xy}\frac{\Delta\bar{\gamma}_{xy}^{(2)}}{\bar{b}} + N_y\frac{\Delta\bar{\epsilon}_y^{(2)}}{\bar{b}}\right] \tag{71}$$

where the sectional forces N_x, N_y, and N_{xy} are computed by using Eq. (68) and the strain data obtained during the first part of the test. This equation again demonstrates the feedback character of the lateral loading. Fig. 4 summarizes the load systems for the two successive tests.

When the strain averages of Eq. (67) and the strain differences of Eq. (70) are measured by the two successive tests on the isothermal analog wing, the stresses in the original heated wing can be computed by using equations similar to Eqs. (62), (63), and (65), replacing $\bar{\bar{\epsilon}}$, $\bar{\bar{\gamma}}$ by $\bar{\epsilon}^{(1)}$, $\bar{\gamma}^{(1)}$ and $\Delta\bar{\epsilon}$, $\Delta\bar{\gamma}$ by $\Delta\bar{\epsilon}^{(2)}$, $\Delta\bar{\gamma}^{(2)}$ of Eqs. (67) and (70), respectively. However, there is one important difference between the test procedure of the present section and the test procedure of the previous one: α can be chosen independent of β, because now β is not necessarily equal to λ. But α and λ are connected because of the condition of Eq. (56). Out of the four constants α, β, λ, and μ, three can be chosen arbitrarily. This greater degree of freedom and simpler

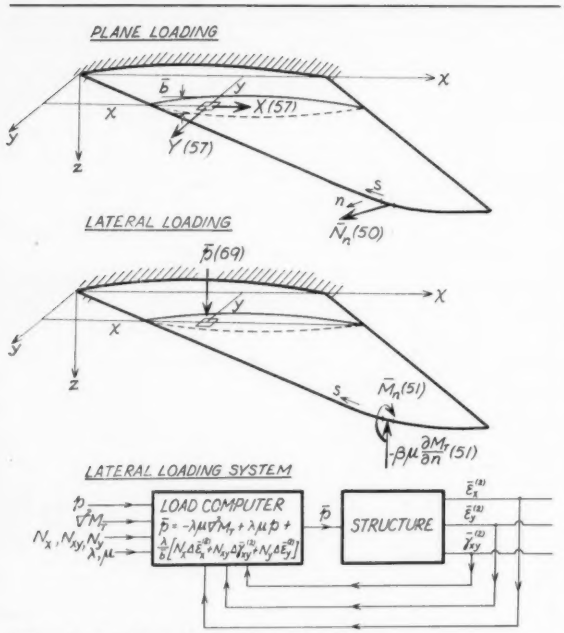

FIG. 4. Loads and boundary conditions of the analog test wing, alternate procedure. (Numbers in parentheses correspond to numbered equations in the text where the appropriate relation with quantities of the original heated wing can be found.)

load system in each stage of tests than the test procedure described in the previous section may prove to be advantageous in actual application.

BOX WING

In the previous sections, the similarity laws for thin solid wings are formulated for obtaining the stresses in a heated wing by testing an analog unheated wing. A majority of actual wing structures is, however, much more complicated than a solid wing. For example, the main load-carrying member of the wing may be a box structure with top and bottom panels, ribs, and deep beams joining the top and bottom panels. Since only the top and bottom panels of such a box wing are exposed to the air stream, the aerodynamic heating of the structure is limited to these panels.

To analyze such a box wing, the different structure elements can be broken down, and each individual part, such as the top panel, can be considered as a plate. To each individual part then, the theory developed in the earlier sections of this paper can be applied. The thickness $\bar{b}$ for the analog unheated plate for each part of the structure can be specified by the method described previously. The only restriction is that the four constants α, β, λ, and μ must be the same for all structure elements. The loads on the individual unheated plates corresponding to the different structure elements can be determined according to equations given in the earlier sections. At the boundary or the junction of the different unheated analog panels, there are now two types of load. One type of load comes from the similarity law. This load system is specified previously as the load system for "free edges." The other type of load comes from the junction condition that the deformations of the different parts of the structure must fit together. If the analog panels are put together, then the junction loads will be automatically supplied by the structure. Therefore the procedure to use the method of similarity is as follows:

The first step is to determine the thickness $\bar{b}$ of the analog isothermal box wing by Eqs. (54) and (56). In a box structure, there is appreciable influence on the sectional forces in the median surface of the plates because of bending deflection. Therefore the separation of bending from the "extensional loads" in the plane of the plates is no longer appropriate. The complete load system for the analog wing must be applied simultaneously. This consists of the body force loads in the plane of the plates, the lateral pressure $\bar{p}$, and the "free edge" loads at the junction of the different parts of the structure. The stresses in the original heated box wing can then be calculated by using Eqs. (12), (63), and (65) with the measured strains.

DISCUSSION

In the previous sections, it is shown that the problem of stressing a heated wing can be solved by tests on an analog unheated wing through the similarity laws. The temperature distribution in the wing is assumed to be given by a theoretical calculation using aerodynamic heating data and the theory of heat transfer in solid materials.[1] The loading system required for the analog wing is indeed complicated. Furthermore, the lateral pressure load $\bar{p}$ specified by either Eq. (59) or Eq. (71) involves the concept of feedback in that $\bar{p}$ is partially dependent upon the measured strains and cannot be predetermined. This is, perhaps, a novel concept in structure testing. The possible justification for this great complication in structural testing is the serious difficulty of simulating aerodynamic heating in a structures laboratory and of measuring strains at high temperatures.

The basic principle of the theory of similarity law can be traced to the well-known fact that the general three-dimensional thermal stress problem can be reduced to a problem in isothermal material by introducing appropriate fictitious three-dimensional body forces and surface forces on the boundary of the body. The general three-dimensional formulation of the "analogy" is, however, not useful for structure testing purposes, because there is no possible method of applying three-dimensional body forces. If one dimension of the body is small, such as a thin plate or a thin shell, then the body force is two-dimensional. The loading for the analog isothermal structure can be done, although not easily, as shown in the previous discussion. From this general argument, it is clear then that the present "similarity theory" for thermal stresses can

certainly be extended to any thin elastic shells, although the actual execution of the analog testing may be more difficult than the flat plate case studied here.

To avoid the task of testing a heated wing, a test wing at room temperature is proposed as an analog. In a sense then, the whole concept of the method of similarity is that of analog-machine computing. There is, however, an advantage of the present method over the recognized machine computer in that the main physical member of the problem, the elastic plate, remains and is not replaced by an approximate system such as electric network. The unheated analog wing is thus the closest analog the aerodynamically heated wing can have and is the most accurate analog. The price of this accuracy and detailed reproduction of the original problem is the complicated test setup required. However, an enterprising structures test engineer will probably welcome such challenge to his ingenuity and demand on his technical skill.

Appendix—Young's Modulus Profile

By writing $f(\eta)$ as

$$f(\eta) = \sqrt{(1/12)\ (\alpha^3/\lambda)}\ g(\eta) \tag{72}$$

Eq. (56) can be written as

$$\left[\int_{-1}^{1} f(\eta)\ d\eta\right]^4 = \left[\int_{-1}^{1} f(\eta)\cdot\eta^2\ d\eta\right]\left[\int_{-1}^{1} f(\eta)\ d\eta\right] - \left[\int_{-1}^{1} f(\eta)\cdot\eta\ d\eta\right]^2 \tag{73}$$

Now any continuous function $f(\eta)$ for $-1 \leq \eta \leq 1$ can be expanded into a series of Legendre polynomials $P_n(\eta)$*—i.e.,

$$f(\eta) = \sum_{n=0}^{\infty} a_n P_n(\eta) \tag{74}$$

where a_n's are constant coefficients. Then[4]

$$\int_{-1}^{1} f(\eta)\ d\eta = \int_{-1}^{1} f(\eta)P_0(\eta)\ d\eta = 2a_0$$

$$\int_{-1}^{1} f(\eta)\eta\ d\eta = \int_{-1}^{1} f(\eta)P_1(\eta)\ d\eta = \frac{2}{3}\ a_1$$

$$\int_{-1}^{1} f(\eta)\eta^2\ d\eta = \frac{2}{3}\int_{-1}^{1} f(\eta)\left[P_2(\eta) + \frac{1}{2}\ P_0(\eta)\right]d\eta = \frac{2}{3}\left(\frac{2}{5}\ a_2 + a_0\right)$$

Therefore Eq. (73) can be written as

$$12\ a_0^2 = 1 + \frac{2}{5}\left(\frac{a_2}{a_0}\right) - \frac{1}{3}\left(\frac{a_1}{a_0}\right)^2 \tag{75}$$

The restriction of Eq. (73) is thus simply a relation among the first three coefficients a_0, a_1, and a_2 of the expansion Eq. (74). The later coefficients, a_n, $n \geq 3$, are entirely free. Therefore the $f(\eta)$, although not entirely arbitrary, has a wide degree of freedom. Hence, it is probable that the Young's modulus profile will conform to the condition of Eq. (56) for the similarity theory up to a high order.

* The author is deeply indebted to Prof. A. Erdélyi, of the California Institute of Technology, for suggesting this method of solving the problem.

References

[1] Kaye, J., *The Transient Temperature Distribution in a Wing Flying at Supersonic Speeds*, Journal of the Aeronautical Sciences, Vol. 17, No. 12, pp. 787–807, 816, December, 1950.

[2] Nádai, A., *Elastische Platten*, p. 264; Julius Springer, Berlin, 1925.

[3] Tsien, H. S., and Cheng, C. M., *A Similarity Law for Stressing Rapidly Heated Thin-Walled Cylinders*, Journal of the American Rocket Society, Vol. 22, p. 144, 1952.

[4] See, for instance, Whittaker, E. T., and Watson, G. N., *Modern Analysis*, Chapt. 15; Cambridge University Press, London, England, 1920.

The Effect of the Torsional Rigidity of a Single Stiffener on the Buckling Characteristics of a Panel Subjected to Axial Compression with Large Deflections*

T. K. STEELE† AND C. T. WANG‡

Bulova Research and Development Laboratories, Inc., and New York University, Respectively

SUMMARY

The solution of von Kármán's fundamental equations for large deflections of plates is presented for the case of a rectangular panel (2:1) with a single stiffener along its center parallel to the applied edge compressive load for the conditions where the stiffener has very low and then very high torsional rigidity relative to the plate. In both cases, the bending rigidity of the stiffener is taken of high order of magnitude compared with the plate itself and is assumed to remain unbuckled under all edge compressive loads considered.

After solving for the deflection coefficients defining the deflection patterns, it is possible to compare the critical buckling loads, effective plate widths, unit plate shortenings, membrane stresses, and bending stresses for the two cases.

On the basis of these comparisons, predictions may be made concerning the increase of permissible load-carrying capacity of panels containing rigid stiffeners against those containing nonrigid stiffeners.

NOMENCLATURE

a	= length of square side of plate
a_e	= effective width of plate
$b_{r,s,p,q}$; $d_{r,s,p,q}$;	
$f_{m,n}$	= coefficients in stress function
c	= moment arm for equivalent normal pressure, p
D	= flexural rigidity of plate $= Eh^3/12(1-\mu^2)$
E	= Young's modulus
F	= stress function
G	= shear modulus
h	= plate thickness
J	= polar moment of inertia
k_m	= edge moment coefficients
m_x	= edge bending moment per unit length about x-axis
m, n, p, q, r, s	= positive integers used as subscripts
$p_{m,n}$	= pressure coefficients for normal pressure
u, v, w	= displacements of a point in the x, y, and z directions, respectively
W	= lateral displacement-thickness ratio $= w/h$
$w_{m,n}$	= coefficients in infinite series for w
x, y, z	= coordinates of a point measured from origin at corner of plate
$\bar{\epsilon}_x, \bar{\epsilon}_y$	= unit plate shortening in x and y directions
$\sigma_x', \sigma_y', \tau_{x,y}'$	= median-fiber stresses (membrane)
$\sigma_x'', \sigma_y'', \tau_{x,y}''$	= extreme-fiber bending and shearing stresses
$\epsilon_x', \epsilon_y', \gamma_{x,y}'$	= median-fiber strains
$\epsilon_x'', \epsilon_y'', \gamma_{x,y}''$	= extreme-fiber bending and shearing strains
$\bar{\sigma}_x, \bar{\sigma}_y$	= average edge compressive stresses
$\sigma_{cr.}$	= critical compressive stress
$\epsilon_{cr.}$	= critical compressive strain
μ	= Poisson's ratio (taken as 0.316)
∇^4	$= \dfrac{\partial^4}{\partial x^4} + 2\dfrac{\partial^4}{\partial x^2 \partial y^2} + \dfrac{\partial^4}{\partial y^4}$

Received June 24, 1952.

* This paper is based on a thesis submitted to New York University by T. K. Steele in partial fulfillment of the requirements for the degree of Doctor of Engineering Science.

† Staff Engineer.

‡ Professor of Aeronautical Engineering, Daniel Guggenheim School of Aeronautics.

INTRODUCTION

IN THE DESIGN OF THIN PLATES that bend under lateral and/or edge loading, formulas based on the Kirchhoff theory, which neglects stretching and shearing in the middle surface, are satisfactory provided that the deflections are small compared with the thickness. If deflections are of the same order as the thickness, the Kirchhoff theory may yield results that are considerably in error, and a more rigorous theory that takes account of deformations in the middle surface should therefore be applied. The fundamental equations for the more exact theory have been derived by von Kármán.[1] The analysis of the postbuckling characteristics of plates in this paper are based upon these nonlinear equations of von Kármán.

The numerical solutions presented herein are based on the trigonometric series method of attack introduced by Levy.[2]

The critical buckling loads, which are independent of the nonlinear terms, have subsequently been determined by using only the linear deflection terms in the von Kármán equations.

EQUATIONS FOR THE DEFORMATION OF THIN PLATES

The fundamental equations governing the deformation of thin plates developed by von Kármán[1] are given by Timoshenko[3] in the following form:

$$\nabla^4 F = E\left[\left(\frac{\partial^2 w}{\partial x \partial y}\right)^2 - \frac{\partial^2 w}{\partial x^2}\frac{\partial^2 w}{\partial y^2}\right] \qquad (1)$$

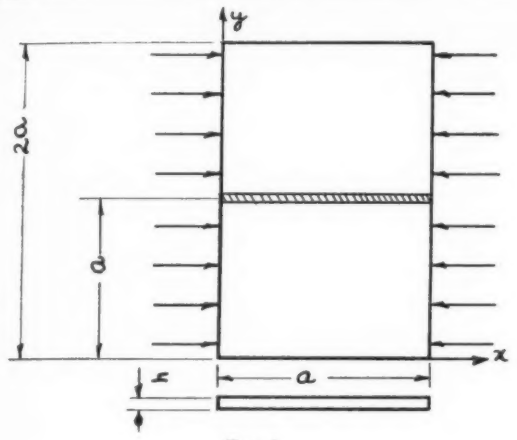

FIG. 1.

$$\nabla^4 w = \frac{p}{D} + \frac{h}{D}\left(\frac{\partial^2 F}{\partial y^2}\frac{\partial^2 w}{\partial x^2} + \frac{\partial^2 F}{\partial x^2}\frac{\partial^2 w}{\partial y^2} - 2\frac{\partial^2 F}{\partial x \partial y}\frac{\partial^2 w}{\partial x \partial y}\right) \tag{2}$$

where the median-fiber stresses are

$$\sigma_x' = \frac{\partial^2 F}{\partial y^2}; \quad \sigma_y' = \frac{\partial^2 F}{\partial x^2}; \quad \tau_{x,y}' = -\frac{\partial^2 F}{\partial x \partial y} \tag{3}$$

and the median-fiber strains are

$$\left.\begin{aligned} \epsilon_x' &= \frac{1}{E}\left(\frac{\partial^2 F}{\partial y^2} - \mu\frac{\partial^2 F}{\partial x^2}\right) \\ \epsilon_y' &= \frac{1}{E}\left(\frac{\partial^2 F}{\partial x^2} - \mu\frac{\partial^2 F}{\partial y^2}\right) \\ \gamma_{x,y}' &= \frac{-2(1+\mu)}{E}\frac{\partial^2 F}{\partial x \partial y} \end{aligned}\right\} \tag{4}$$

The extreme-fiber bending and shearing stresses are

$$\left.\begin{aligned} \sigma_x'' &= -\frac{Eh}{2(1-\mu^2)}\left[\frac{\partial^2 w}{\partial x^2} + \mu\frac{\partial^2 w}{\partial y^2}\right] \\ \sigma_y'' &= -\frac{Eh}{2(1-\mu^2)}\left[\frac{\partial^2 w}{\partial y^2} + \mu\frac{\partial^2 w}{\partial x^2}\right] \\ \tau_{x,y}'' &= [Eh/2(1+\mu)](\partial^2 w/\partial x \partial y) \end{aligned}\right\} \tag{5}$$

GENERAL SOLUTION OF THE PLATE EQUATIONS

Fig. 1 represents a 2:1 rectangular plate with a single centered stiffener subjected to an end compressive load parallel to the stiffener. From the symmetry of the figure, each plate half may be considered as a square of length a.

If the stiffener has a very low torsional rigidity, it will tend to twist freely under load so that the plate would be analogous to one with four edges simply supported. The high bending rigidity of the stiffener will resist any lateral deflection so that a node will exist at the center of the plate face.

The boundary conditions for this case are

$$\left.\begin{aligned} w]_{x=0,a} &= 0; \quad w]_{y=0,a} = 0 \\ \frac{\partial^2 w}{\partial x^2}\Big]_{x=0,a} &= 0; \quad \frac{\partial^2 w}{\partial y^2}\Big]_{y=0,a} = 0 \end{aligned}\right\} \tag{6}$$

This problem has been treated extensively by Levy.[2, 4] The pertinent results of his work will be presented for comparison purposes in this paper. The method of attack will not be included here.

If the stiffener has a very high torsional rigidity, it will resist twisting under load so that the plate will act as one with three edges simply supported and the fourth edge clamped rigidly.

The boundary conditions for this case are

$$\left.\begin{aligned} w]_{x=0,a} = 0; \quad w]_{y=0,a} = 0: \quad \frac{\partial w}{\partial y}\Big]_{y=a} &= 0 \\ m_y = -D\left(\frac{\partial^2 w}{\partial y^2} + \mu\frac{\partial^2 w}{\partial x^2}\right)_{x=0,a} &= 0 \\ m_x = -D\left(\frac{\partial^2 w}{\partial x^2} + \mu\frac{\partial^2 w}{\partial y^2}\right)_{y=0} &= 0 \end{aligned}\right\} \tag{7}$$

Condition of Straight Edges:

If the elongation of the plate $\bar{\epsilon}_x$ in the x-direction and $\bar{\epsilon}_y$ in the y-direction and if the edges of the plate are straight, then $\bar{\epsilon}_x$ and $\bar{\epsilon}_y$ must be independent of the position along the length or width at which they are measured, or

$$\left.\begin{aligned} a\bar{\epsilon}_x &= \int_0^a \left[\frac{1}{E}\left(\frac{\partial^2 F}{\partial y^2} - \mu\frac{\partial^2 F}{\partial x^2}\right) - \frac{1}{2}\left(\frac{\partial w}{\partial x}\right)^2\right] dx \\ a\bar{\epsilon}_y &= \int_0^a \left[\frac{1}{E}\left(\frac{\partial^2 F}{\partial x^2} - \mu\frac{\partial^2 F}{\partial y^2}\right) - \frac{1}{2}\left(\frac{\partial w}{\partial y}\right)^2\right] dy \end{aligned}\right\} \tag{8}$$

Load on the Edges:

If the average stress in the plane of the plate is $\bar{\sigma}_x$ in the x-direction and $\bar{\sigma}_y$ in the y-direction, then

$$\left.\begin{aligned} a\bar{\sigma}_x &= \left[\left(\frac{\partial F}{\partial y}\right)_{y=a} - \left(\frac{\partial F}{\partial y}\right)_{y=0}\right] \\ a\bar{\sigma}_y &= \left[\left(\frac{\partial F}{\partial x}\right)_{x=a} - \left(\frac{\partial F}{\partial x}\right)_{x=0}\right] \end{aligned}\right\} \tag{9}$$

General Solution:

The lateral deflection is taken in Eq. (1) as

$$w = \sum_{m=1}^{\infty}\sum_{n=1}^{\infty} w_{m,n} \sin\frac{m\pi x}{a}\sin\frac{n\pi y}{a} \tag{10}$$

Eq. (10) can be made to satisfy all the boundary conditions of Eqs. (7) if the value of the moment, m_x, along edge $y = a$ were known.

To facilitate this solution, the required edge moment, m_x, will be replaced by an auxiliary pressure distribution $p(x, y)$ near the edge $y = a$, as shown in Fig. 2. This method was first suggested by Levy.[5]

If this pressure distribution is expressed by a Fourier series and the value of c approaches zero, the auxiliary pressure is

$$p(x, y) = \sum_{n=1}^{\infty} \frac{2\pi m_x}{a^2} n \sin \frac{n\pi y}{a} \tag{11}$$

If m_x is expressed by a Fourier series with k_m as an undetermined coefficient, then

$$m_x = \frac{a^2}{2\pi} \sum_{m=1}^{\infty} k_m \sin \frac{m\pi x}{a} \tag{12}$$

Inserting Eq. (12) into Eq. (11) gives

$$p(x, y) = \sum_{m=1}^{\infty} \sum_{n=1}^{\infty} p_{m,n} \sin \frac{m\pi x}{a} \sin \frac{n\pi y}{a} \tag{13}$$

where

$$p_{m,n} = (-1)^{n-1} nkm \tag{14}$$

From boundary conditions (7), $\partial w/\partial y]_{y=a} = 0$, it follows that

$$\sum_{n=1}^{\infty} n w_{m,n} (-1)^n = 0; \quad m = 1, 3, \ldots . \tag{15}$$

In order to satisfy Eq. (1) and the boundary conditions of Eqs. (9), F is taken as

$$F = \frac{\bar{\sigma}_x y^2}{2} + \frac{\bar{\sigma}_b x^2}{2} + \sum_{m=0}^{\infty} \sum_{n=0}^{\infty} f_{m,n} \cos \frac{m\pi x}{a} \cos \frac{n\pi y}{a} \tag{16}$$

Substituting Eqs. (16) and (10) simultaneously into Eq. (1) and equating coefficients of like trigonometric terms on the two sides of the equation results in a relation between the coefficients $f_{m,n}$ and $w_{m,n}$.

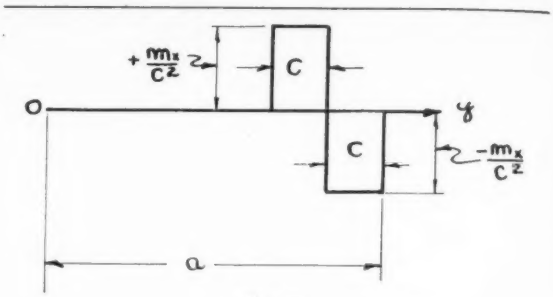

FIG. 2.

This relation can be simplified to

$$f_{m,n} = \frac{E}{4(m^2 + n^2)^2} \sum b_{r,s,p,q} w_{r,s} w_{p,q} \tag{17}$$

where (1) the summation includes all products $w_{r,s}w_{p,q}$ for which m is equal to either the sum or difference of r and p, and for which n is equal to either the sum or difference of s and q; and (2) the coefficient $b_{r,s,p,q}$ is given by

$$b_{r,s,p,q} = 2rspq \pm (r^2q^2 + s^2p^2) \tag{17a}$$

where the sign before the parenthesis is positive if m is the sum of r and p and n is the difference of s and q, or if m is the difference of r and p and n is the sum of s and q. It is negative otherwise. When $r = p$ and $s = q$, $b_{r,s,p,q}$ is one-half the value given by Eq. (17a).

It remains to show the necessary relation between the coefficients $w_{m,n}$, Eq. (10); $p_{m,n}$, Eq. (13); and $f_{m,n}$ Eq. (17).

TABLE 1
Equations for the Stress Coefficients in Eq. (17)

$f_{0,1} = (E/4)(-w_{1,1}w_{1,2} - w_{1,2}w_{1,3} - 9w_{3,1}w_{3,2} - 9w_{3,2}w_{3,3})$
$f_{0,2} = (E/32)(w_{1,2}^2 + 9w_{3,1}^2 - 2w_{1,1}w_{1,3} - 18w_{3,1}w_{3,3})$
$f_{0,3} = (E/36)(w_{1,1}w_{1,2} + 9w_{3,1}w_{3,2})$
$f_{0,4} = (E/128)(2w_{1,1}w_{1,3} + w_{1,2}^2 + 18w_{3,1} + 9w_{3,2}^2)$
$f_{0,5} = (E/100)(w_{1,2}w_{1,3} + 9w_{3,2}w_{3,3})$
$f_{0,6} = (E/288)(w_{1,3}^2 + 9w_{3,3}^2)$
$f_{2,0} = (E/32)(w_{1,1}^2 + 4w_{1,2}^2 + 9w_{1,3}^2 - 2w_{1,1}w_{3,1} - 8w_{1,2}w_{3,2} - 18w_{1,3}w_{3,3}$
$f_{2,1} = (E/100)(9w_{1,1}w_{1,2} - w_{1,1}w_{3,2} + 25w_{1,2}w_{1,3} - 25w_{1,2}w_{3,1} - 9w_{1,2}w_{3,3} - 49w_{1,3}w_{3,2})$
$f_{2,2} = (E/64)(4w_{1,1}w_{1,3} - 12w_{1,1}w_{3,1})$
$f_{2,3} = (E/676)(-w_{1,1}w_{1,2} + 25w_{1,1}w_{3,2} + 49w_{1,2}w_{3,1})$
$f_{2,4} = (E/400)(-w_{1,1}w_{1,3} + 9w_{1,1}w_{3,3} + 16w_{,1}2w_{3,2} + 25w_{1,3}w_{3,1})$
$f_{2,5} = (E/3,364)(-w_{1,2}w_{1,3} + 81w_{1,2}w_{3,3} + 121w_{1,3}w_{3,2})$
$f_{2,6} = (E/1,600)(36w_{1,3}w_{3,3})$
$f_{4,0} = (E/64)(w_{1,1}w_{3,1} + 4w_{1,2}w_{3,2} + 9w_{1,3}w_{3,3}$
$f_{4,1} = (E/1,156)(25w_{1,1}w_{3,2}\ 49w_{1,2}w_{3,1} + 81w_{1,2}w_{3,3} + 121w_{1,3}w_{3,2})$
$f_{4,2} = (E/400)(-w_{1,1}w_{3,1} + 9w_{1,1}w_{3,3} + 25w_{1,3}w_{3,1})$
$f_{4,3} = (E/2,500)(-w_{1,1}w_{3,2} - 25w_{1,2}w_{3,1})$
$f_{4,4} = (E/256)(-w_{1,2}w_{3,2} - 4w_{1,3}w_{3,1})$
$f_{4,5} = (E/6,724)(-9w_{1,2}w_{3,3} - 49w_{1,3}w_{3,2})$
$f_{4,6} = (E/2,704)(-9w_{1,3}w_{3,3})$
$f_{6,0} = (E/288)(w_{3,1}^2 + 4w_{3,2}^2 + 9w_{3,3}^2)$
$f_{6,1} = (E/5,476)(81w_{3,1}w_{3,2} + 225w_{3,2}w_{3,3})$
$f_{6,2} = (E/1,600)(36w_{3,1}w_{3,3})$
$f_{6,3} = (E/900)(-w_{3,1}w_{3,2})$
$f_{6,4} = (E/2,704)(-9w_{3,1}w_{3,3})$
$f_{6,6} = (E/3,721)(-9w_{3,2}w_{3,3})$

Substituting Eqs. (10), (13), and (17) simultaneously into the lateral equilibrium Eq. (2) and equating coefficients of like trigonometric terms on the two sides of the equation results in the relation given by

$$p_{m,n} = Dw_{m,n}\pi^4\left(\frac{m^2}{a^2}+\frac{n^2}{a^2}\right) - \bar{\sigma}_x h w_{m,n}\frac{m^2\pi^2}{a^2} - \bar{\sigma}_y h w_{m,n}\frac{n^2\pi^2}{a^2} + \frac{h\pi^4}{4a^4}\sum d_{r,s,p,q} f_{r,s} w_{p,q} \tag{18}$$

where (1) the summation includes all products $f_{r,s}w_{p,q}$ for which m is equal to either the sum or difference of r and p, and for which n is equal to either the sum or difference of s and q; and (2) the coefficients $d_{r,s,p,q}$ are given by

$$d_{r,s,p,q} = \pm(rq \pm sp)^2 \text{ if } r \neq 0,\ s \neq 0 \tag{18a}$$

and are twice this value if either r or s is zero. The signs in Eq. (18a) are determined by the following rules:

The first sign is positive if either $r - p = m$ or if $s - q = n$ but not if both conditions are true. It is negative in all other cases.

The second sign is positive if m is the sum of r and p and n is the difference of s and q; or if m is the difference of r and p and n is the sum of s and q. It is negative otherwise.

The boundary condition for straight edges, Eqs. (8), can be shown to be satisfied by the chosen expressions for F and w by substituting Eqs. (10) and (16) into Eqs. (8) and performing the indicated differentiation and integration. After simplification, requiring the use of Eq. (17), it is found that the edges $x = 0$ and $x = a$ separate by an amount

$$a\bar{\epsilon}_x = -\frac{\bar{\sigma}_x a}{E} + \mu\frac{\bar{\sigma}_y a}{E} - \frac{\pi^2}{8a}\sum_{m=1}^{\infty}\sum_{n=1}^{\infty} m^2 w_{m,n}^2 \tag{19a}$$

while the edges $y = 0$ and $y = a$ separate by an amount

$$a\bar{\epsilon}_y = -\frac{\bar{\sigma}_y a}{E} + \mu\frac{\bar{\sigma}_x a}{E} - \frac{\pi^2}{8a}\sum_{m=1}^{\infty}\sum_{n=1}^{\infty} n^2 w_{m,n}^2 \tag{19b}$$

Since the right-hand sides of Eqs. (19a) and (19b) are independent of x and y, the boundary conditions for straight edges are satisfied.

Equations (15), (17), and (18) each represent infinite sets of equations. An exact solution for this problem should satisfy all of these equations. A good approximate solution can, however, be obtained by assuming that only a limited number of $w_{m,n}$ coefficients differ from zero and that, of these, only a few will have large enough values so that they cannot be neglected where third-order terms appear.

The values of $f_{m,n}$ in Eq. (17) for these coefficients are listed in Table 1.

Eq. (18) represents a doubly infinite family of equations. In each of the equations of the family, the coefficients $f_{r,s}$ may be replaced by their values listed in Table 1.

The resulting equations will involve the unknown normal pressure coefficients, $p_{m,n}$, the cubes of the deflection coefficients, $w_{m,n}$, and the known average edge compressive stresses, $\bar{\sigma}_x$ and $\bar{\sigma}_y$. For this problem $\bar{\sigma}_y$ is equal to zero. The number of these equations is equal to the number of unknown deflection coefficients $w_{m,n}$ and is consequently six.

By utilizing Eq. (14), the six unknown pressure coefficients, $p_{m,n}$, can be replaced by two moment coefficients, k_1 and k_3.

These six equations are solved for the linear-deflection term in terms of the remaining terms and the values used for the first three terms in the summations of the two of Eqs. (15) obtained by taking $m = 1$ and $m = 3$ (the remaining deflection coefficients being taken as zero). The two cubic equations listed in Table 3 result. Thus, there are eight simultaneous cubic equations with eight unknowns. A direct solution is virtually impossible so that iterative methods must be employed.

It will be noted that the equations in Tables 2 and 3 are cubics, and their solution therefore gives three values for each of the deflection coefficients, $w_{m,n}$. Some of these values correspond to stable equilibrium, whereas the remaining values are either imaginary or correspond to unstable equilibrium. Fortunately, if the equations in Tables 2 and 3 are solved by a method of successive approximations, the successive approximations approach values corresponding to stable equilibrium.

The final solution for the deflection coefficients and edge moment coefficients are shown in Table 4.

With the values of the deflection coefficients known, the horizontal unit plate shortening may be calculated from Eq. (19a). The variation of the horizontal unit plate shortening with the average edge compressive stress is represented in Fig. 3.

The effective width of plate, defined by

$$a_e = [(\bar{\sigma}_x/\sigma_{cr,x})/(\bar{\epsilon}_x/\epsilon_{cr,x})]a \tag{20}$$

TABLE 2

	0 =	0 =	0 =	0 =	0 =	0 =
$a^4\pi^4Eh^4$	$-k_1$	$2k_1$	$-3k_1$	$-k_3$	$2k_3$	$-3k_3$
1	$0.3703W_{1,1}$	$2.3145W_{1,2}$	$9.2578W_{1,3}$	$9.2578W_{3,1}$	$15.6457W_{3,2}$	$29.9953W_{3,3}$
$\bar{\sigma}_x a^2/Eh^2$	$-0.1013W_{1,1}$	$-0.1013W_{1,2}$	$-0.1013W_{1,3}$	$-0.9119W_{3,1}$	$-0.9119W_{3,2}$	$-0.9119W_{3,3}$
$W_{1,1}^3$	0.0626	0	−0.0313	−0.0313	0	0
$W_{1,1}^2W_{1,2}$	0	0.4531	0	0	−0.2823	0
$W_{1,1}^2W_{1,3}$	−0.0312	0	0.6591	0.2500	0	−0.3042
$W_{1,1}^2W_{3,1}$	−0.0938	0	0.2500	0.9091	0	−0.3042
$W_{1,1}W_{1,2}^2$	0.4529	0	0.6562	−0.7059	0	−0.2025
$W_{1,1}W_{1,3}^2$	0.6587	0	0	−1.3438	0	0
$W_{1,1}W_{1,2}W_{1,3}$	0	1.3124	0	0	−1.2050	0
$W_{1,1}W_{3,1}^2$	0.6587	0	−1.3438	0	0	0
$W_{1,1}W_{1,2}W_{3,1}$	0	−1.1615	0	0.0625	2.3457	0
$W_{1,2}^3$	0	0.5312	0	0	−1	0
$W_{1,2}^2W_{1,2}$	0.6562	0	2.8126	−1.5625	0	−1.6936
$W_{1,2}W_{1,3}^2$	0	2.8126	0	0	−5.3220	0
$W_{1,3}^3$	0	0	2.5632	0	0	−2.5317
$W_{1,2}^2W_{3,1}$	−0.7056	0	0	2.9700	0	1.7019
$W_{3,1}^3$	0	0	0	2.5632	0	−2.5317
$W_{1,3}^2W_{3,1}$	−1.3438	0	0	7.3746	0	0
$W_{1,2}W_{3,1}^2$	0	3.0325	0	0	0	0
$W_{1,3}W_{3,1}^2$	−1.3438	0	7.3746	0	0	0
$W_{1,2}W_{1,3}W_{3,1}$	0	−3.1250	0	0	5.4075	0
$W_{1,1}^2W_{3,2}$	0	−0.1570	0	0	0.3689	0
$W_{1,1}^2W_{3,3}$	0	0	−0.3042	−0.3042	0	0.4050
$W_{1,1}W_{1,2}W_{3,2}$	−0.3136	0	−1.2050	2.1585	0	1.3824
$W_{1,1}W_{1,2}W_{3,3}$	0	−0.4050	0	0	1.3831	0
$W_{1,1}W_{1,3}W_{3,1}$	0.5000	0	−2.6875	−2.6875	0	3.3732
$W_{1,1}W_{1,3}W_{3,2}$	0	−1.2050	0	0	2.1144	0
$W_{1,1}W_{1,3}W_{3,3}$	−0.6075	0	0	3.3740	0	0
$W_{1,1}W_{3,1}W_{3,2}$	0	3.4075	0	0	0	0
$W_{1,1}W_{3,1}W_{3,3}$	−0.6075	0	3.3740	0	0	0
$W_{1,1}W_{3,2}^2$	0.3689	0	1.0571	0	0	0
$W_{1,1}W_{3,3}^2$	0.4050	0	0	0	0	0
$W_{1,1}W_{3,2}W_{3,3}$	0	1.3824	0	0	0	0
$W_{1,2}^2W_{3,2}$	0	−1.5000	0	0	3.9364	0
$W_{1,2}^2W_{3,3}$	−0.2025	0	−1.6935	−1.7020	0	2.1130
$W_{1,2}^2W_{3,2}$	0	−4.1967	0	0	10.3481	0
$W_{1,3}^2W_{3,3}$	0	0	−7.5942	0	0	11.2473
$W_{1,2}W_{1,3}W_{3,2}$	−1.2050	0	−8.3931	5.9700	0	9.5931
$W_{1,2}W_{1,3}W_{3,3}$	0	−3.3871	0	0	11.8426	0
$W_{1,2}W_{3,1}W_{3,2}$	2.4081	0	5.9700	0	0	0
$W_{1,2}W_{3,2}W_{3,3}$	0	3.4047	0	0	0	
$W_{1,3}W_{3,1}W_{3,2}$	0	5.9700	0	0	0	0
$W_{1,3}W_{3,1}W_{3,3}$	4.4364	0	0	0	0	0
$W_{3,1}^2W_{3,2}$	0	0	0	0	5.4907	0
$W_{1,2}W_{3,2}^2$	0	1.9368	0	0	0	0
$W_{1,2}W_{3,3}^2$	0	2.1130	0	0	0	0
$W_{1,3}W_{3,2}^2$	1.0581	0	10.3481	0	0	0
$W_{1,3}W_{3,3}^2$	0	0	11.2455	0	0	0
$W_{1,2}W_{3,2}W_{3,3}$	1.3831	0	8.8640	0	0	0
$W_{1,3}W_{3,2}W_{3,3}$	0	9.5927	0	0	0	0
$W_{3,1}W_{3,2}^2$	0	0	0	5.7223	0	8.4258
$W_{3,1}W_{3,3}^2$	0	0	0	11.2455	0	0
$W_{3,1}W_{3,2}W_{3,3}$	0	0	0	0	11.7889	0
$W_{3,2}^3$	0	0	0	0	3.0312	0
$W_{3,2}^2W_{3,3}$	0	0	0	8.4256	0	13.5641
$W_{3,2}W_{3,3}^2$	0	0	0	0	13.5650	0
$W_{3,3}^3$	0	0	0	0	0	5.0706

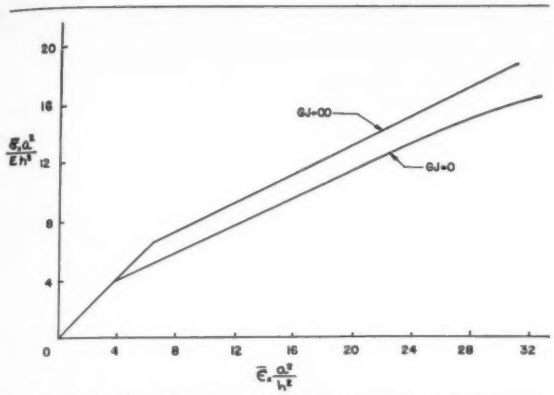

FIG. 3. Variation of horizontal unit plate shortening with average edge compressive stress.

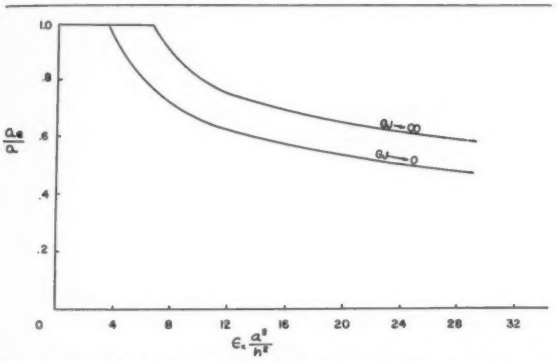

FIG. 4. Variation of effective width ratio with horizontal unit plate shortening.

is plotted against horizontal unit plate shortening in Fig. 4.

The error resulting from the omission of more deflection terms in the solution can be judged to some extent by comparison of the critical stress constant $\bar{\sigma}_x a^2/Eh^2 = 6.45$, Table 4, with the value 5.24 of the same constant computed from the tables in reference 6 for a square plate having one edge parallel to the load clamped and the other edges simply supported. Since the results given in reference 6 correspond to an exact solution of the differential equations in the small deflection range that governs buckling, the difference is a measure of the error in the present solution. It is estimated that the error in the large deflection range is slightly larger than this, since the relative magnitude of higher modes (subscript 3) increases slowly with load.

TABLE 3

	0 =	0 =
$a^4/\pi^4 Eh^4$	$5.4009k_1$	$0.6637k_3$
$\bar{\sigma}_x a^2/Eh^2$	$0.2736W_{1,1}$	$0.0985W_{3,1}$
$\bar{\sigma}_x a^2/Eh^2$	$-0.0875W_{1,2}$	$-0.1166W_{3,2}$
$\bar{\sigma}_x a^2/Eh^2$	$0.0328W_{1,3}$	$0.0912W_{3,3}$
$W_{1,1}{}^3$	−0.1590	0.0034
$W_{1,1}{}^2W_{1,2}$	0.3915	−0.0361
$W_{1,1}{}^2W_{1,3}$	−0.1293	0.0034
$W_{1,1}{}^2W_{3,1}$	0.1723	−0.0678
$W_{1,1}W_{1,2}{}^2$	−1.4357	0.0965
$W_{1,1}W_{1,3}{}^2$	−1.7788	0.1452
$W_{1,1}W_{1,2}W_{1,3}$	1.1340	−0.1540
$W_{1,1}W_{3,1}{}^2$	−1.3433	0
$W_{1,1}W_{1,2}W_{3,1}$	−1.0036	0.2931
$W_{1,2}{}^3$	0.4590	−0.1278
$W_{1,2}{}^2W_{1,3}$	−2.6835	0.3382
$W_{1,2}W_{1,3}{}^2$	2.4305	−0.6803
$W_{1,3}{}^3$	−0.8306	0.2532
$W_{3,1}{}^3$	0	−0.0237
$W_{1,2}{}^2W_{3,1}$	3.6289	−0.7966
$W_{1,2}W_{3,1}{}^2$	2.6203	0
$W_{1,3}W_{3,1}{}^2$	1.2391	0
$W_{1,2}W_{1,3}W_{3,1}$	−2.7003	0.6912
$W_{1,1}{}^2W_{3,2}$	−0.1357	0.0472
$W_{1,1}{}^2W_{3,3}$	0.0986	−0.0076
$W_{1,2}{}^2W_{3,1}$	1.9055	−0.4910
$W_{1,1}W_{1,2}W_{3,2}$	1.2374	−0.3714
$W_{1,1}W_{1,2}W_{3,3}$	−0.3500	0.1768
$W_{1,1}W_{1,3}W_{3,1}$	−0.4713	−0.0471
$W_{1,1}W_{1,3}W_{3,2}$	−1.0412	0.2703
$W_{1,1}W_{1,3}W_{3,3}$	1.6406	−0.3644
$W_{1,1}W_{3,1}W_{3,2}$	2.9444	0
$W_{1,1}W_{3,1}W_{3,3}$	0.5472	0
$W_{1,1}W_{3,2}{}^2$	−1.3388	0
$W_{1,1}W_{3,3}{}^2$	−1.0937	0
$W_{1,1}W_{3,2}W_{3,3}$	1.1945	0
$W_{1,2}{}^2W_{3,2}$	−1.2961	0.5032
$W_{1,2}{}^2W_{3,3}$	1.0957	−0.3951
$W_{1,3}{}^2W_{3,2}$	−3.6263	1.3228
$W_{1,3}{}^2W_{3,1}$	2.4609	−1.1249
$W_{1,2}W_{1,3}W_{3,2}$	5.9739	−1.6044
$W_{1,2}W_{1,3}W_{3,3}$	−2.9267	1.5138
$W_{1,2}W_{3,1}W_{3,2}$	−8.4377	0
$W_{1,2}W_{3,1}W_{3,3}$	2.9419	0
$W_{1,3}W_{3,1}W_{3,2}$	5.1586	0
$W_{1,3}W_{3,1}W_{3,3}$	−11.9806	0
$W_{3,1}{}^2W_{3,2}$	0	0.7019
$W_{3,1}{}^2W_{3,3}$	0	−0.3046
$W_{1,2}W_{3,2}{}^2$	1.6736	0
$W_{1,2}W_{3,3}{}^2$	1.8258	0
$W_{1,2}W_{3,2}{}^2$	−6.2107	0
$W_{1,2}W_{3,2}W_{3,3}$	−6.6075	0
$W_{1,3}W_{3,2}W_{3,3}$	8.2889	0
$W_{3,1}W_{3,2}{}^2$	0	−1.4608
$W_{3,1}W_{3,3}{}^2$	0	−1.2147
$W_{3,1}W_{3,2}W_{3,3}$	0	1.5070
$W_{3,2}{}^3$	0	0.3875
$W_{3,2}{}^2W_{3,3}$	0	−2.2667
$W_{3,2}W_{3,3}{}^2$	0	1.7340
$W_{3,3}{}^3$	0	−0.5071

TABLE 4

$\bar{\sigma}_x a^2/Eh^2$	$W_{1,1}$	$W_{1,2}$	$W_{1,3}$	$W_{3,1}$	$W_{3,2}$	$W_{3,3}$	k_1	k_3
6.450	0	0	0	0	0	0	0	0
6.556	0.1	0.0350	−0.0100	0	0	0	−0.0290	0
6.869	0.5	0.1732	−0.0512	0.0042	0.0020	−0.0005	−0.1485	−0.0027
7.916	1.0	0.3386	−0.0179	0.0315	0.0128	−0.0024	−0.3207	−0.0122
9.451	1.5	0.4919	−0.1721	0.0866	0.0351	−0.0053	−0.5303	−0.0300
11.526	2.0	0.6312	−0.2457	0.1588	0.0693	−0.0064	−0.7984	−0.0454
14.162	2.5	0.7554	−0.3293	0.2407	0.1175	−0.0022	−1.1449	−0.0586
17.464	3.0	0.8620	−0.4258	0.3230	0.1842	+0.0136	−1.6108	−0.0464

Conclusions

The outstanding advantage resulting from the use of a stiffener of high torsional rigidity with respect to the plate as illustrated in Fig. 3 is the substantial increase in the critical stress constant, $\bar{\sigma}_x a^2/Eh^2$, from the value of 3.66 to 6.45. In this manner, a reduction of about 33 per cent in plate area is possible for constant thickness plates having a stiffener of high torsional rigidity in preference to plates having a stiffener of low torsional rigidity.

Figs. 3 and 4 show a reduction of unit plate shortening of about 25 per cent and an increase of effective plate width of about 20 per cent for the plate containing a torsionally rigid stiffener.

The quantitative value of the results is limited by the number of terms used in the determination of the deflection patterns. With the use of six deflection coefficients, a reasonably close approximation of the deflection patterns is attained. In both cases, the $w_{1,1}$ coefficients are far greater numerically than any of the other coefficients.

The nonlinear character of plate problems makes possible, under certain conditions, more than one stable solution. In this paper, only one real root for each deflection coefficient resulted from the solution of the cubic equations. However, if a lateral pressure existed in the conjunction with the edge load, a load might be reached where one stable deflection configuration "oil-cans" into another stable configuration. This stability problem might well be treated in some future work.

References

[1] von Kármán, Th., *Festigkeitsprobleme im Maschinenbau*, Encyk. der Math. Wiss., Vol. IV, p. 349, 1910.

[2] Levy, S., *Bending of Rectangular Plates with Large Deflections*, N.A.C.A. T.R. No. 737, 1942.

[3] Timoshenko, S., *Theory of Elastic Stability*, pp. 322–323; McGraw-Hill Book Company, Inc., 1936.

[4] Levy, S., *Large Deflection of Rectangular Plates*, Proc. of Symposia in Applied Math., Vol. I, p. 179, 1949.

[5] Levy, S., *Square Plate with Clamped Edges under Normal Pressures Producing Large Deflections*, N.A.C.A. T.R. No. 740, 1942.

[6] Kroll, W. D., *Tables of Stiffness and Carry Over Factor for Flat Rectangular Plates under Compression*, N.A.C.A., A.R.R. No. 3K27, 1943.

Changes of Address

Since the Post Office Department does not as a rule forward magazines to forwarding addresses, it is important that the Institute be notified of changes in address 30 days in advance of publishing date to ensure receipt of every issue of the JOURNAL and REVIEW.

Notices should be printed legibly and sent directly to.

Institute of the Aeronautical Sciences, Inc.

2 East 64th Street, New York 21, New York

Boundary-Layer Stability and Transition in Subsonic and Supersonic Flow

*A Review of Available Information with New Data in the Supersonic Range**

CARL GAZLEY, JR.†

General Electric Company

SUMMARY

Accurate prediction of the aerodynamic characteristics of a body at high flight speeds requires knowledge of the characteristics of the existing boundary layer. Although the effects of compressibility on the characteristics of both laminar and turbulent boundary layers are known rather well, little information has been available as to how the transition between the two types of flow is affected by compressibility and other factors. Even in subsonic flow, the effects of such variables as free-stream turbulence, surface curvature, pressure gradient, surface roughness, and surface temperature are known only qualitatively.

While the theory of laminar boundary-layer stability yields the conditions necessary for instability, it does not permit prediction of the transition point. This theory is, however, useful in indicating possible effects of the several variables on transition. It has recently been extended to compressible flows with heat transfer and with pressure gradient.

This paper presents the available data in subsonic and supersonic flow for the effects of free-stream turbulence, surface curvature, pressure gradient, surface roughness, surface temperature, and Mach Number on the transition position. New supersonic data are included from rocket flights, firing-range tests, and wind-tunnel tests. The effects of the several variables on transition are compared with the theoretically predicted effects on boundary-layer stability.

In general, the experimental data for transition confirm the trends indicated by the stability theory. Perhaps the most significant deviation from the trend expected from the stability theory is the relative insensitivity of supersonic transition to surface-temperature variation. The transition Reynolds Number range appears to increase with increasing Mach Number in both firing-range tests, where relatively low surface temperatures occur, and in wind-tunnel tests, where relatively high surface temperatures occur.

NOMENCLATURE

B = width of roughness element in flow direction
k = height of roughness element above surface
f_1 = function of
f_2 = function of
l = characteristic dimension of turbulence-producing device
M = Mach Number
p = pressure
R = Reynolds Number
T = absolute temperature
u = velocity in x-direction (time average)
u' = fluctuating component of u
u_* = friction velocity, $\sqrt{\tau_w/\rho}$
x = distance in flow direction from leading edge or nose apex
θ = boundary-layer momentum thickness
λ = Pohlhausen (or Weil) parameter
μ = absolute viscosity of fluid
ν = kinematic viscosity of fluid
ρ = fluid density
τ = shearing stress

Subscripts

aw = adiabatic-wall condition
r = roughness element position
t = transition position
w = wall condition
x = based on x
θ = based on θ
1 = condition just outside boundary layer
∞ = free-stream condition

INTRODUCTION

THE POSITION OF BOUNDARY-LAYER TRANSITION is one of the factors necessary for the prediction of aerodynamic performance in high-speed flight. This is apparent when one considers that the condition of the boundary layer (i.e., whether laminar, turbulent, or separated) determines the skin-friction drag, the base-pressure drag, the form drag of the afterbody, and the effectiveness of control surfaces that are partially immersed in the body boundary layer. The effects of the boundary layer on the various types of "pressure" drags and control-surface effectiveness become more important as the flight speed increases. This is due to the fact that boundary-layer thickness increases with Mach Number (at constant Reynolds Number).

When the present investigation was initiated about 2 years ago, there was little quantitative information available regarding the effects of various quantities on boundary-layer transition, especially in supersonic flow. Researches in subsonic flow had shown that the transition Reynolds Number is affected by surface temperature, surface roughness, pressure gradient, surface curvature, and free-stream turbulence. Investigations in transonic flow indicated that shock-wave-boundary-layer interaction also influences transition. However,

Received May 21, 1952.

* This investigation was made as a part of Army Ordnance Contract No. DA-30-115-ORD-23.

† Development Engineer, General Engineering Laboratory, Schenectady, N.Y. Now with The RAND Corporation, Santa Monica, Calif.

only the qualitative effects of these variables were known; little quantitative information was available about the effect of these variables, either singly or interrelated. Quantitative information about boundary-layer stability resulted from the theories of Tollmien[1] and Schlichting[2] and was confirmed by the experiments of Schubauer and Skramstad.[3] However, this theory and its extensions only yield the Reynolds Number above which disturbances can be amplified in the boundary layer and does not give the Reynolds Number where the disturbances have been sufficiently amplified to cause turbulence. The theories are practically useful, however, for indicating possible qualitative effects of various quantities on transition.

Because of the many factors that affect boundary-layer transition, the experimental study of the effect of one of these variables on transition is difficult. For example, the effects of free-stream turbulence in wind-tunnel studies tend to mask out the effects of other variables. This is especially true of supersonic flow, since little is known about turbulence in supersonic flow or its effects; furthermore, the turbulence characteristics of most supersonic tunnels have not been determined. The desirable method of experiment is, of course, tests in flight; however, they are expensive and can be used only in cases where other methods are not possible. An attractive possibility appears to be the use of firing-range tests for transition study. There is no free-stream turbulence present, and it is possible to evaluate the transition position from spark shadowgraphs of the projectile in flight.

This paper presents the available data in subsonic and supersonic flow for the effects of free-stream turbulence, surface curvature, pressure gradient, surface roughness, surface temperature, and Mach Number. New supersonic data are included from rocket flights, firing-range tests, and wind-tunnel tests. The effects of the several variables on transition are compared with the theoretically predicted effects on boundary-layer stability.

Theory of Laminar Boundary-Layer Stability

The theory of the stability of laminar flows was first formulated mathematically by Rayleigh.[4] Successful solutions for the laminar boundary layer on a flat plate were obtained by Tollmien[1] and by Schlichting.[2] The results of this theory indicate that instability in the laminar boundary layer originates in small disturbances that are either damped or amplified depending on their frequency and the Reynolds Number. This selective amplification is predicted only if the Reynolds Number is greater than a certain value, called the "minimum critical Reynolds Number." This Reynolds Number is, of course, somewhat smaller than the transition Reynolds Number, since the regular disturbances in the laminar boundary layer must be amplified to a magnitude sufficient to produce the irregular oscillations characteristic of turbulence. For several years, no experimental evidence was found of the laminar boundary-layer oscillations predicted by the Tollmien-Schlichting theory.

In 1935, a somewhat different theoretical approach was suggested by Taylor.[5] The theory of Taylor, originally thought to be in opposition to that of Tollmien and Schlichting, involves the supposition that turbulence in the free stream outside the boundary layer imposes local adverse pressure gradients on the laminar boundary layer. These local adverse gradients are thought to cause local boundary-layer separation with subsequent transition.

The apparent difference between these two theories was finally resolved by the experimental studies of Schubauer and Skramstad,[3] at the National Bureau of Standards. In connection with a study of wind-tunnel turbulence, these investigators observed the regular laminar boundary-layer oscillations predicted by Tollmien and Schlichting in a wind tunnel having an exceptionally low turbulence level. The predicted ranges of damping and amplification were closely confirmed. It was found that the oscillations and their damping or amplification to eventual turbulence could be detected only when the magnitude of the free-stream turbulent fluctuations is less than about 0.001 of the mean velocity. For larger magnitudes of the free-stream turbulence, the boundary-layer oscillations are difficult to identify because of the near coincidence of their appearance and the point of transition to turbulence.

With the aid of the Schubauer-Skramstad experiments, the Tollmien-Schlichting theory and the Taylor theory can be reconciled, and a unified picture of the mechanism leading to transition in the boundary layer can be obtained. In the case of low free-stream turbulence ($u'/u_1 < 0.001$), any small disturbances that are initially present may be due to either internal or external disturbances such as surface roughness, vibration, noise, or free-stream turbulence. The amplified oscillations cannot be classified as turbulence because of their regularity; it is only when these oscillations or waves become large enough to roll up into eddies that turbulence is initiated. The eddies, formed close to the solid surface, break away and dissipate in an irregular turbulent motion. The process is well illustrated in the interferometer photographs of Eckert[6] and is somewhat analogous to the growth and breaking of waves on an air-water interface. In case of a high free-stream turbulence level ($u'/u_1 > 0.001$), the free-stream fluctuations are large enough to produce local adverse pressure gradients that cause local separation with subsequent transition in the manner described by Taylor's theory.

Since the Tollmien-Schlichting oscillations have been confirmed experimentally, revisions and extensions of the theory have appeared. Lin[7] has made some revisions and mathematical clarifications. Schlichting and Ulrich[8] and Hahneman, Freeman, and Finston[9] ex-

tended the theory to flows with pressure gradient and found that a positive pressure gradient destabilized, and a negative pressure gradient stabilized, the boundary layer. The minimum critical Reynolds Number is shown in Fig. 3 as a function of the pressure-gradient parameter. Lees and Lin[10, 11] and Van Driest[12] have studied flat-plate compressible flows with heat transfer. Weil[13] studied the effect of pressure gradient in compressible flow.

While the theories of the Tollmien-Schlichting type permit prediction of the effect of various factors on laminar boundary-layer stability and prediction of the Reynolds Number below which disturbances are not amplified, they give no indication of the transition Reynolds Number. Presumably, the original small disturbances must be amplified to the point where they become unstable. While the theory permits calculation of the initial amplification rate, it is applicable only when the disturbances are infinitely small. That this amplification takes considerable time and distance is exemplified by a comparison of the minimum critical Reynolds Number with the transition Reynolds Number. For incompressible flow along a flat plate, the minimum critical Reynolds number is calculated as 60,000; this figure was confirmed by Schubauer and Skramstad,[3] who also found the Reynolds Number range of the transition region to be 2,800,000 to 3,900,000. For this case, then, there is about a sixty-fold difference between the Reynolds Numbers at which amplification begins and at which turbulence begins.

Liepmann[14] has made an interesting attempt to compute the transition Reynolds Number using the maximum initial rates of amplification given by the Tollmien-Schlichting theory. He estimates that transition to turbulence will begin when the apparent shear stress of the amplified disturbances becomes equal to existing laminar shear stress. The resulting relationship gives the transition Reynolds Number as a function of the magnitude of the initial disturbance having the frequency of maximum amplification. However, this latter quantity is dependent on the magnitude and frequency of the free-stream turbulence, of the surface roughness, and/or of noise and vibration; the quantitative dependence of this factor on these variables is not known. Therefore, Liepmann's calculation cannot be compared directly with experiment; however, for reasonable values of the initial disturbances, the predicted ratio of transition Reynolds Number to minimum critical Reynolds Number is of the same order as that found experimentally.

Emmons[15] has recently evolved a theory of transition based on the idea that every point on a body is turbulent part of the time; the fraction of the time that a given spot is turbulent is derived from probability considerations. The results of this theory, while not enabling prediction of the absolute value of transition range of Reynolds Numbers, give the variation of skin friction or heat-transfer rate in the transition region and the effect of flow geometry (flat plate, cone, swept wing) on the transition.

Experimental Studies of the Effects of Various Factors on Transition

Because of the importance of the position of transition to the practical aerodynamicist, many experimental determinations have been made of the effects of various factors on transition, and many experimental techniques have been devised to detect transition. Most of the available experimental data are in the low subsonic-flow range but are useful for giving an insight into the effects of such factors as pressure gradient, free-stream turbulence, surface roughness, etc. While these data enable qualitative knowledge of the effect of a given variable upon transition, they do not usually allow a quantitative correlation. This is generally due to the fact that other variables, also affecting transition, were not controlled or measured during the experiments. Thus it is frequently necessary to compare data taken under different conditions, although in recent years the appreciation of the sensitivity of transition to a great variety of factors has yielded several valuable studies in which extraneous factors have been carefully controlled. Notable among these are the investigations of Liepmann, at the California Institute of Technology,[14, 16] and Dryden and coworkers, at the National Bureau of Standards.[3] These investigators carefully controlled the free-stream turbulence, pressure gradient, and surface condition and used a hot-wire anemometer to detect transition. This is probably the most sensitive technique used for detecting the progress of transition. Other techniques involve the difference in velocity distribution, skin friction, transfer rates, or temperature recovery factor in the laminar and turbulent boundary layers.

Free-Stream Turbulence.—As noted above, Taylor[5] has developed a theory for the effect of free-stream turbulence on transition. The result of this theory indicated that the transition Reynolds Number is a function of the intensity and scale of the free-stream turbulence:

$$R_{xt} = f_1\,[(u'/u_1)(x/l)^{1/5}] \qquad (1)$$

where

- u' = free-stream velocity fluctuation
- u_1 = free-stream velocity
- x = distance downstream from turbulence-producing device
- l = characteristic dimension of turbulence-producing device

This relationship was confirmed experimentally for transition on spheres at the National Bureau of Standards.[17] Recent studies of turbulence characteristics[18] have indicated that the intensity and scale of iso-

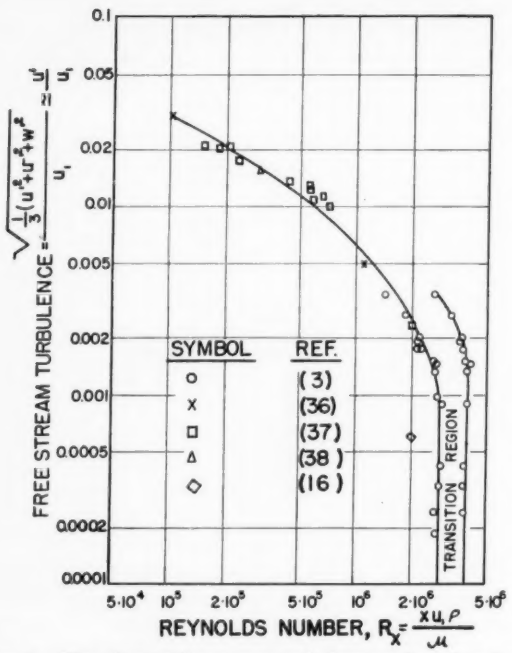

FIG. 1. The effect of free-stream turbulence on boundary-layer transition in subsonic flow.

tropic turbulence can be related approximately as

$$x/l \simeq u_1/u' \tag{2}$$

Thus Eq. (1) may be simplified to

$$R_{xt} = f_2\,(u'/u_1) \tag{3}$$

Of course, these relationships would be expected to hold only under conditions where the scale of the turbulence is of the same order of magnitude as the boundary-layer thickness. For example, atmospheric turbulence is presumably of such a large scale that it would have only a negligible effect on transition.

The available data for the change in transition Reynolds Number with free-stream turbulence intensity are shown in Fig. 1 for the case of subsonic flow over smooth flat plates aligned with the stream. It is seen that the general form of Eq. (3) is confirmed and that the variation of free-stream turbulence can change the transition Reynolds Number by as much as thirtyfold. It is interesting to note that even the higher levels of free-stream turbulence (fluctuations of about 3 per cent of the mean velocity) do not produce transition Reynolds Numbers below the minimum critical value calculated by Lin.[7]

Surface Curvature.—The effect of surface curvature on flow stability has been analyzed by many investigators. Qualitative considerations by Rayleigh[4] and Prandtl[19] indicate that flow along a concave wall is less stable than flow along a convex wall. Quantitative studies by Schlichting[20] and Görtler[21] of two-dimensional disturbances indicate the opposite. Recent studies by Taylor[22] and Görtler[23] of three-dimensional disturbances indicate that flow along a concave wall is less stable than flow along flat or convex walls.

The effects of surface curvature on boundary-layer transition observed by Liepmann[14] confirm approximately the theory of Görtler[23]—i.e., that the boundary-layer stability is dependent on the value of the parameter $R_\theta\sqrt{\theta/r}$ which, for zero pressure gradient, is proportional to $R_x^{1/4}\sqrt{x/r}$. The experimental transition Reynolds Numbers observed by Liepmann, for zero pressure gradient, are shown in Fig. 2 in comparison with lines of constant Görtler parameter. The data for low turbulence levels ($u'/u_1 = 0.0006$, 0.002) give a Görtler parameter of about 9.0 and for a higher turbulence level a value of about 5.5. The effects of curvature in the region of convex curvature seem to be negligible, as Görtler's theory indicates.

Pressure Gradient.—The effects of pressure gradient on laminar boundary-layer stability have been computed by Schlichting and Ulrich[8] and Hahneman, et al.,[9] for incompressible flow and by Weil[13] for compressible flow. The results of these calculations, shown in Fig. 3,† indicate that a negative pressure gradient tends to stabilize the boundary layer while a positive gradient has the opposite effect. The predicted effect of pressure gradient is greatest at a Mach Number of 1.5 and is al-

† These results are shown in terms of the momentum-thickness Reynolds Number, since the x Reynolds Number is without significance in flows with pressure gradient.

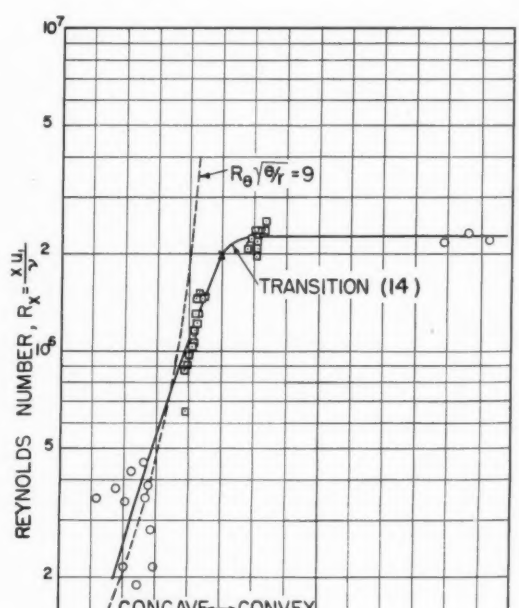

FIG. 2. The effect of surface curvature on boundary-layer transition in subsonic flow. Data of Liepmann[14] for $dp/dx = 0$ and $u'/u_1 = 0.0006$.

most negligible at a Mach Number of 4. General experience in subsonic flow confirms qualitatively the effects predicted theoretically—e.g., transition frequently occurs shortly after the minimum pressure point on an airfoil. Furthermore, the experiments of Schubauer and Skramstad[3] confirmed qualitatively the predicted effects of pressure gradient on the damping or amplification of laminar boundary-layer oscillations. However, only one set of systematic experiments for the effects of pressure gradient on transition is known (those of Liepmann[14]), and none is known in compressible flow. The results of Liepmann, also shown in Fig. 3, follow the same trend as that predicted by the theory. As is to be expected, the transition measured by Liepmann occurs at higher Reynolds Numbers than the theoretical minimum critical Reynolds Numbers.

Surface Roughness.—Both the surface finish and any single surface discontinuities are known to affect transition in the boundary layer. Small irregularities in the surface finish presumably contribute to the initiation of oscillations in the laminar boundary layer which are selectively amplified until transition occurs. However, no known quantitative information exists on the relationship between the scale and characteristics of a surface finish and the resulting boundary-layer oscillations. Larger single roughness elements may bring about an almost immediate transition if they are large enough to produce a turbulent wake. Considerable data exist for the effects of two-dimensional roughness elements on transition, such as wires and ridges, and a few data exist for three-dimensional elements, such as rivet heads. Most of the data lies in the subsonic-flow region, although a few data are becoming available in supersonic flow.

The available data for the effects of two-dimensional roughness elements cover a variety of shapes and sizes mounted on bodies of revolution, flat plates, and airfoils. Measurements have been made in a water tunnel,[24] several wind tunnels,[25] and in flight.[25] Fage and Preston[24] formulated an empirical criterion for the size of wire necessary to cause immediate transition—i.e., transition directly behind the wire. Tani, et al.,[26] proposed a somewhat similar correlation for the effect of a wire. Goldstein[27] proposed a similar criterion for the size of a surface wire which has no effect on the transition position. Fage[25] tested various types of two-dimensional elements and devised another empirical correlation for the effect of the roughness elements on the transition position. All of these correlations can be reduced to the form

$$R_{xt} = f(k^3/Bx_t) \tag{4}$$

where

R_{xt} = transition Reynolds Number
k = height of roughness element
B = width of roughness element
x_t = distance to transition point from leading edge

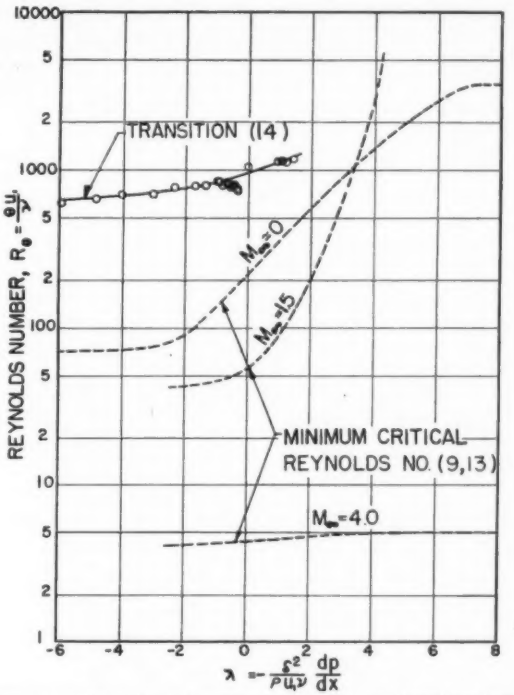

FIG. 3. The effect of pressure gradient on boundary-layer stability and transition. Transition data of Liepmann[14] for subsonic flow; stability calculations of Hahneman, et al.,[9] for incompressible flow and of Weil[13] for compressible flow over 5 per cent thick biconvex airfoil.

The available data for the effect of two-dimensional roughness elements on transition are shown in Fig. 4, together with the several proposed correlations. It is apparent that Fage and Preston's correlation for wires[24] fits the data well in the lower Reynolds Number range, while Fage's correlation for a variety of other shapes[25] follows the data at higher Reynolds Numbers. It is apparent that any general correlation should asymptotically approach the smooth-surface value of the transition Reynolds Number for extremely small roughness elements. None of the heretofore proposed correlations has this characteristic. A proposed correlation, covering the entire Reynolds Number range and approaching the smooth-surface transition Reynolds Number at small roughness values, is shown by the solid lines in Fig. 4. Admittedly, the degree of correlation is not too good but is perhaps as good as can be expected considering the variety of conditions under which the data were procured—i.e., with different body geometries, pressure gradients, and degrees of free-stream turbulence. Undoubtedly the effect of roughness is dependent on the free-stream turbulence. Most of the high Reynolds Number data shown in Fig. 4 was taken either in flight or in low turbulence-level tunnels; however, it may be seen from Fig. 1 that smooth-surface transition may occur at lower Reynolds Numbers if the free-stream turbulence is appreciable. Therefore, a variety of curves might be drawn for the roughness

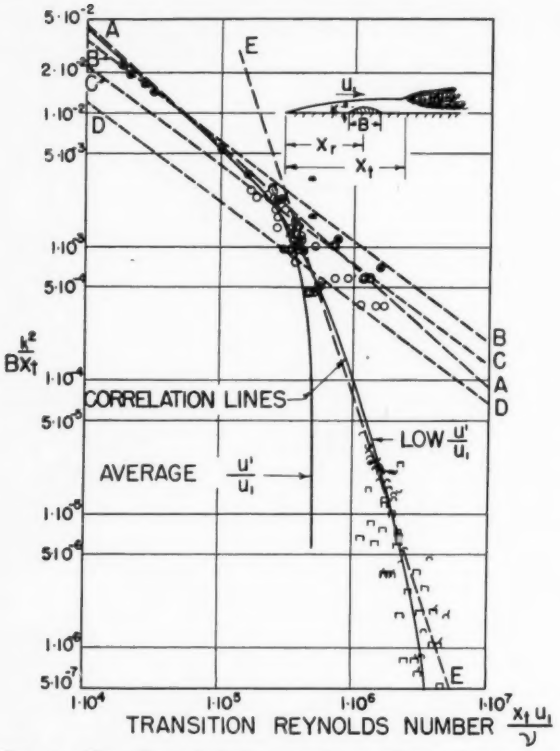

FIG. 4. The effect of single spanwise roughness elements on boundary-layer transition in subsonic flow.

Line A-A, limit of buffer layer in resulting turbulent boundary layer, $ku_{*\,(\text{turb.})}/\nu = 30$.

Line B-B, suggested correlation of Fage and Preston,[24] $ku_*/\nu = 20$.

Line C-C, suggested correlation of Tani, et al.,[26] $ku_*/\nu = 13$.

Line D-D, suggested correlation of Goldstein,[27] $ku_*/\nu = 7$.

Line E-E, suggested correlation of Fage.[25]

Symbol shapes denote roughness shapes: ○ = wire;[24–26] ⌒ = smooth bulge or half wire;[25, 27] ⌣ = smooth hollow;[25] — = flat ridge.[26] Solid points indicate $x_r = x_t$; flagged points indicate flight data.

correlation for various turbulence levels. Two are shown in Fig. 4, one for low turbulence and one for "average" turbulence.

The surprising fact deducible from this correlation is that the relative position of the roughness element does not affect the position of boundary-layer transition. Fage[25] indicates that such an effect does exist only when the roughness element is located at relatively small values of x. However, the inclusion of this factor into the correlation, as suggested by Fage, does not appreciably improve it. The apparent fact that transition is not appreciably affected by the relative location of the roughness element indicates that, as the roughness element is moved downstream, the decreasing disturbance due to the element and the increasing inherent instability of the laminar boundary layer are combined to produce a constant instability due to the roughness element. It may be noted that the critical size of roughness elements indicated in Fig. 4 is quite a different function of the Reynolds Number than is the boundary-layer thickness, the critical roughness size varying from the same order of magnitude to a small fraction of the boundary-layer thickness.

Data on the effects of three-dimensional roughness elements are rather meager; however, the data of Loftin[28] and of Williams and Brown[29] for rivets agree reasonably well with the correlation for two-dimensional elements when the rivet-head diameter is used for the factor B. A small amount of data for backward lapped joints[29] indicates that the joint has approximately the same effect as a wire whose diameter is one-half the joint height. The data of Holstein[30] for various grades of emery cloth on a flat plate correlate reasonably well in the form shown in Fig. 4 but lie somewhat below the line shown for two-dimensional elements, approaching Goldstein's line at low Reynolds Numbers. Unfortunately, Holstein's results appear to be affected by a variation of tunnel turbulence level occurring during a change in tunnel pressure level.

There is little information available about the effects of roughness in supersonic flow; a few data are shown in Fig. 5 and tend to confirm the trend indicated in

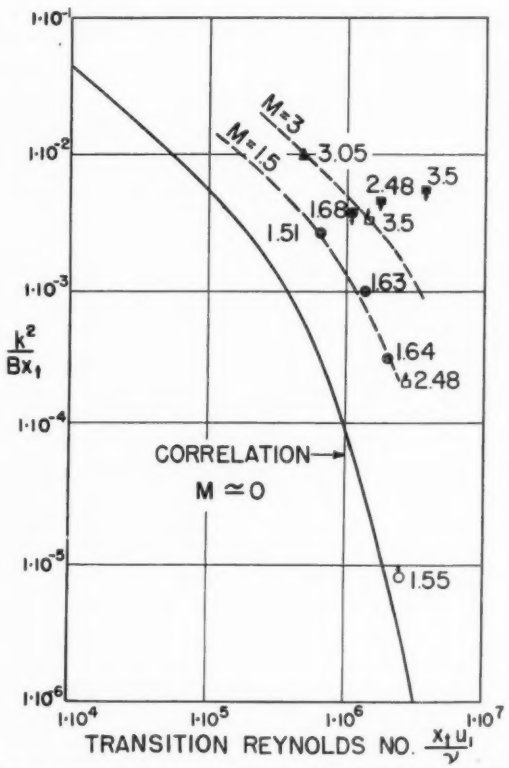

FIG. 5. The available data for the effect of roughness elements on boundary-layer transition in supersonic flow. Symbol shapes denote source of data: Δ = Station H of V-2 No. 27;[35] ○ = cone in Aberdeen Firing Range; □ missile model in wind tunnel. Shading of points indicate position of transition: open points denote no transition, shaded points denote transition downstream of roughness ($x_t > x_r$), and solid points denote transition at roughness ($x_t = x_r$). Arrows on open and solid points indicate probable position of a corresponding shaded point.

Fig. 4 with the Mach Number effect shown in Fig. 8 superimposed.

Surface Temperature.—The theory of boundary-layer stability[10–12] indicates that surface cooling has a stabilizing effect while surface heating has a destabilizing effect. The results of Van Driest's recent calculations[12] are shown in Fig. 6. It is apparent that the predicted effect of surface temperature is appreciable, although not so great as originally calculated by Lees.[11] The available experimental data[31–34] for the effect of surface temperature on transition are also shown in Fig. 6. While the observed effect of surface temperature on the transition Reynolds Number is seen to be qualitatively similar to the predicted effect on the minimum critical Reynolds Number, the quantitative effect is somewhat less. The data shown are internally consistent as far as the effects of surface temperature are concerned; however, the various sets of data are probably not comparable, since the turbulence level in the supersonic tunnels and its effect on transition are not known.

Compressibility.—The theoretical works of Lin and Lees[10, 11] and of Van Driest[12] for flat-plate flow indicate that the effects of both Mach Number and heat transfer on laminar boundary-layer stability are appreciable, as is indicated in Fig. 6. Van Driest's results (which are extensions and corrections to the earlier work of Lees) indicate that, between Mach Numbers of 1 and 9, the boundary layer may be completely stabilized by means of a considerable degree of cooling. Fig. 7 shows Van Driest's computed minimum critical Reynolds Number as a function of Mach Number and surface temperature. If the surface temperature is maintained in constant ratio to the free-stream temperatures, an increase in Mach Number is predicted to increase the stability of the boundary layer; if the surface temperature is maintained in constant ratio to the adiabatic-surface temperature, an increase in Mach Number is predicted to destabilize generally the boundary layer, except for the intermediate Mach Number range when $T_w < 3T_{aw}/4$, where complete stability is predicted to exist. As noted above (Fig. 6), the meager transition data available confirm the predicted trend of the effect of surface temperature on stability, although the transition trend is not so pronounced as the predicted stability trend. However, no systematic experimental investigations have been made of the combined effects of surface temperature and Mach Number.

Because of the effects of free-stream turbulence on transition (Fig. 1), the study of the effects of Mach Number on transition in wind tunnels is of questionable value unless the free-stream turbulence is suppressed to a point where it no longer influences transition. Unfortunately, the turbulence characteristics of supersonic wind tunnels are not known; in fact the characterization of turbulence in compressible flow has no firm foundation. Furthermore, the effects of free-stream turbulence on transition have not been estab-

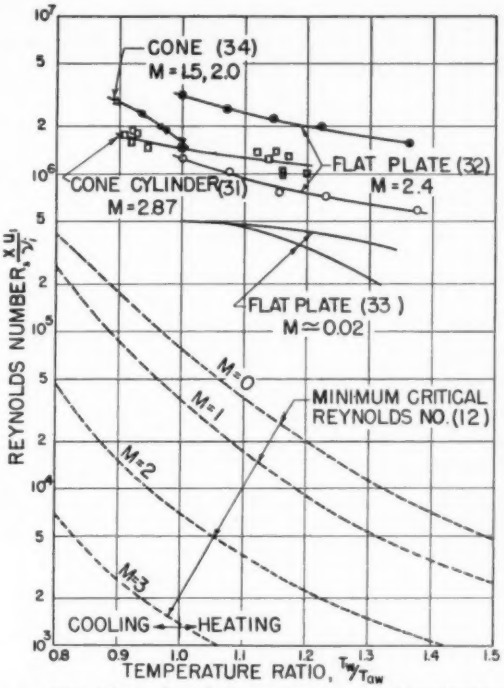

FIG. 6. The effect of surface temperature on boundary-layer stability and transition on nominally smooth surfaces. The transition data shown at the top of the figure indicate the beginning or middle of the transition region, except for the data of Higgins and Pappas,[32] which show the beginning and end of the transition region. The stability calculations[12] are for a flat plate.

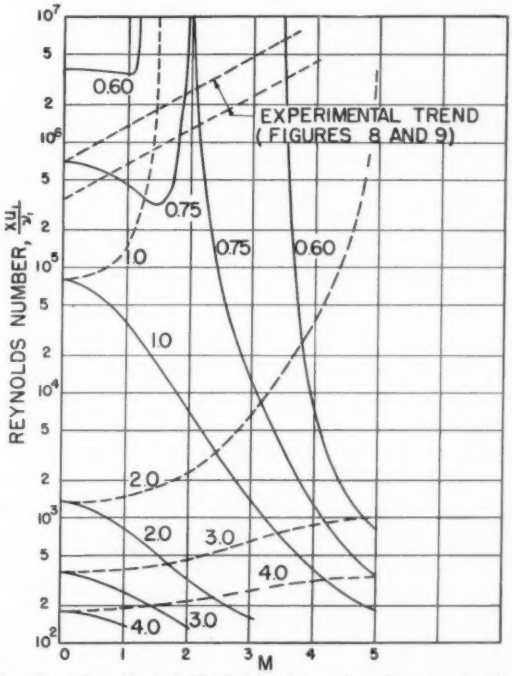

FIG. 7. The effect of Mach Number and surface temperature on boundary-layer stability. The calculated stability trends[12] are for constant values of T_w/T_{aw} (solid lines) and for constant values of T_w/T_1 (dotted lines). The numbers adjacent to the curves denote values of these temperature ratios.

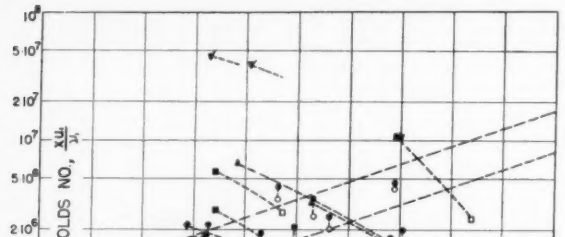

FIG. 8. The effect of Mach Number on boundary-layer transition in firing range ($T_w \simeq T_1$) and in rocket flight ($T_w \simeq 1.3\,T_1$). ○ = cones in Aberdeen Firing Range; □ = V-2 No. 27;[35] Δ V-2 No. 21; ▽ V-2 No. 12; and ◇ rocket flight. Open points denote beginning of transition region; solid points denote the end.

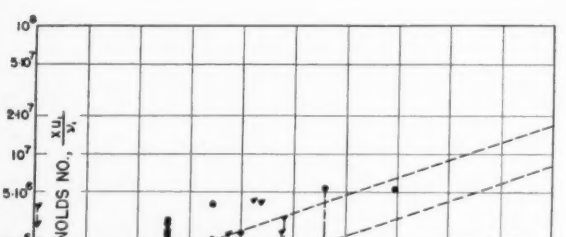

FIG. 9. The effect of Mach Number on boundary-layer transition in wind tunnels. ◁ = flat plates and airfoils;[32, 39, 40, 16, 38, 3, 41, 42] ○ = bodies of revolution[31, 43, 34] (including unpublished G-E data). Open points denote beginning of transition, shaded points denote average transition point, and solid points denote end of transition.

lished in supersonic flow. Because of these considerations, measurements in flight or in a firing range appeared to be attractive possibilities. Some flight skin-temperature data had already been obtained by the author's organization on V-2 rockets;[35] these data, when used to compute convective heat-transfer rates, indicated the transition point of the boundary layer. Some additional skin-temperature data later became available from other rocket flights. In the rocket flights, the measured skin temperature lay between the temperature outside the boundary layer and the adiabatic-wall temperature. Most of the measurements were made on the smooth conical noses of these rockets; thus the effects of pressure gradient, as well as free-stream turbulence, were eliminated from these results. Additional free-flight data were obtained from firing-range shadowgraphs of cone-cylinder models loaned by A. C. Charters and J. D. Nicolaides, of the Ballistics Research Laboratory, Aberdeen Proving Ground. By careful examination of these shadowgraphs it was possible to detect the apparent position of the beginning and end of transition on the conical nose of the models, where again a zero pressure gradient existed. In these firings, the time of flight was so short that the surface temperature remained close to ambient temperature. Effects of surface finish, however, may have been present in the firing-range tests, since the models were only machine-finished. The transition Reynolds Number ranges estimated from the rocket flights and the firing-range tests are shown in Fig. 8 as a function of the local Mach Number outside the boundary layer. Although the data show considerable scatter, there appears to be an increase in stability with increasing Mach Number. This is the trend predicted for these surface temperature conditions by the stability theory, although the effect of Mach Number on transition is not so great as the predicted effect on stability.

Although wind-tunnel transition data are suspect because of the unknown effects of tunnel turbulence level, the available data are shown in Fig. 9. These data were obtained from continuous-flow tunnels where the models had presumably reached equilibrium temperature. For this surface-temperature condition, the stability theory predicts decreasing stability with Mach Number. The wind-tunnel data, however, show a trend similar to that shown by the flight and firing-range data. Thus it may be tentatively concluded that the trend of boundary-layer transition with surface temperature is considerably less than the predicted trend of stability. This agrees with the rather slight trend with surface temperature shown in Fig. 6. Both sets of data (Figs. 8 and 9) indicate an increase in transition Reynolds Number with Mach Number.

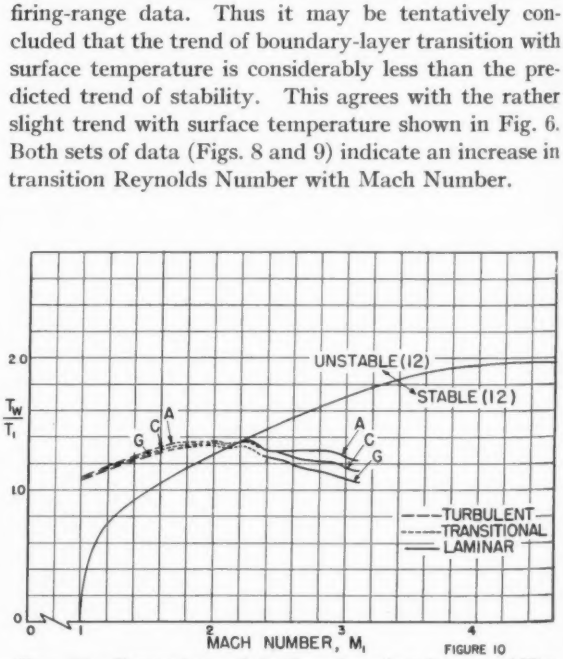

FIG. 10. Comparison of laminar boundary-layer stability theory with boundary-layer condition on smooth nose cone of V-2 rocket in flight. Data of Fischer and Norris[35] for Stations A, C, and G on the smooth nose cone of V-2 No. 27.

These must be considered as tentative conclusions, however, because of the possible effects of surface roughness on the firing-range results and of tunnel turbulence in the wind-tunnel results. The only data that may be considered free from these restrictions are those of Fischer and Norris[35] for Stations A, C, and G on the nose cone of V-2 No. 27. These data are shown in Fig. 10 compared with the predicted region of complete stability calculated by Van Driest.[12] It is seen that stabilization of the boundary layer takes place close to the theoretical prediction. This is not true, however, for stations preceded by surface roughness, as Fig. 11 indicates. Station H was located on the nose cone opposite Station G but was preceded by an $^1/_8$-in. trip wire. Stations K and M were located back on the ogival nose of the missile in a region of negative pressure gradient but were preceded by door joints and other surface discontinuities. The wind-tunnel and firing-range data are also indicated in Fig. 11; it is seen that the appearance of turbulence in the wind-tunnel tests is compatible with the theory, since they lie in the "unstable" region. However, in the firing-range tests, turbulence appears in the "stable" region; this may be due to the machine-finish of the firing-range projectiles.

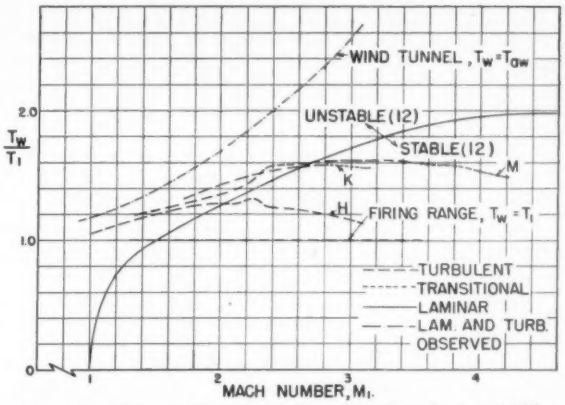

FIG. 11. Comparison of laminar boundary-layer stability theory with boundary-layer on "rough" nose of V-2 rocket in flight. Data of Fischer and Norris[35] for Stations H, K, and M on nose of V-2 No. 27.

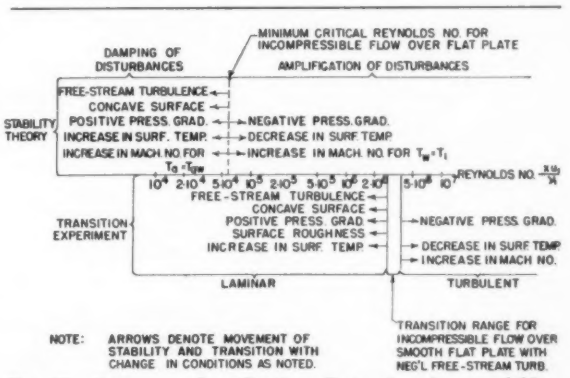
MINIMUM CRITICAL REYNOLDS NO. FOR INCOMPRESSIBLE FLOW OVER FLAT PLATE
DAMPING OF DISTURBANCES
AMPLIFICATION OF DISTURBANCES
STABILITY THEORY
FREE-STREAM TURBULENCE
CONCAVE SURFACE
POSITIVE PRESS. GRAD.
INCREASE IN SURF. TEMP.
INCREASE IN MACH NO. FOR $T_o = T_{aw}$
NEGATIVE PRESS. GRAD.
DECREASE IN SURF. TEMP.
INCREASE IN MACH. NO. FOR $T_w = T_t$
REYNOLDS NO. $\frac{x\,u_1}{\nu}$
10^4 $2\cdot10^4$ $5\cdot10^4$ 10^5 $2\cdot10^5$ $5\cdot10^5$ 10^6 $2\cdot10^6$ $5\cdot10^6$ 10^7
TRANSITION EXPERIMENT
FREE-STREAM TURBULENCE
CONCAVE SURFACE
POSITIVE PRESS. GRAD.
SURFACE ROUGHNESS
INCREASE IN SURF. TEMP.
NEGATIVE PRESS. GRAD.
DECREASE IN SURF. TEMP.
INCREASE IN MACH NO.
LAMINAR
TURBULENT
TRANSITION RANGE FOR INCOMPRESSIBLE FLOW OVER SMOOTH FLAT PLATE WITH NEG'L FREE-STREAM TURB.
NOTE: ARROWS DENOTE MOVEMENT OF STABILITY AND TRANSITION WITH CHANGE IN CONDITIONS AS NOTED.

FIG. 12. Summary of qualitative effects of various variables on boundary-layer stability and transition.

CONCLUSIONS

A review of the available boundary-layer transition data and a comparison with theory have yielded certain conclusions as to the effects of several variables on transition. These conclusions are summarized qualitatively in Fig. 12. The predicted effects of several of these variables on laminar boundary-layer stability are shown, as well as their experimental effect on transition. It is apparent that, in general, the experimental transition trends follow the predicted stability trends. The only exception appears to be the effects of surface temperature and Mach Number on supersonic transition, which are much less than, and sometimes opposite to, the predicted effects on stability.

It is evident that, while the qualitative effects of the several variables on transition are well established in subsonic flow and partially in supersonic flow, quantitative information is rarely available. This is particularly true of the combined effects of several of the variables that affect transition. Additional data on the effects of surface roughness, surface temperature, and pressure gradient in supersonic flow would be particularly valuable. The use of a firing range appears especially attractive for this work, at least until the turbulence level in supersonic wind tunnels and its effects on transition are established.

REFERENCES

[1] Tollmien, W., *General Instability Criterion of Laminar Velocity Distributions*, N.A.C.A. T.M. No. 792, 1936.

[2] Schlichting, H., *Zur Entstehung der Turbulenz bei der Plattenströmung*, Nach. Ges. Wiss. Gött. Math. physik. Klasse, 181 (1933); *Amplitudenverteilung und Energie Bilanz der keinen Störungenbeider Plattenströmung*, Nach. Ges. Wiss. Gött., Math. physik. Klasse, Vol. I, p. 47, 1935.

[3] Schubauer, G. B., and Skramstad, H. K., *Laminar Boundary-Layer Oscillations and Transition on a Flat Plate*, Jour. of Research of the Nat. Bureau of Standards, Vol. 38, p. 281, 1947.

[4] Rayleigh, Lord, *On the Stability or Instability of Certain Fluid Motions I, II*, Proc. London Math. Soc., Vol. 11, pp. 57–70; Vols. 18 and 19, pp. 67–74, 1887.

[5] Taylor, G. I., *Effect of Turbulence on Boundary Layer*, Proc. Roy. Soc., Vol. A156, pp. 307–310, 1936.

[6] Eckert, E. R. G., and Soehngen, E., *Interferometric Studies on the Stability and Transition to Turbulence of a Free-Convection Boundary Layer*, General Discussion on Heat Transfer, London Conference, 1951.

[7] Lin, C. C., *On the Stability of Two-Dimensional Parallel Flows, Part I*, Q. Appl. Math., Vol. III, pp. 117–142, 1945; Part II, Vol. III, pp. 218–234, 1945; Part III, Vol. III, pp. 277–391, 1946.

[8] Schlichting, H., and Ulrich, A., *Über die Berechrung der Umschlagsstelle laminar-turbulent*, Jahrb. der Deutschen Luftfahrtforschung, Part I, pp. 8–35, 1942.

[9] Hahneman, E., Freeman, J. C., and Finston, M., *Stability of Boundary Layers and of Flow in Entrance Section of a Channel*, Journal of the Aeronautical Sciences, Vol. 15, pp. 493–496, 1948.

[10] Lees, L., and Lin, C. C., *Investigation of the Stability of the Laminar Boundary Layer in a Compressible Fluid*, N.A.C.A. T.N. No. 1115, 1946.

(*Concluded on next page*)

[11] Lees, L., *The Stability of the Laminar Boundary Layer in a Compressible Fluid*, N.A.C.A. T.N. No. 1360, 1947.

[12] Van Driest, E. R., *Calculation of the Stability of the Laminar Boundary Layer in a Compressible Fluid on a Flat Plate with Heat Transfer*, Journal of the Aeronautical Sciences, Vol. 19, No. 12, pp. 801–812, December, 1952.

[13] Weil, H., *Effects of Pressure Gradient on Stability and Skin Friction in Laminar Boundary Layers in Compressible Fluids*, Journal of the Aeronautical Sciences, Vol. 18, pp. 311–318, 1951.

[14] Liepmann, H. W., *Investigation of Boundary Layer Transition on Concave Walls*, N.A.C.A. A.C.R. 4J28, 1945 (Wartime Report W-87).

[15] Emmons, H. W., *The Laminar-Turbulent Transition in a Boundary Layer—Part I*, Journal of the Aeronautical Sciences, Vol. 18, pp. 490–498, 1951.

[16] Liepmann, H. W., *Investigations on Laminar Boundary-Layer Stability and Transition on Curved Boundaries*, N.A.C.A. A.C.R. 3H30, 1943 (Wartime Report W-107).

[17] Dryden, H. L., *Reduction of Turbulence in Wind Tunnels*, N.A.C.A. Report No. 392, 1931.

[18] Dryden, H. L., *A Review of the Statistical Theory of Turbulence*, Q. Appl. Math, Vol. 1, pp. 7–42, 1943.

[19] Prandtl, L., *Effect of Stabilizing Forces on Turbulence*, N.A.C.A. T.M. No. 625, 1931.

[20] Schlichting, H., *Über die Enstehung der Turbulenzin einem rotierender Zylinder*, Nach. Ges. Wis. Gött., Math. physik. Klasse, 160, 1932.

[21] Görtler, H., *Über den Einfluss der Wandkrümmung auf die Enstehung der Turbulenz*, Z.f.a. M.M., Vol. 20, pp. 138–147, 1940.

[22] Taylor, G., *Stability of a Viscous Liquid Contained Between Two Rotating Cylinders*, Phil. Trans. Roy. Soc. London, Vol. A223, pp. 289–343, 1923.

[23] Görtler, H., *Übereine dreidimensionale Instabilität laminarer Grenzschichten an konkaven Wänden*, Göttinger Nachrichten, Neue Folge, Vol. 2, Nr. 1.

[24] Fage, A., and Preston, J. H., *On Transition from Laminar to Turbulent Flow in the Boundary Layer*, Proc. Roy. Soc., Vol. A178, pp. 201–227, 1941.

[25] Fage, A., *The Smallest Size of a Spanwise Surface Corrugation Which Affects Boundary-Layer Transition on an Aerofoil.* British A.R.C. R.&M. 2120, 1943.

[26] Tani, I., Hama, R., and Mituisi, S., *On the Permissible Roughness in the Laminar Boundary Layer*, Aero. Res. Inst. Tokyo Rep., Vol. 15, p. 199, 1940.

[27] Goldstein, S., *A Note on Roughness*, British A.R.C. R&M. 1763, 1936.

[28] Loftin, L. K., Jr., *Effects of Specific Types of Surface Roughness of Boundary-Layer Transition*, N.A.C.A. A.C.R. L5J29A (Wartime Report L-48).

[29] Williams, D. H., Brown, A. F., *Tests on Rivets and Backward Lapped Joints in the Compressed Air Tunnel*, British A.R.C. R.& M. 1789, 1937.

[30] Holstein, H., *Tests on a Flat Plate in a Uniform Airstream on the Influence of Roughness on the Transition from Laminar to Turbulent Flow*, U.M. No. 3110, 1944.

[31] Eber, G. R., *Recent Investigation of Temperature Recovery and Heat Transmission on Cones and Cylinders in Axial Flow in the N.O.L. Aeroballistics Wind Tunnel*, Journal of the Aeronautical Sciences, Vol. 19, pp. 1–6, 1952.

[32] Higgins, W., and Pappas, C. C., *An Experimental Investigation of the Effect of Surface Heating on Boundary-Layer Transition on a Flat Plate in Supersonic Flow*, N.A.C.A. T.N. No. 2351, 1951.

[33] Liepmann, H. W., and Fila, G. H., *Investigations of Effects of Surface Temperature and Single Roughness Elements on Boundary-Layer Transition*, N.A.C.A. T.N. No. 1196, 1947.

[34] Scherrer, R., *Boundary-Layer Transition on a Cooled 20° Cone at Mach Numbers of 1.5 and 2.0*, N.A.C.A. T.N. No. 2131, 1950.

[35] Fischer, W. W., and Norris, R. H., *Supersonic Convective Heat Transfer Correlation from Skin-Temperature Measurements on a V-2 Rocket in Flight*, Trans., A.S.M.E., Vol. 71, pp. 457–467, 1949.

[36] Dryden, H. L., *Airflow in the Boundary Layer Near a Plate*, N.A.C.A. Report No. 562, 1936.

[37] Hall, A. A., and Hislop, G. S., *Experiments on the Transition of the Laminar Boundary Layer on a Flat Plate*, British A.R.C. R.&M. 1843, 1938.

[38] Van der Hegge Zignen, B. G., *Measurements of the Velocity Distribution in the Boundary Layer along a Plane Surface*, Thesis, Delft (1924), printed by J. Waltmen, Jr., Delft.

[39] Holder, D. W., *Transition Indication in the National Physical Laboratory 20 in. × 8 in. High Speed Tunnel*, British A.R.C. R.&M. 2079, 1941.

[40] Ladenburg, R., and Bershader, D., *On Laminar and Turbulent Boundary Layer in Supersonic Flow*, Rev. of Mod. Phys., Vol. 21, pp. 510–515, 1949.

[41] Stalder, J. R., Rubesin, M. W., and Tendeland, T., *A Determination of the Laminar, Transitional, and Turbulent Boundary-Layer Temperature Recovery Factors on a Flat Plate in Supersonic Flow*, N.A.C.A. T.N. No. 2077, 1950.

[42] Wilson, R. E., Young, E. C., and Thompson, M. J., *2nd Interim Report on Experimentally Determined Turbulent Boundary Layer Characteristics at Supersonic Speeds*, DRL/UT Report CM-501, 1949.

[43] Hilton, W. F., *Wind-Tunnel Tests for Temperature Recovery Factors at Supersonic Velocities*, Journal of the Aeronautical Sciences, Vol. 18, pp. 97–100, 1951.

Equilibrium Temperature of an Unheated Icing Surface as a Function of Air Speed*

BERNARD L. MESSINGER†

Lockheed Aircraft Corporation

ABSTRACT

The thermal analysis of a heated surface in icing conditions has been extensively treated in the literature.[8] Except for the work of Tribus,[1] however, little has been done on the analysis of an unheated icing surface. This latter analysis is significant in the design of cyclic thermal deicing systems that are attractive for small high-speed aircraft for which thermal anti-icing requirements have become severe.

In this paper, a complete analysis of the temperature of an unheated surface in icing conditions is presented for the several significant régimes (i.e., less than 32°F., at 32°F., and above 32°F.) as a function of air speed, altitude, ambient temperature, and liquid water content.

The results are presented in graphical form and permit the rapid determination of surface temperature for a wide range of variables. Curves are presented to determine the speeds beyond which no ice accretion will occur. Curves are also presented to indicate the surface temperature and the rate of ice sublimation which takes place when an ice-covered surface emerges into clear air.

One significant result of this study is the introduction of a new basic variable referred to as the "freezing-fraction," which denotes the proportion of the impinging liquid which freezes in the impingement region. The fact that some of the liquid does not freeze in the impingement region tends to explain the observed variation in ice formation shape with temperature, speed, and water catch.

New test data obtained at Mt. Washington, N.H., for stagnation-point surface temperatures of an unheated plastic cylinder in natural and artificial icing conditions are included in the Appendix. These data substantiate the validity of the assumptions made in the theoretical analysis.

(1) INTRODUCTION

AIRFOILS MAY BE PROTECTED against icing in two basic ways. The ice may be entirely prevented from forming (anti-icing) as, for example, by thermal or chemical means; or it may be allowed to form to a tolerable thickness and periodically removed (deicing) as in the case of the inflatable boot or the cyclic application of heat. Until recently, almost all aircraft employed either an inflatable boot type of deicing or a thermal system of anti-icing, the latter being the preferred method.

The advent of transonic aircraft speeds and very thin airfoils has made the application of thermal ice prevention extremely difficult or impractical, and, as a result, increased attention has been given to the possibilities offered by the cyclic thermal deicing method. The publication of reference 1 has been an important factor in directing attention to the significant economy of energy that is possible by the use of cyclic thermal deicing as compared to the continuous thermal anti-icing method. A more recent report, reference 2, contains experimental results of preliminary N.A.C.A. research with cyclic electrothermal deicing using a relatively low-intensity system. By using a short duration, high-intensity "on" period, the average energy can be of the order of one-tenth to one-twentieth of energy required for continuous anti-icing. This large reduction in energy requirements makes electrical power appear to be an ideal source of heat for a cyclic thermal system. These general characteristics have been experimentally verified by numerous flight and laboratory tests recently conducted by the Lockheed Aircraft Corporation.

Of the thermal types, the continuous anti-icing system has predominated in the last decade. Hence, the theoretical studies and methods of analysis developed in this period have been almost entirely concerned with the energy balance that exists when an anti-iced surface is maintained at a temperature considerably above the freezing point, generally at about 100°F. Little if any attention (except in reference 1) has been directed toward determining the temperature of an unheated icing surface.

If, in designing a cyclic thermal deicing system, high-intensity heating (about 30 to 40 watts per sq.in.) is used, a short "on" period as low as 2 sec. may be employed. This permits a ratio of "off" to "on" time of as much as 50 or 75 to 1. With this large a ratio of "off" time, the *initial temperature* of the iced surface just prior to an "on" period is essentially the *equilibrium temperature of an unheated airfoil surface.* Although the exact mechanics of the ice removal process in a cyclic thermal system is not fully understood, it is believed that this initial surface temperature has a significant bearing on the net energy required. Other factors that may be involved are related to the effect of ice thickness and liquid surface tension on the removal process. It was pointed out in reference 1 that one

Presented at the Design and Structures Session, Annual Summer Meeting, I.A.S., Los Angeles, June 27–28, 1951. Revised and received July 2, 1952.

* The author is indebted to M. M. Friedlander for assistance in preparation of the curves and to P. J. Valentine for suggestions relative to the "freezing fraction" concept. Both are members of the Thermodynamics Group at Lockheed Aircraft Corporation.

† Department Manager, Thermodynamics.

advantage of the deicing method is that a high rate of water catch results in a higher initial temperature in the ice impingement area due to the release of the latent heat of fusion, whereas an anti-icing system is severely taxed at high rates of water impingement because not only is the heat of fusion unavailable but, in addition, the entire latent heat of evaporation must be supplied, as well as the usual loss by convection heat transfer. By using high-intensity thermal deicing, it is possible to achieve nearly instantaneous, dry removal of ice, thus avoiding the effect of "runback" and consequent refreezing.

During the early phases of the development of aircraft ice-protection systems, it was usually assumed that, when the day came that airplanes would fly fast enough to result in stagnation temperatures of 32°F. or more, the problem of icing would be eliminated. As that day approached, however, it became increasingly obvious that the surface temperature rise in icing conditions would be different from that which would prevail in dry air. It is now evident that ice *can* be deposited on a surface even though the speed corresponds to a clear-air surface temperature of more than 32°F.

One of the early attempts to analyze the effect of free moisture on the kinetic heating of the boundary layer was made by J. K. Hardy, a visiting British anti-icing specialist who was temporarily stationed at the Ames Aeronautical Laboratory of the N.A.C.A. The results of his work were reported in 1944 in reference 3 and somewhat later in references 4 and 5. In reference 4, Hardy introduced the concept of a "datum temperature," which he considered to be a basic reference parameter for use in computing the unit heat- and mass-transfer rates for a heated surface in icing flight. This "datum temperature" parameter was adopted and used in many subsequent reports and articles on ice protection.[6–9] In some of these articles (particularly reference 6), the suggestion is made that the "datum temperature" cannot be measured in an icing cloud because of the release of the heat of fusion. In the opinion of the author of the present paper, there are certain fallacies in the manner in which the "datum temperature" parameter has been employed, and these will be discussed in detail later in the article.

It is the purpose of this paper to present a complete analysis of the conditions that govern the equilibrium temperature of an insulated, unheated surface exposed to icing. The analysis is, in part, based on the approach begun in reference 1 but goes beyond the scope of that work. The latter considered icing conditions for a surface temperature *above* and *below* 32°F. but not *at* 32°F. The present analysis includes an important range of conditions at a 32°F. surface temperature using the concept of the "freezing fraction." In extending the results of this analysis to the problem of airfoil ice protection, some consideration must be given to the limitations of some of the simplifying assumptions involved in certain of the parameters that are employed.

In that range of conditions in which a surface temperature of *more* than 32°F. is attained during icing, an analysis has also been developed using a parameter that will be referred to as the "evaporation fraction." This latter analysis includes conditions up to and including the speed for complete evaporation of all intercepted water.

Also of interest to the aircraft designer are those factors that govern the ability of the airplane to rid itself of ice accretions collected on unprotected surfaces after it has emerged from icing conditions into clear air. For this reason, an analysis is presented which permits the determination of (a) the rate of sublimation of ice from a surface at less than 32°F. in clear air, (b) the speed required to attain a surface temperature of 32°F. on an ice-covered surface in clear air, and (c) the rate of melting from a wet surface of ice at 32°F. in clear air.

(2) Symbols

A = surface area, sq.ft.
B = ambient absolute pressure, in. of mercury
b = "relative heat factor," $R_w c_w / f_c$, dimensionless
c_i = unit heat capacity of ice, B.t.u./lb. °F.
c_p = unit heat capacity of air, B.t.u./lb. °F.
c_w = unit heat capacity of water, B.t.u./lb. °F.
δ_m = linear melting rate, in. per hour
δ_s = linear sublimation rate, in. per hour
E_m = water droplet catch efficiency, dimensionless
f_c = unit convection conductance, B.t.u./hour ft.^{2} °F.
g = gravitational constant, 32.2 ft./sec.^{2} or lbs. per slug
γ_i = density of ice, lbs. per cu.ft.
J = mechanical equivalent of heat, 778 ft.lbs. per B.t.u.
L_e = latent heat of vaporization of H_2O, B.t.u. per lb.
L_f = latent heat of fusion of H_2O, B.t.u. per lb.
L_s = latent heat of sublimation of ice, B.t.u. per lb.
m = evaporation fraction, dimensionless
n = freezing fraction, dimensionless
P = vapor pressure of atmospheric moisture, in. of mercury
P_{si} = vapor pressure over ice at t_{s_e}, in. of mercury
P_{sw} = vapor pressure over water at t_{s_e}, in. of mercury
q = rate of heat flow, B.t.u. per hour [subscripts defined in paragraphs (3.1), (3.2), and (6.2)]
r = "recovery" factor applying to kinetic heating, dimensionless
R_w = unit rate of water catch, lbs./hour ft.^{2}
R_{w_e} = unit rate of evaporation of water, lbs./hour ft.^{2}
R_{w_m} = unit rate of melting of water, lbs./hour ft.^{2}
t_∞ = ambient free-stream temperature, °F.
t_{s_e} = equilibrium surface temperature, °F.
θ = heat balance parameters, °F. [defined in paragraph (4)]
V_∞ = free-stream velocity, ft. per sec.

(3) Modes of Energy Transfer to an Unheated Icing Surface

(3.1) *Equilibrium Surface Temperature Less Than 32°F.*

For an icing surface having a steady-state temperature, t_{s_e}, of less than 32°F., the actual value of t_{s_e} will be largely dependent on the result of an energy balance involving the simultaneous interchange of the following quantities (see Fig. 1):

(3.1.1) Heat *lost* by convection:

$$q_c = f_c A(t_{s_e} - t_\infty)$$

(3.1.2) Heat *lost* by sublimation:

$$q_s = 2.90 L_s f_c A[(P_{s_1} - P_\infty)/B]^*$$

(3.1.3) Heat *lost* due to being absorbed by the warming of the impinging subcooled liquid:

$$q_w = R_w A c_w(32 - t_\infty)$$

(3.1.3) Heat *gained* due to the release of the latent heat of fusion as the subcooled liquid impinges and changes to the solid state at 32°F. and, then, as a solid, cools to t_{s_e}:

$$q_f = R_w A[144 + c_i(32 - t_{s_e})]$$

(3.1.5) Heat *gained* due to the viscous or frictional heating in the boundary layer:

$$q_v = f_c A(rV_\infty^2/2gJc_p)\dagger$$

(3.1.6) Heat *gained* equivalent to the kinetic energy of the liquid particles as they strike the icing surface:

$$q_k = R_w A(V_\infty^2/2gJ)$$

Because, in this case, the value of t_{s_e} is assumed to be less than 32°F., all of the impinging water is considered to have solidified so that no mass transfer by direct "blowoff" of liquid takes place and the accretion rate will be R_w. In addition, the effect of heat *loss* by radiation has been entirely disregarded, since it is relatively insignificant.

(3.2) t_{s_e} *Equal to 32°F.*

For a surface having an equilibrium temperature of 32°F., the energy balance is basically similar to that outlined above, *except* that an additional variable (hereafter referred to as the "freezing fraction," n) is involved in energy quantity (3.1.4). When operating conditions result in the value of t_{s_e} just reaching 32°F., n will be equal to 1.0, which signifies that *all* of the impinging liquid is converted to ice. When conditions correspond to the release of a somewhat greater net amount of heat to the ice formation (as with increased speed), part of the impinging water will not solidify but will persist as a 32°F. liquid, so that the value of n, the "freezing fraction," will be *less* than 1.0. Whenever n is less than 1.0, the heat quantity (3.1.2) corresponds to the latent heat of *evaporation* rather than heat of sublimation, even though a large part of the water may be present as ice.

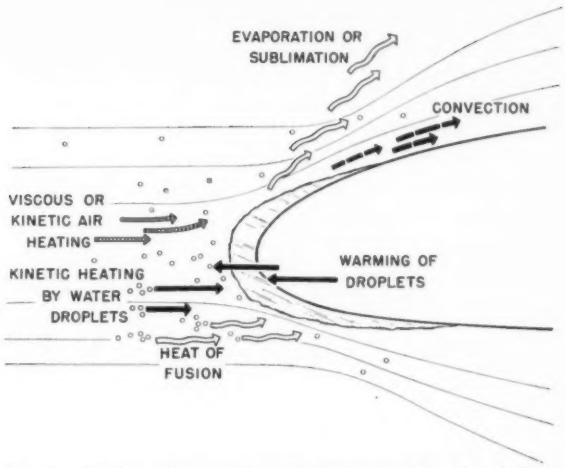

FIG. 1. Modes of energy transfer for an unheated airfoil in icing conditions.

The energy balance for a 32°F. surface temperature, t_{s_e}, in icing, therefore involves:

(3.2.1) Heat *lost* by convection:

$$q_c = f_c A(32 - t_\infty)$$

(3.2.2) Heat *lost* by evaporation (unless $n = 1$):

$$q_e = 2.90 L_e f_c A[(P_{s_0} - P_\infty)/B]$$

(3.2.3) Heat *lost* due to warming of the liquid:

$$q_w = R_w A c_w(32 - t_\infty)$$

(3.2.4) Heat *gained* due to the latent heat of fusion:

$$q_f = 144 n R_w A$$

(3.2.5) Heat *gained* due to viscous or frictional heating:

$$q_v = f_c A(rV_\infty^2/2gJc_p)$$

(3.2.6) Heat *gained* due to the kinetic energy of the impinging liquid:

$$q_k = R_w A(V_\infty^2/2gJ)$$

As the value of n becomes smaller, it is probable that a significant part of the impinging liquid will leave the surface by "blowoff" or "runoff." When the value of n becomes zero, none of the impinging water freezes and the surface may be at 32°F. *or above*. Note that the actual ice accretion rate in this range will be equal to nR_w.

(3.3) t_{s_e} *Greater Than 32°F.*

For above-freezing surface temperatures, at least some of the impinging water will probably run off the trailing edge of the airfoil during actual icing conditions. At the same time, however, part of the impinging water

* The constant 2.90 is an empirical factor relating mass transfer to convection heat transfer. In reference 1 this constant appears erroneously as being equal to 2.29 because of a numerical error in the derivation. Also, to be completely accurate, the values of P_∞ and B should be replaced by their corresponding *local* values just outside the boundary layer. Thus the areas of low static pressure promote increased evaporation and high static pressure areas suppress evaporation. The magnitude of this effect is considered negligible in this paper.

† This term is usually combined with that of paragraph (3.1.1) to give the *net* convection loss.

will leave the airfoil by evaporation, and that fraction that is evaporated in the impingement area is denoted by the symbol, m, and can be determined analytically as will be shown in a later section. At certain conditions corresponding to $m = 1.0$, the net energy gained by the surface will permit *complete evaporation* of the impinging liquid; hence, there will be no runback and presumably the surface will approach a dry condition.

The energy balance for a surface temperature, t_{s_e}, greater than 32°F. in icing, therefore involves:

(3.3.1) Heat *lost* by convection:

$$q_c = f_c A(t_{s_e} - t_\infty)$$

(3.3.2) Heat *lost* by evaporation:

$$q_e = 2.90 L_e f_c A[(P_{s_w} - P_\infty)/B] = mR_w L_e A$$

(3.3.3) Heat *lost* due to warming of the liquid:

$$q_w = R_w A c_w (t_{s_e} - t_\infty)$$

(3.3.4) Since *none* of the liquid freezes, there is no term representing the heat of fusion.

(3.3.5) Heat *gained* due to frictional heating:

$$q = f_c A(r V_\infty^2/2gJc_p)$$

(3.3.6) Heat *gained* due to the kinetic energy of the impinging liquid:

$$q_k = R_w A(V_\infty^2/2gJ)$$

(4) Evaluation of the Basic Heat Balance Equations

(4.1) When $t_{s_e} \leq 32$°F.

Arranging the terms of paragraph (3.1) in a single heat balance equation yields:

$$\text{Net heat loss} = q = f_c A\left[\left(t_{s_e} - t_\infty - \frac{rV_\infty^2}{2gJc_p}\right) + 2.90L_s\left(\frac{P_{s_i} - P_\infty}{B}\right)\right] + R_w A\left[c_w(32 - t_\infty) - 144 - c_i(32 - t_{s_e}) - \frac{V_\infty^2}{2gJ}\right]$$

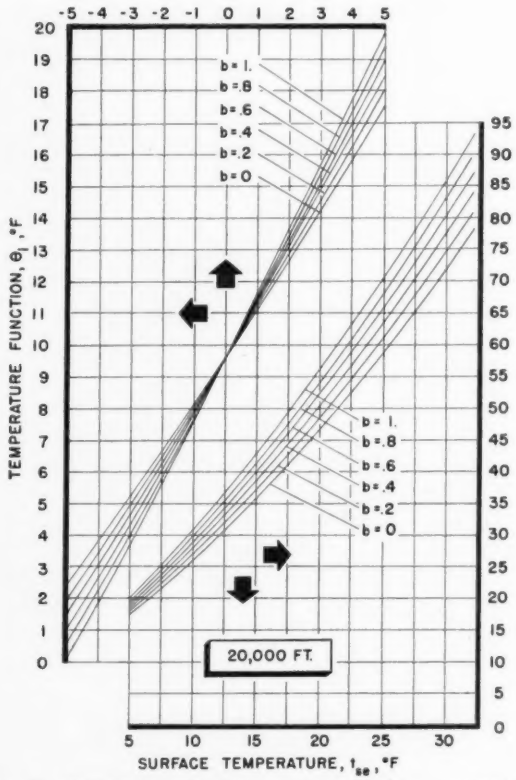

FIG. 2. Temperature function θ_1 versus surface temperature t_{s_e} for 20,000-ft. altitude.

The last term can be evaluated at $c_w = 1.0$ and $c_i = 0.47$,

$$\ldots + R_w A[0.47t_{s_e} - t_\infty - 127 - (V_\infty^2/2gJ)]$$

By introducing* the dimensionless ratio $b = R_w c_w/f_c$ and three new groupings of the variables—namely,

$$\theta_1 = t_{s_e}(1 + 0.47b) + (2.90L_s P_s/B)$$

$$\theta_2 = t_\infty(1 + b) + (2.90L_s P_\infty/B) + 127b$$

$$\theta_3 = [(r/c_p) + b](V_\infty^2/2gJ)$$

the combined equation then becomes

$$q = f_c A(\theta_1 - \theta_2 - \theta_3)$$

For the case of an unheated surface under equilibrium conditions, $q = 0$ and therefore $\theta_1 = \theta_2 + \theta_3$.

For any given altitude, the function θ_1 can be plotted in terms of t_s and b; θ_2, in terms of t_∞ and b; and θ_3 for an arbitrary value of r [$r = 0.875$, a compromise value for laminar (0.85) and turbulent (0.90) flow],† in terms of V_∞ and b. Such plots are shown in Figs. 2, 3, and 4. These θ functions have the dimensions of temperature °F. and, except where they are independent of altitude, have been plotted for 20,000 ft.

* These parameters were first presented in reference 1.

† A more precise form for r is $[1 - (V^2/V_\infty^2)(1 - Pr^n)]$, where $n = 1/2$ for a laminar and $n = 1/3$ for a turbulent boundary layer.

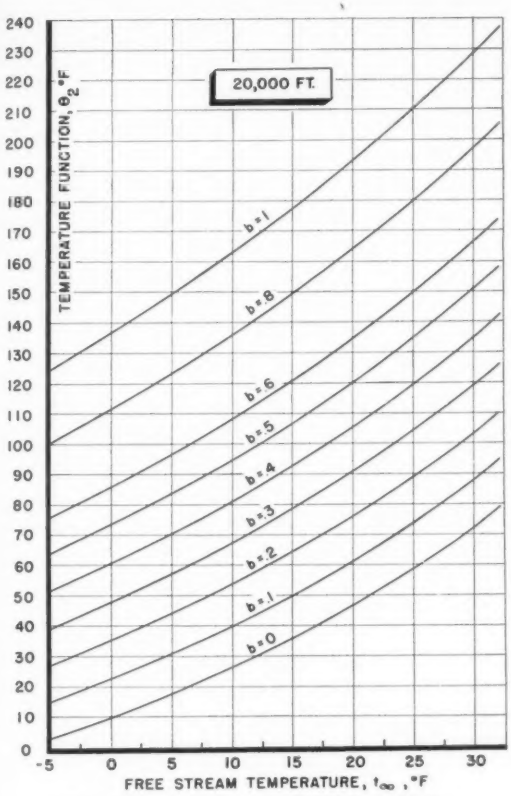

FIG. 3. θ_2 versus t_∞ for 20,000-ft. altitude.

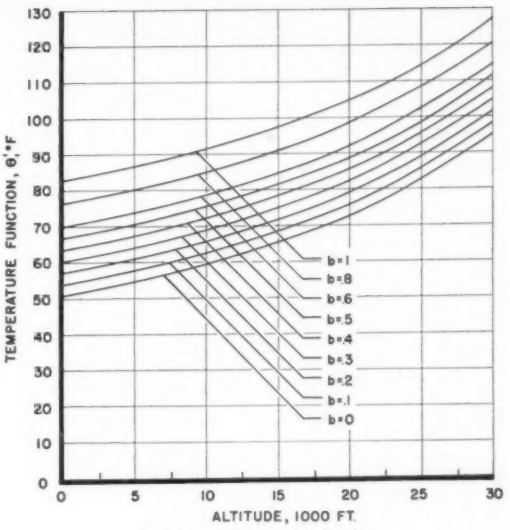

FIG. 5. θ_1' versus altitude.

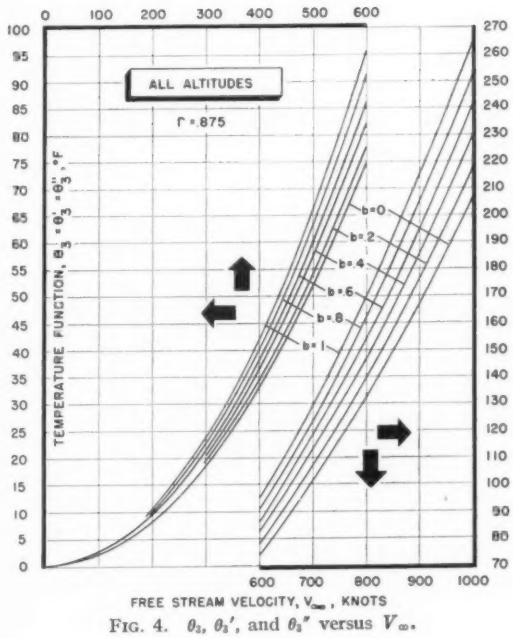

FIG. 4. θ_3, θ_3', and θ_3'' versus V_∞.

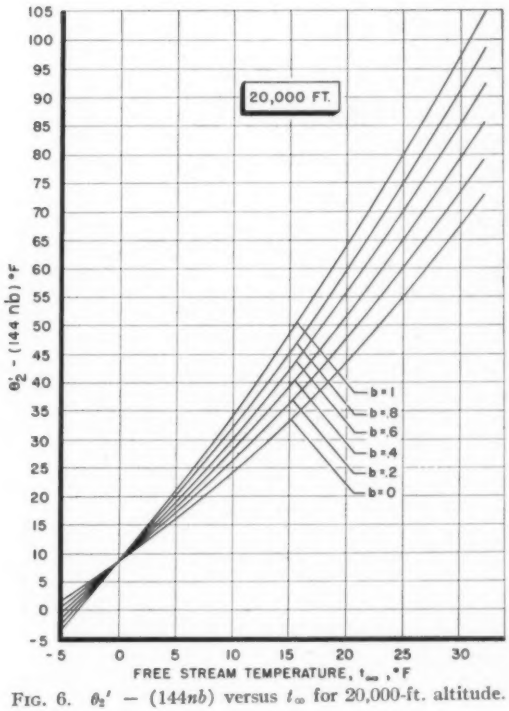

FIG. 6. $\theta_2' - (144nb)$ versus t_∞ for 20,000-ft. altitude.

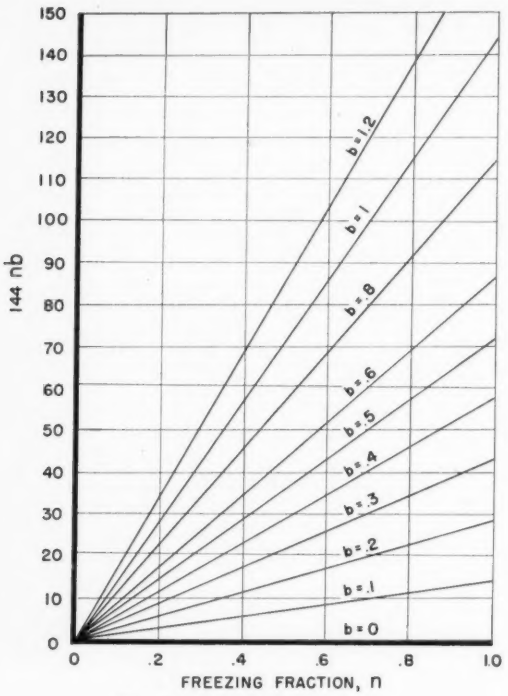

FIG. 7. Plot of $144nb$ versus n.

(4.2) When $t_{s_e} = 32°F.$ and $0 < n < 1$

For this case, the terms of paragraph (3.2) can be conveniently correlated by means of a second group of θ' functions:

$$\theta_1' = 32(1 + b) + (560/B)$$

(based on $L_e = 1{,}075$ for $t_{s_e} = 32°\text{F.}$),

$$\theta_2' = t_\infty(1 + b) + (3{,}120P_\infty/B) + 144nb$$

$$\theta_3' = \theta_3 = [(r/c_p) + b](V_\infty^2/2gJ)$$

and also, in this case, since $q = 0$,

$$\theta_1' = \theta_2' + \theta_3'$$

For any given altitude θ_1' is a function only of b as shown in Fig. 5, and θ_2' can be plotted in two steps as indicated in Figs. 6 and 7.

(4.3) When $t_{s_e} \geq 32°F.$ and $n = 0$

The terms of paragraph (3.3) can be expressed by a third group of θ'' functions:

$$\theta_1'' = t_{s_e}(1 + b) + (3{,}100P_s/B)$$

(based on $L_e \cong 1{,}070$ when $32°\text{F.} < t_{s_e} < 50°\text{F.}$),

$$\theta_2'' = t_\infty(1 + b) + (3{,}100P_\infty/B)$$

(based on $L_e \cong 1{,}070$ for $32°\text{F.} < t_{s_e} < 50°\text{F.}$), and

$$\theta_3'' = \theta_3' = \theta_3 = [(r/c_p) + b](V_\infty^2/2gJ)$$

and again

$$\theta_1'' = \theta_2'' + \theta_3''$$

As indicated in Fig. 8, both θ_1'' and θ_2'' can be represented by a single plot.

(4.4) When $t_{s_e} \geq 32°F.$ and $n < 1$

In order to determine the extent of the evaporation in the impingement area when $t_{s_e} \geq 32°\text{F.}$ and $n < 1$, the following energy balance can be solved in terms of m, the evaporation fraction:

The energy required for evaporation:

$$q_e = mR_wL_eA$$

The energy available for evaporation:

$$q_e' = 2.9f_cL_eA[(P_{s_w} - P_\infty)/B]$$

Equating the two forms,

$$m = \frac{2.9f_c}{R_w}\left(\frac{P_{s_w} - P_\infty}{B}\right) = \frac{2.9f_c}{b}\left(\frac{P_{s_w} - P_\infty}{B}\right)$$

This latter equation can also be used to determine the speed beyond which a surface exposed to icing conditions will be maintained *ice-free and dry* ($m = 1$):

$$P_{s_w} = b(B/2.9) + P_\infty$$

After finding P_{s_w}, the corresponding value of t_{s_e} can be found in any table of steam properties. The speed corresponding to this value of t_{s_e} can then be determined by means of Fig. 4 from $\theta_3'' = \theta_1'' - \theta_2''$.

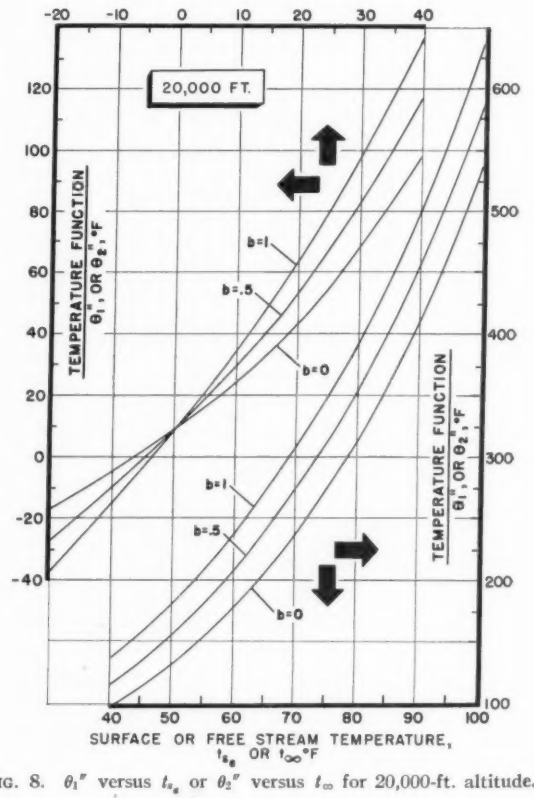

FIG. 8. θ_1'' versus t_{s_e} or θ_2'' versus t_∞ for 20,000-ft. altitude.

(5) Equilibrium Surface Temperature in Icing Conditions as a Function of the Significant Parameters

(5.1) *Characteristics of the Parameters*

By means of the graphical presentations of the θ functions, it is a simple matter to evaluate the heat balance equation and determine the equilibrium temperature t_{s_e} for any part of the range of flight speeds in icing conditions regardless of whether this temperature is above, at, or below the freezing point, provided, however, that the local value of b can be determined with reasonable accuracy.

The dimensionless ratio b (which is equal to $R_w c_w / f_c$) can be considered a measure of the ratio of the sensible heat-absorbing capacity of the impinging water per unit of surface area to the unit convective heat-dissipating capacity of the same surface. It has been proposed that this ratio be called the "relative heat factor."

No general statement can be made about the variations of the value of b except that, for a given position in the impingement area of an airfoil and for a constant air speed, it will vary directly as the liquid water content.

Another characteristic of the parameter, b, is that it tends to increase with altitude, since R_w increases and f_c becomes smaller for a given speed.

The variation of b with air speed depends, in turn, on the relationship between the variation of R_w and f_c with air speed for a given position on the airfoil. For an area in which the initial catch efficiency is close to 100 per cent, the value of R_w will vary directly with speed; if the initial catch efficiency is low, R_w will increase at a more rapid rate than the air speed. If the external boundary is locally laminar, f_c will vary as the square root of the air speed; if turbulent, it will vary as the 0.8 power of the air speed; in the transition region, it may vary as an air-speed power function greater than 1.0. It is therefore apparent that no simple single relationship will express the variation of b with air speed.

By making a survey of the local values of R_w and f_c around the periphery of a typical thin airfoil, it is possible to investigate the range of variation of b in the impingement area. Based on a laminar conductance, the maximum value of b is about three to four times the stagnation point value and seems to occur at about 5 per cent chord on the lower surface for an airfoil angle of attack at 4°. A typical stagnation point value for b is 0.5 based on a 6-ft. chord N.A.C.A. series 65-210 airfoil at 20,000 ft., 435 knots, 0°F., 30 micron drop size, and a liquid water content of 0.5 Gm. per cu.m.

A study of the θ function characteristics for equilibrium conditions yields the following relationships:

(5.1.1) θ_2 cannot be greater than θ_1 since θ_3 cannot be negative.

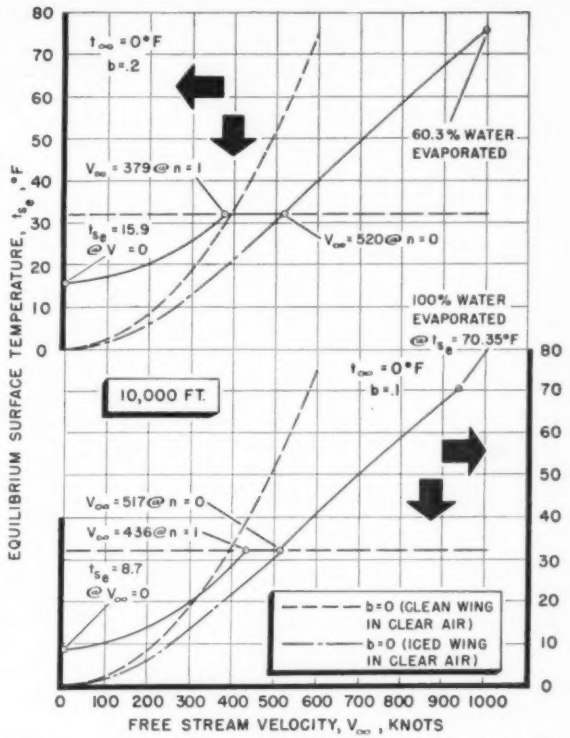
EQUILIBRIUM SURFACE TEMPERATURE, t_{s_e}, °F
FREE STREAM VELOCITY, V_∞, KNOTS
t_∞ = 0°F
b=.2
60.3% WATER EVAPORATED
V_∞ = 379 @ n = 1
t_{s_e} = 15.9 @ V = 0
V_∞ = 520 @ n = 0
100% WATER EVAPORATED @ t_{s_e} = 70.35°F
10,000 FT.
t_∞ = 0°F
b=.1
V_∞ = 517 @ n = 0
V_∞ = 436 @ n = 1
t_{s_e} = 8.7 @ V_∞ = 0
b=0 (CLEAN WING IN CLEAR AIR)
b=0 (ICED WING IN CLEAR AIR)

FIG. 9. t_{s_e} versus V for $b_\infty = 0.1$ and $b = 0.2$ at 10,000-ft. altitude.

(5.1.2) When $\theta_2 = \theta_1$, a purely hypothetical condition prevails—i.e., $\theta_3 = 0$ ($V_\infty = 0$)—and yet both water impingement and heat transfer are assumed to exist. This relationship, however, does establish the minimum t_{s_e} that can exist at subfreezing conditions for *a given value of b*. [See paragraph (5.2) and Fig. 10a for a detailed analysis of an actual condition.]

(5.1.3) If θ_2 is greater than that value of θ_1, which corresponds to 32°F., than n must be less than 1.0—i.e., *a wet icing surface exists*—and the θ' functions should be used.

(5.1.4) If $n = 0$ and $t_{s_e} = 32$°F., for a given value of t_∞, θ_2'' can be read directly and then subtracted from θ_1'' (corresponding to $t_{s_e} = 32$°F.) to give the required values of θ_3'' and thus the speed for *a surface that is wet but on which no ice is depositing*. This method was used to construct Fig. 11 from Fig. 4 and Fig. 8 for 20,000 ft. and from the equations for θ_1'' and θ_2'' of paragraph (4.3) for 10,000 and 30,000 ft.

(5.1.5) If the speed falls in the range between the two conditions defined by (5.1.3) and (5.1.4) above (i.e., $0 < n < 1$), the following steps can be used to determine the freezing fraction, n, for given values of V_∞, t_∞, b, and altitude or to determine V_∞ for given values of n, t_∞, b, and altitude:

(5.1.5.1) For the given value of altitude and b, determine the corresponding value of θ_1' using Fig. 5.

(5.1.5.2) If V_∞ is given, determine θ_3' using Fig. 4.

(5.1.5.3) Calculate $\theta_2' = \theta_1' - \theta_3'$.

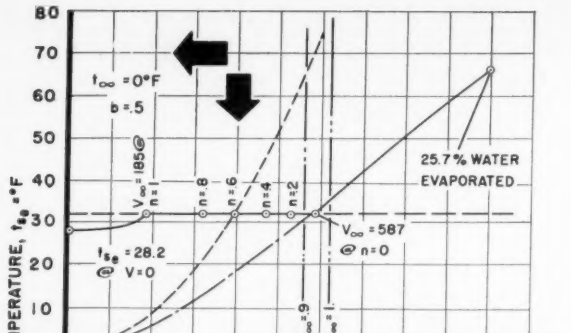
EQUILIBRIUM SURFACE TEMPERATURE, t_{se}, °F
FREE STREAM VELOCITY, V_∞, KNOTS
t_∞ = 0°F
b = .5
V_∞ = 185 @ n = 1
n = 8
n = 6
n = 4
n = 2
25.7% WATER EVAPORATED
V_∞ = 587 @ n = 0
t_{se} = 28.2 @ V = 0
M_∞ = .9
M_∞ = 1
64.9% WATER EVAPORATED
20,000 FT.
t_∞ = 0° F
b = .2
V_∞ = 570 @ n = 0
V_∞ = 439 @ n = 1
t_{se} = 14.1 @ V_∞ = 0
b = 0 (CLEAN WING IN CLEAR AIR)
b = 0 (ICED WING IN CLEAR AIR)

FIG. 10a. t_{se} versus V_∞ at $b = 0.2$ and $b = 0.5$ at 20,000-ft. altitude.

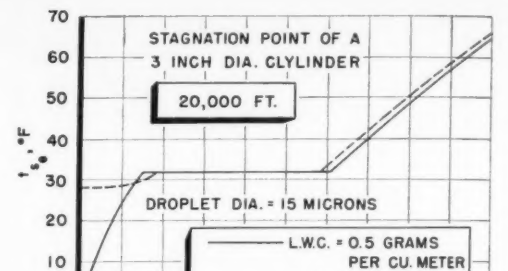
STAGNATION POINT OF A 3 INCH DIA. CYLINDER
20,000 FT.
DROPLET DIA. = 15 MICRONS
L.W.C. = 0.5 GRAMS PER CU. METER
b = 0.5, REPLOTTED FROM FIG. 10
t_{se}, °F
$b, \frac{R_w c_w}{t_c}$
DROPLET TRAJECTORY DATA OF DOUBTFUL ACCURACY ABOVE THIS APPROX. VELOCITY
FREE STREAM VELOCITY, V_∞, KNOTS

FIG. 10b. t_{se} versus V_∞ for variable value of b computed for constant liquid water content.

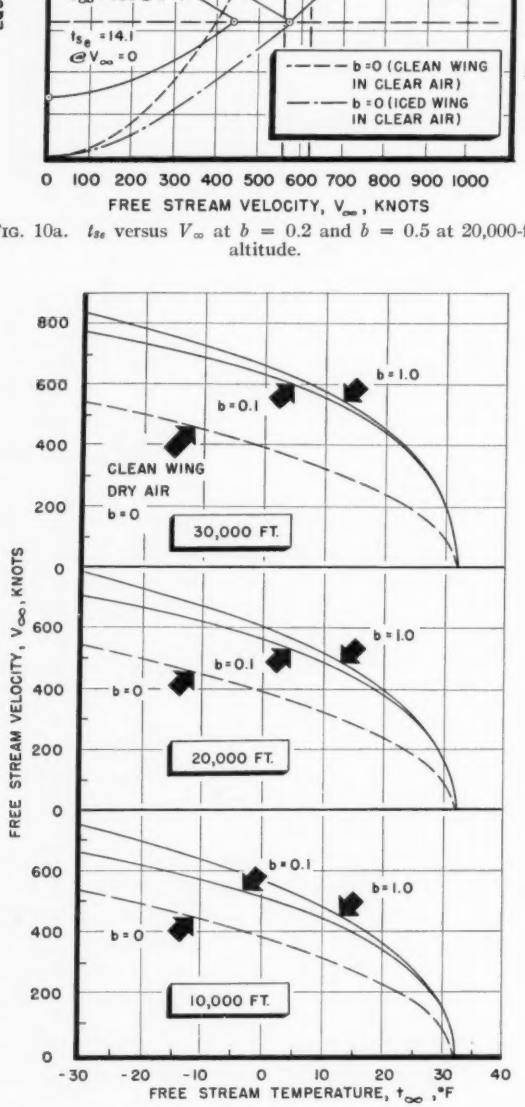

FIG. 11. V_∞ versus t_∞ for $n = 0$ at $t_{se} = 32°F$.

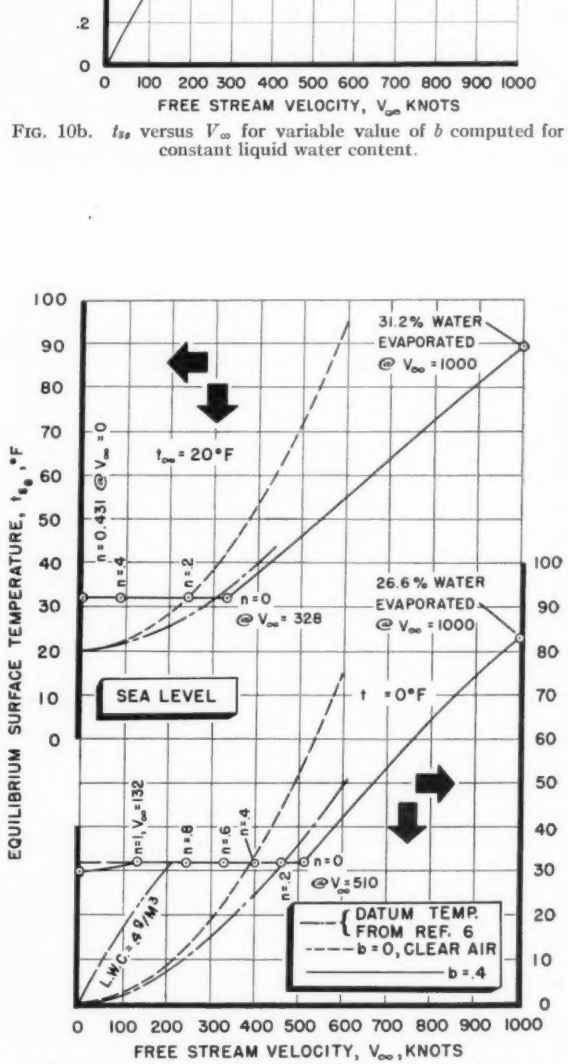
EQUILIBRIUM SURFACE TEMPERATURE, t_{se}, °F
t_∞ = 20°F
n = 0.431 @ V_∞ = 0
n = 4
n = 2
n = 0 @ V_∞ = 328
31.2% WATER EVAPORATED @ V_∞ = 1000
26.6% WATER EVAPORATED @ V_∞ = 1000
SEA LEVEL
t = 0°F
n = 1, V_∞ = 132
n = 8
n = 6
n = 4
n = 2
n = 0 @ V_∞ = 510
L.W.C. = .9 g/M³
DATUM TEMP. FROM REF. 6
b = 0, CLEAR AIR
b = .4
FREE STREAM VELOCITY, V_∞, KNOTS

FIG. 12. t_{se} versus V_∞ at sea level for comparison with values replotted from reference 6.

(5.1.5.4) For given value of t_∞, determine $\theta_2' - (144nb)$ using Fig. 6, and then calculate $(144nb)$ using θ_2' as obtained in (5.1.5.3).

(5.1.5.5) Using Fig. 7, determine n for the given value of b.

(5.1.5.6) If n is a known value and it is necessary to determine the corresponding value of V_∞, then step (5.1.5.2) should consist of determining θ_2' by adding $(144nb)$ obtained from Fig. 7 to the value of $\theta_2' - (144nb)$ obtained from Fig. 6.

(5.1.5.7) Using Fig. 4, V_∞ can then be determined from θ_3', which is the sum of θ_1' and θ_2'.

(5.2) *Surface Temperature Characteristics*

In order to illustrate the general trend of t_{s_e} as a function of airplane altitude, speed, water catch rate, and surface conductance, Figs. 9 and 10 have been constructed by use of the θ functions of Parts (4.1), (4.2), and (4.3).

Although each of these plots of t_{s_e} versus air speed is shown for constant values of b, it should be noted that b will vary somewhat with speed as indicated above. It has been suggested by J. P. Lewis, one of the coauthors of references 2, 6, and 9, that, since Figs. 9, 10, and 12 do not present a realistic picture of the true variation of surface temperature with air speed, it would be desirable to construct these curves for constant values of liquid water content as would be the case in actual icing flight. Unfortunately, it is only possible to construct such a plot for a given location on a given configuration of aerodynamic body. In order to illustrate the differences between the general plot using b as the independent parameter and a specific plot using liquid water content as the independent parameter, Fig. 10a has been prepared based on the stagnation region of a 3-in. diameter cylinder. The lower part of the figure shows the variation of b with air speed for this point on the cylinder, and the shaded area of the upper part of the figure indicates the nature of the discrepancy that results from the use of the simplifying assumption that b remains constant. As noted on this figure, the accuracy of the catch efficiency in the higher speed range is doubtful, but it can be seen that a large variation in b has little influence on t_{s_e} at the higher speeds.

A line of constant liquid water content (= 0.4 Gm. per cu.m.) has also been added to the lower part of Fig. 12 to illustrate the same effect at sea level.

Fig. 10 shows that the effect of a high rate of water catch ($b = 0.5$) is to maintain the impingement area at 32°F. over a wide range of speeds, in this case from 185 to 587 knots. Note that, while a temperature of 32°F. is attained at only 185 knots, there is at least some ice accretion all the way up to 587 knots. Even at 395 knots for $b = 0.50$, Fig. 10 indicates that 60 per cent of the deposit is ice. There is as yet no experimental indication that, under these conditions, the liquid water present (40 per cent at 395 knots) acts in any way that would assist aerodynamic forces in blowing away the ice formation. In fact, a few high-speed icing flights have been unofficially reported for at least moderate icing conditions, at which time heavy, rapidly forming deposits of ice were observed. The liquid water present when $n < 1$ may form runback ice beyond the impingement region if the "wet adiabatic" surface temperature (see reference 6 curve in Fig. 12) is less than 32°F. for the air speed in question.

Plotted for comparison purposes in Figs. 9 and 10 are the dotted curves of t_{s_e} for (a) an ice-free surface in clear air and (b) an ice-covered surface in clear air.

In the lower part of Fig. 10 is a plot of the same variables at the same altitude but for a lower water-catch rate ($b = 0.2$). Note that the speed at which $n = 0$ (ice-free) is almost as high (570 knots) as the corresponding speed for $b = 0.5$ (587 knots).

Note by comparing Figs. 9 and 10 that, for a given value of b (in this case 0.2), the effect of changing altitude from 10,000 to 20,000 ft. (without changing the ambient temperature) is to lower t_{s_e} slightly at all speeds (except in the 32°F. range), which fact is undoubtedly due to the increased rate of evaporation or sublimation due in turn to the lower barometric pressure.

Certain general conclusions can be drawn from a study of the four comparative plots. These are:

(a) *High rates of water catch* (and correspondingly high values of b) tend to produce higher surface temperatures in the range of speeds up to about 500 knots.

(b) In the speed range up to that for $n = 1$ (dry surface of ice) for a given value of ambient temperature, speed, and b, the surface temperature decreases slightly with altitude.

(c) The speed beyond which the surface is ice-free, even in moderate icing conditions, is much higher than the speed for a 32°F. clean surface temperature in clear air. For example, in Fig. 10 the speed for $n = 0$ and $b = 0.5$ is 587 knots compared with 393 knots for a 32°F. surface at $b = 0$.

Fig. 11 was plotted to show how this critical ice-free speed at $n = 0$ and $t_{s_e} = 32$°F. varies with b, t_∞, and altitude.

(5.3) *"Wet Adiabatic" or "Datum Temperature"*

As indicated in Part (1), the "datum temperature" developed in reference 4 and later used in references 6, 7, 8, and 9 has been employed in the past as a measure of the temperature of an unheated icing surface. The following form of this parameter has been copied from reference 8:

$$t_{0_k} = t_0 + \frac{V^2}{2gJc_p}\left[1 - \frac{U^2}{V^2}(1 - Pr^{1/3})\right] - 0.622\frac{L_v}{c_p}\left(\frac{e_{0_k} - e_1}{P_1}\right)$$

where

t_{0k} = datum temperature
t_0 = ambient static temperature
V = free-stream velocity
U = local velocity just outside the boundary layer
Pr = Prandtl Number
L_s = latent heat of vaporization (L_e)
e_{0k} = saturation vapor pressure of water at t_{0k}
e_1 = saturation vapor pressure of water just outside of the boundary layer
P_1 = barometric pressure just outside the boundary layer

The term within the bracket represents the local recovery factor.

An examination of the above equation indicates that this parameter might be more aptly named the "dynamic wet bulb temperature" rather than "datum temperature." Since it does not include terms to account for the sensible heating of the impinging droplets or the release of the latent heat of fusion, it cannot represent the true equilibrium temperature of an unheated icing surface or even the temperature of a surface that is wetted by an above-freezing-temperature cloud. It does represent the temperature in clear air of a surface that is wetted by water (possibly from within the surface) supplied at the temperature of the surface itself. This corresponds exactly to the wet bulb temperature and, as defined by the above equation, is in a general form that can be evaluated at any velocity. In fact, it is this form that permits the determination of the ambient wet bulb temperature from data obtained in high-speed flight.

Of related interest is the fact that in references 6, 8, and 9 the basic equation for the energy transfer from a heated airfoil contains two terms that are based on this "dynamic wet bulb" temperature. The convection loss term is presented as

$$q_c = f_c(t_s - t_{0k})$$

which would indicate that the difference between surface temperature and wet bulb temperature is the controlling potential. This is obviously contrary to the definition of the conductance. If this were actually the case, there could be no wet bulb thermometer depression at low velocity, since the convection gain that just balances the evaporation loss would be zero because the wick surface would itself be at the wet bulb temperature and, hence, the above definition would not permit the transfer of heat by convection to the wick.

Similarly, the evaporation term is stated in these references as

$$q_e = f_c(X - 1)(t_s - t_{0k})$$

or

$$q_e = f_c \frac{0.622 L_s}{c_p}\left(\frac{e_s - e_{0k}}{P_1}\right)$$

Here again, there could be no mass transfer from the wet bulb thermometer, since in this case e_s would be equal to e_{0k} and the evaporation term would be zero.

Fortunately, the two terms q_c and q_e are invariably used in combination with each other in solving anti-icing design problems, and, because of the definition of the term X,

$$X = 1 + \frac{0.622 L_s}{c_p P_1}\left(\frac{e_s - e_{0k}}{t_s - t_{0k}}\right)$$

the sum of the above two terms is equivalent to the sum of the two corresponding conventional terms:

$$q_c + q_e = f_c\left(t_s - t_0 + r\frac{V^2}{2gJc_p}\right) + f_c\left(\frac{0.622\, L_s}{c_p}\right)\left(\frac{e_s - e_1}{P_1}\right)$$

which satisfy the requirements of the psychrometric energy balance. The use individually of either of the terms of q_c or q_e as defined in references 6, 7, 8, and 9 would yield inaccurate results.

In order to illustrate the nature of the divergence between the results obtained by the methods of the present paper and those of references 6, 7, 8, and 9, Fig. 12 has been prepared. Curves of "datum temperature" for two ambient temperatures, 0° and 20°F., were copied directly from Fig. 2 of reference 6. The curves of t_{s_e} are plotted for an arbitrary value of b. Note that the region of greatest divergence is in the speed range below 300 to 400 knots, where the effect of the latent heat of fusion is noticeable. In the higher speed range, the difference between the two curves is small and is apparently due entirely to the cooling effect of the impinging liquid which is not taken into account in the datum temperature.

(6) Modes of Energy Transfer to an Unheated Ice-Covered Surface in Clear Air

(6.1) t_s, Less Than, or Just Equal to, 32°F.

(6.1.1) Heat *lost* by convection:

$$q_c = f_c A(t_{s_e} - t_\infty)$$

(6.1.2) Heat *lost* by sublimation:

$$q_s = 2.90 L_s f_c A[(P_{s_i} - P_\infty)/B]$$

(6.1.3) Heat *gained* due to viscous heating:

$$q_v = f_c A(r V_\infty{}^2/2gJc_p)$$

(6.2) t_s, Greater Than 32°F. (Wet Ice Surface)

When the air speed of the ice-covered surface is sufficient to result in the surface temperature t_{s_e} exceeding the melting point, a rather complex condition exists.

A water film of some indeterminate thickness will cover the surface of the ice. The thickness of this film will be related to factors such as the liquid-surface tension and viscosity, as well as the boundary-layer drag forces. The net heat gained due to the viscous heating can only produce melting in the ice after having traversed the liquid film by conduction. A film of finite thickness will therefore contain a finite temperature gradient, the differential being $(t_{s_e} - 32°\text{F.})$ since the melting ice temperature can only be 32°F.

The water that is evolved in the melting process may leave the surface by two means: (a) evaporation or (b) mechanical blowoff or runoff. It has been determined by the numerical evaluation of typical operating conditions that the ice will be melted much more rapidly than it can be evaporated, and therefore most of it will leave the airfoil by mechanical runoff. For example, in order for the rate of evaporation to equal the rate of melting at a speed of 800 knots at an altitude of 10,000 ft. and a conductance of 20 B.t.u./hour °F. ft.², the equilibrium thickness of the water film would have to be 0.45 in., an unlikely condition. If it were possible for a water film of this thickness to persist, it would involve a temperature differential of 31°F. between the ice face and the external surface of the water film. If, as is probably the case, the actual film thickness is small—say, for example, 0.001 in.—its thermal resistance is small, and it has been determined that little error is involved if it is entirely neglected as was the case in constructing the curves of Fig. 15.

The energy balance, based on this latter assumption for a wet melting ice surface just slightly above 32°F. will therefore include the following terms:

(6.2.1) Heat *lost* by convection:

$$q_c = f_c A(t_{s_e} - t_\infty) \cong f_c A(32 - t_\infty)$$

(6.2.2) Heat *lost* by evaporation:

$$q_e = 2.90 f_c L_e A[(P_{s_w} - P_\infty)/B] \cong 2.90 f_c L_e A[(0.1803 - P_\infty)/B]$$

(6.2.3) Heat *lost* by melting of ice:

$$q_m = R_{w_m} A L_f$$

(6.2.4) Heat *gained* by viscous heating:

$$q_v = f_c A(r V_\infty^2/2gJc_p)$$

(7) Sublimation and Melting Rates from an Unheated Ice-Covered Surface in Clear Air

(7.1) *Sublimation*

The combined heat balance equation for the terms listed in Part (6.1) can be written as

$$q_v - q_c = q_s$$

or

$$f_c A\left[t_\infty + \left(\frac{rV^2}{2gJc_p}\right) - t_{s_e}\right] = 2.9 L_s f_c A\left(\frac{P_{s_i} - P_\infty}{B}\right)$$

In the latter form, this equation can be evaluated for arbitrary values of t_∞, P_∞, and B in terms of V_∞ and t_{s_e}. In order to avoid a trial-and-error solution, t_{s_e} is selected as the independent variable.

Having obtained t_{s_e} in terms of V_∞, it is then possible to determine the rate of sublimation R_{w_s} or $\gamma_i \delta_s/12$ from

$$q_s = 2.9 L_s f_c A[(P_{s_i} - P_\infty)/B] = \gamma_i(\delta_s/12) L_s A$$

Since P_{s_i} has already been determined, it is possible to determine $\gamma_i \delta_s$ for an arbitrary series of values of f_c.

Fig. 13 is a plot of such values for three altitudes. The corresponding ambient temperatures for each altitude are N.A.C.A. standard.

The right-hand terminal points of each series of curves in Fig. 13 occur at the speed for a 32°F. surface temperature, and a general plot corresponding to these points is given in Fig. 14.

Note that in Fig. 13 the rate of sublimation is generally small, so that, once ice has accumulated on an airplane, its removal by sublimation alone is a slow process. Note also that for a given value of f_c the rate of sublimation at 32°F. (right end of each curve) is greater at high altitude than at low altitude, principally because of the lower value of B and also of P_∞. For a given speed the removal rate at high altitude is slower due entirely to the lower ambient temperature assumed. It is significant that these high-altitude removal rates would probably require more time for shedding even a minor ice accretion than the entire duration of an in-

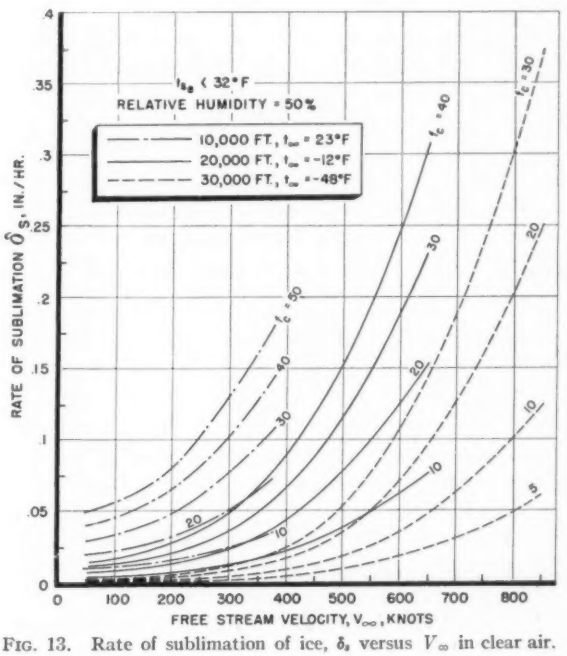

FIG. 13. Rate of sublimation of ice, δ_s versus V_∞ in clear air.

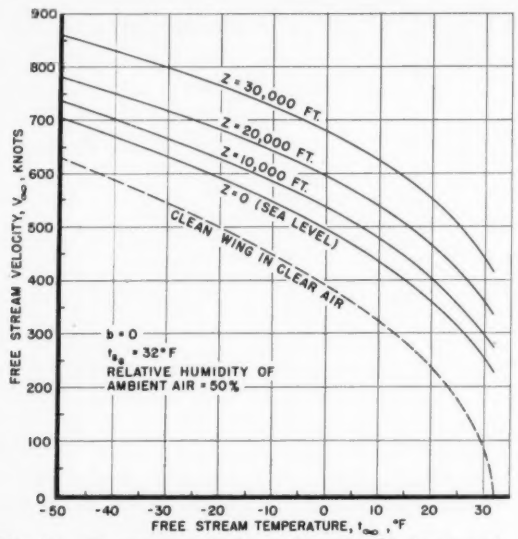
FREE STREAM VELOCITY, V_∞, KNOTS
FREE STREAM TEMPERATURE, t_∞, °F
Z = 30,000 FT.
Z = 20,000 FT.
Z = 10,000 FT.
Z = 0 (SEA LEVEL)
CLEAN WING IN CLEAR AIR
b = 0
t_{s_e} = 32°F
RELATIVE HUMIDITY OF AMBIENT AIR = 50%

FIG. 14. V_∞ versus t_∞ for ice surface at 32°F. in clear air.

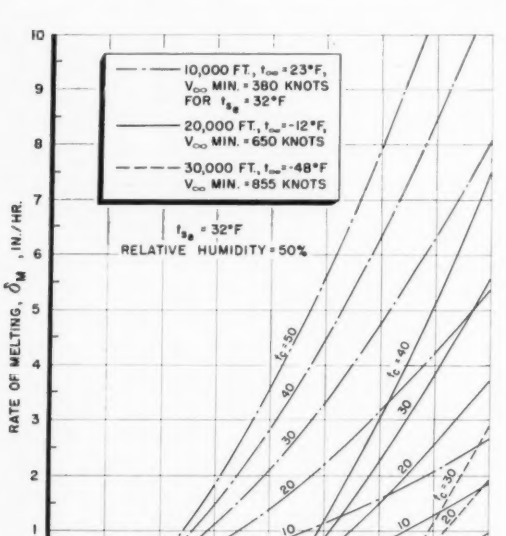

FIG. 15. Rate of melting of ice, δ_m versus V_∞ in clear air.

terceptor type of aircraft, the high-speed performance of which might be seriously crippled.

(7.2) *Melting*

When the speed exceeds the values given by Fig. 14, a wet surface will exist and the controlling factor for ice removal is the melting rate, although as indicated in Part (6.2) evaporation also occurs but its contribution to the removal is small compared to the runoff rate resulting from the melting.

The combined heat balance for the terms of paragraph (6.2) is

$$q_v - q_c - q_e = q_m$$

or, since $t_{s_e} = 32°\text{F.}$,

$$f_c A\left[t_\infty - \left(\frac{rV_\infty^2}{2gJc_p}\right) - 32\right] - 2.9L_e f_c A\left(\frac{0.1803 - P_\infty}{B}\right) = \gamma_f(\delta_m/12)L_f A$$

This equation was evaluated for the same arbitrary series of conditions used in Part (7.1), and the results are plotted in Fig. 15. Note that, although the melting rates are high, the speeds required to achieve them are also high.

In using Fig. 13 or 15 it should be remembered that, as the speed increases, the value of f_c also increases, so that for a given airfoil the sublimation or melting rate will increase faster with speed than indicated by the slope of the lines of constant f_c.

(8) Conclusions

At least some ice can collect on an unheated surface in normal low-temperature icing conditions at speeds up to about 600 knots (690 m.p.h.).

High rates of water catch tend to maintain an unheated icing surface at 32°F. over a wide range of speeds, but, except at the high speed end, a 32°F. surface temperature does not signify an ice-free surface.

Surface temperatures predicted by the "datum temperature" or "wet adiabatic" method of analysis are lower in the low-speed range and slightly higher in the high-speed range than are obtained by the methods developed in this paper.

Once an unheated surface has been allowed to collect ice, the period required to remove it by sublimation alone is long. It is of the order of 5 hours for $^1/_4$ in. of ice at an air speed of 500 knots at 30,000 ft. and N.A.C.A. standard ambient temperature.

The air speed required to attain a 32°F. ice surface temperature in clear air at 30,000 ft. and at N.A.C.A. standard temperature is about 850 knots. Beyond this speed, melting and evaporation occur.

There are few reliable experimental data available which would permit checking the accuracy of the results developed analytically in this paper. Such data, obtained in natural icing conditions, would be valuable for establishing the validity of the various foregoing assumptions (see Appendix).

References

[1] Tribus, Myron, *Intermittent Heating for Protection in Aircraft Icing*, University of California, Los Angeles, Ph.D. Thesis, August, 1949. (See also A.S.M.E. Trans., Vol. 73, No. 8, p. 1117, November, 1951.

[2] Lewis, James P., and Bowden, Dean T., *Preliminary Investigation of Cyclic De-icing of an Airfoil Using an External Electric Heater*, N.A.C.A. Research Memorandum No. R.M. E51J30, February 4, 1952.

[3] Hardy, J. K., *An Analysis of the Dissipation of Heat in Conditions of Icing from a Section of the Wing of the C-46 Airplane*, N.A.C.A. T.R. No. 831, 1945.

TABLE 1

EQUILIBRIUM STAGNATION POINT TEMPERATURE OF AN UNHEATED LUCITE CYLINDER IN MT. WASHINGTON ICING TUNNEL

January 7 to 21, 1952 — Cylinder Diameter = 3.75 inches

Run Number	Type of Icing:- N=Natural; A= Artificial	True Airspeed M.P.H	Liquid Water Content Grams/Cubic Meter	Droplet Diameter Microns	Wet Static Temperature °F (Equivalent Ambient)	Tunnel Total Temperature °F (Actual Ambient)	Droplet Reynolds Number R_u	Scale Modulus	Stagnation Point Water Catch Ratio	b, Relative Heat Factor	θ_3 or θ_3' *	θ_2 or θ_2' *	θ_1 or θ_1' *	n, Calculated Freezing Fraction	°F Calculated Surface Temperature	°F Measured Surface Temperature
1	A	244	.64	6.8	6.8	14.5	43.1	122.8	.18	.275	10	52.3	62.3	1.0	31.1	31.
2-A	A	252	.70	9.7	4.6	13.2	63.8	86.	.31	.527	11.3'	62.7'	74.0'	.65	32.	34.
2-B	A	252	2.00	7.6	4.6	13.2	49.9	110.	.22	1.065	12.5'	78.7'	91.2'	.402	32.	31.
2-C	A	252	.26	10.5	4.6	13.2	69.1	79.5	.335	.211	10.5	40.1	50.6	1.0	26.3	27.
3	A	235	1.10	8.5	10.1	16.8	51.6	98.2	.25	.645	10.1'	67.9'	78.'	.46	32.	33.
4	A	226	.32	12.0	0.9	8.3	71.3	69.5	.375	.276	8.5	41.95	50.45	1.0	25.8	25.
5	A	227	.27	20.7	4.1	11.	122.8	40.35	.59	.367	9.0'	59.6'	68.6'	.90	32.	30.
6-A	N	221	.27	9.8	5.4	11.7	56.5	85.2	.29	.178	7.9	36.6	44.5	1.0	23.4	22.
6-B	N	207	.27	10.	6.2	11.5	53.8	83.5	.29	.17	6.9	37.2	44.1	1.0	23.3	21.
7	A	220	.50	18.2	6.7	13.3	103.9	45.9	.53	.603	8.6'	64.6'	73.2'	.535	32.	32.
8	A	210	.81	17.1	17.9	22.7	91.2	48.8	.50	.90	8.5'	77.5'	86.'	.237	32.	33.
9	N	238	.70	16.4	12.8	19.0	94.5	50.9	.495	.796	9.4'	73.1'	82.5'	.35	32.	33.
10	N	234	.16	13.8	2.5	10.0	84.6	60.5	.44	.165	8.9	30.4	39.3	1.0	20.4	20.
11	N	228	.43	13.2	20.8	26.5	75.8	63.3	.41	.407	9.1'	60.9'	70.0'	.282	32.	31.
12-A	N	243	.17	8.9	0.8	9.0	56.9	93.8	.27	.107	9.4	20.9	30.3	1.0	16.	16.
12-B	N	243	.145	10.0	-0.2	7.7	64.0	83.5	.32	.111	9.4	19.1	28.5	1.0	15.2	18.
13	A	238	.34	13.0	7.7	14.7	80.1	64.2	.415	.334	9.7'	58.1'	67.8'	.83	32.	31.
14	N	232	.34	16.0	15.7	22.0	94.5	52.1	.49	.388	9.4'	59.8'	69.2'	.475	32.	32.

* The θ values shown are based on an average tunnel static altitude of 7800 feet. It was subsequently found that the actual average tunnel altitude was more nearly 8200 ft. but the θ values have not been revised since the net effect on t_{s_e} is believed to be small.

[4] Hardy, J. K., *Kinetic Temperature of Wet Surfaces, A Method of Calculating the Amount of Alcohol Required to Prevent Ice, and the Derivation of the Psychrometric Equation*, N.A.C.A. A.R.R. No. 5G13, September, 1945.

[5] Hardy, J. K., *Protection of Aircraft Against Ice*, Royal Aircraft Establishment, Report No. S.M.E. 3380, July, 1946.

[6] Gelder, Thomas F., and Lewis, James P., *Ice Protection for Turbojet Transport Airplane, Part II—Determination of Heat Requirements*, Institute of Aeronautical Sciences, Sherman M. Fairchild Fund Paper No. FF-1, March 24, 1950.

[7] Lewis, William, *Meteorological Factors in the Design and Operation of Thermal Ice Protection Equipment for High Speed, High Altitude Transport Airplanes*, Part 7 of a Compilation of the Paper Presented at N.A.C.A., "Conference on Some Problems of Aircraft Operation," October 9 and 10, 1950.

[8] Neel, Carr B., Jr., Bergrun, Norman R., Jukoff, David, and Schlaff, Bernard A., *The Calculation of the Heat Required for Wing Thermal Ice Prevention in Specified Icing Conditions*, N.A.C.A. T.N. No. 1472, December, 1947.

[9] Gelder, Thomas F., and Lewis, James P., *Comparison of Heat Transfer from Airfoil in Natural and Simulated Icing Conditions*, N.A.C.A. T.N. No. 2480, September, 1951.

APPENDIX

Since the time of the original presentation of this paper, the Lockheed Aircraft Corporation conducted a series of icing tests at the Aeronautical Ice Research Laboratory, Mt. Washington, N.H., which facility is operated jointly by the U.S. Air Force and the Navy Bureau of Aeronautics. One phase of this test program included a series of surface temperature measurements on an unheated Lucite cylinder, which had a 3.75-in. outside diameter and a $^1/_8$-in. wall thickness and was approximately 12 in. long. Surface thermocouple readings were obtained at the forward stagnation point, as well as at the 100° and 180° positions.

The principal purpose of recording these cylinder temperatures was to obtain experimental data with which to check the validity of the theoretical analysis presented in the subject paper.

The test facility used for this investigation consisted of a duct attached to the inlet of a radial-flow jet engine. This duct, having a cross-sectional area of approximately 3 sq.ft., acted as a small icing wind tunnel by induction of the ambient icing cloud conditions that prevail at the top of Mt. Washington during the winter months of the year. By this means, the natural icing conditions which flow over the mountain top at velocities ranging from about 30 to 90 m.p.h. are accelerated in this tunnel to about 250 m.p.h.

Table 1 contains the data obtained for 18 individual icing runs under a variety of meteorological conditions. Rotating multiple cylinders were used to obtain the liquid water content and mean droplet diameter in the vicinity of the test cylinder. The ambient temperature

of the air prior to its entry into the tunnel was taken to be the most reliable measure of the actual tunnel total temperature. The equivalent flight ambient temperature was then computed from this total temperature by making an allowance for the adiabatic acceleration of the water-laden air, including the effect of condensation of additional moisture due to the cooling of the air-water mixture resulting from the acceleration.

From the mean droplet diameter data shown, the corresponding droplet Reynolds Number R_u and Scale modulus ψ were computed. These values permitted the determination of the stagnation point water catch ratio (or catch efficiency) β_0 and, finally, the theoretical value of b, the relative heat factor. The θ values shown in the table were determined by using the θ curves of the subject paper, together with a set of unpublished curves which permitted correcting the θ values to the altitude indicated in the note under the table.

From the θ values, the theoretical value of n, the freezing fraction, and t_{se}, the equilibrium stagnation point temperature, were determined. In the last column the actual measured values are tabulated for comparison. The agreement is extremely good in spite of the obvious limitations of the instrumentation. For example, in Run No. 2A, a measured temperature of 34°F. is indicated even though the cylinder is unheated, an ice formation was observed in the thermocouple region, and the *total* temperature of the tunnel was 13.2° F. Similarly, the measured temperatures of 33°F. in runs 3, 8, and 9 indicate that the thermocouple inaccuracy was as high as 1 or 2°F. under some conditions. It is interesting to note that, in runs 5 and 13 where the predicted values of t_{se} are 1° or 2° higher than the measured, the value of n is only slightly less than 1.0, which would be the true value of n based on the *measured* temperature.

Note in the second column that the proportion of the runs obtained in natural icing was about equal to that using artificial spray water icing. The fact that the agreement in the last two columns did not appear to be influenced by this factor is an indication that, under the proper control, artificial icing is a valid research technique. The fact that it has been reported to the writer that the full effect of the latent heat of fusion has not been observed in the N.A.C.A. icing tunnel or in the Canadian N.R.C. icing tunnel is an indication that the spray water systems used in these facilities are not producing 100 per cent *subcooled* liquid droplets and may be hampered by the presence of partial "freeze-out" prior to impingement. That this does not seem to occur in the Mt. Washington tunnel may be the fortuitous result of the necessarily short distance, and, hence, time span, between the spray nozzles and the test section.

In conclusion, it is the opinion of the author that the experimental data presented in this appendix are strong evidence that the basic equations of the foregoing paper are valid. The extent of the agreement shown in the table between measured and predicted temperatures cannot be mere coincidence, since the conditions of the tests covered a wide range of icing conditions.

Blade Adjustment in Axial-Flow Compressor Stages*

ALLAN W. McCOY† AND ALTON V. HOOPER‡
*Sverdrup & Parcel, Inc.***

SUMMARY

An investigation of blade adjustment as a means of achieving volume regulation of an axial-flow compressor stage is presented. The effectiveness of such blade control is established and defined as the relative change of volume flow per unit of adjustment angle at constant pressure rise.

In the case of a grid element, the effectiveness of blade control is shown to be dependent upon the principal design parameters of reaction ratio, flow, and pressure coefficients. Low reaction ratios should be employed for stator-blade control, and for corresponding use of rotor-blade adjustment the preference is toward high reaction ratios.

Radial distribution of blade-control effectiveness is shown for several conventional stage types without consideration of radial equilibrium and nonuniform energy addition. In case of stator grid adjustment, the distribution of effectiveness indicates maximum values at the blade root section—i.e., with the adjustment for increase in flow, the axial velocities tend to rise rapidly at the hub. Rotor-blade control in these conventional stage diagrams affords a somewhat more uniform distribution of effectiveness. Special stage designs for uniform spanwise distribution of adjustment effectiveness are also discussed.

INTRODUCTION

FOR EFFICIENT COMPRESSION OF FLUID with high rates of flow, the axial-flow compressor offers definite advantages over competitive turbomachines. A significant limitation, however, is its narrow range of flow at constant speed due to the inherent steepness of the pressure-volume characteristic. Certain applications of axial-flow compressors require a wide range of both pressure ratio and volume flow, and the usual compressor characteristics must be modified in some manner. This requirement of a wide operational range is particularly evident in the case of compressors for high-speed wind tunnels, such as those at the Arnold Engineering Development Center of the U.S. Air Force. In such high-speed wind tunnels, the pressure and flow requirements are no longer satisfied by the usual compressor performance characteristics with variable drive speed; a new method of effective wind tunnel and compressor matching must be employed. Because of the large size of these wind tunnels and compressors, considerable benefits accrue from application of design principles permitting high mass-flow ratios[1] and attainment of required operating range by use of adjustable blading at a constant rotational speed.

Although the use of stator-blade control offers less mechanical difficulty than similar adjustment of the rotor blades, both types of control will be considered for purposes of generality and comparison. Considerations are based upon a single "normal" stage that is capable of multistage application.

Received April 23, 1951. Revised and received July 7, 1952.
* The authors wish to express their grateful appreciation to Miss Catherine Neville, of Sverdrup & Parcel, Inc., for her part in the mathematical computations and preparation of the plots associated with this paper.
† Senior Aeronautical Engineer.
‡ Project Engineer, Southern Cooperative Wind Tunnel, California Institute of Technology.
** Consulting Engineers, St. Louis.

NOTATION

A listing of the nomenclature is given below. In addition, a sketch of a typical blade diagram of a normal stage, with much of this notation indicated, is shown in Fig. 1. This normal stage velocity diagram is such as to produce exit flow conditions corresponding to those prevailing at the stage inlet. The major portion of the notation used in the subsequent analysis is given by Rannie.[2] The reference velocity for securing this nondimensionality is usually the peripheral velocity of the rotor tip, although in some cases the rotational velocity of a particular element is used. In this latter instance, all flow terms are said to be "local" values.

- ϕ = flow coefficient (dimensionless axial velocity)
- λ = rotational component of absolute velocity
- μ = rotational component of relative velocity
- ψ = pressure coefficient (dimensionless pressure rise)
- U = rotational speed of rotor tip element, used for nondimensionalizing above velocity terms
- ξ = radius ratio
- R = reaction ratio (ratio of static pressure rise in rotor to static pressure rise of complete stage)
- n = relative change of compressor flow or axial velocity
- E = effectiveness of blade control
- β = rotor flow angle
- γ = stator flow angle
- δ = reset angle of adjusted grid

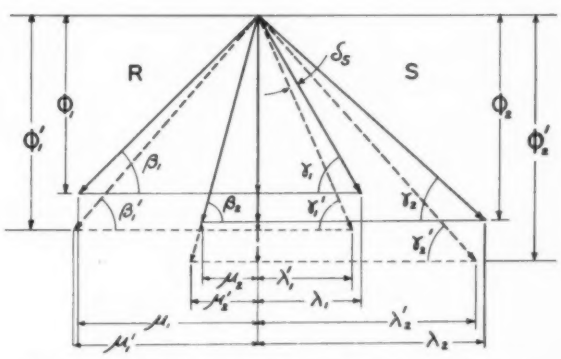

FIG. 1. Typical compressor diagram with stator grid reset.

Subscripts

R = rotor
S = stator
0 = hub conditions
1 = rotor inlet conditions
2 = rotor exit conditions

General Theory

(1) Definition of Control Effectiveness

The use of blade adjustment in axial-flow compressor stages results in relocation of the constant speed pressure-volume characteristics. Such typical characteristics are indicated in Fig. 2 for resetting of either the stator or rotor grid. In this case, as well as in the following sections, the grid adjustment angle is taken as positive when the action is such as to increase the volume flow.

For establishing the effectiveness of blade control, attention is centered upon design operation at zero resetting and operation at an increased flow with adjustment of either rotor or stator grid by an amount δ. When either grid is reset to this latter position, an operating condition

$$\left.\begin{aligned} \phi_e &= \phi + \Delta\phi_e \\ \psi_e &= \psi + \Delta\psi_e \end{aligned}\right\} \begin{aligned} &\delta = a \\ &\psi_e \neq \psi \end{aligned} \tag{1}$$

exists where the blade grids are aerodynamically loaded equivalent to design values. In general, this equivalent operating point would be at a slightly different pressure rise than the original value. However, blade adjustment is considered primarily as a means of volume regulation, since the usual multistage compressor characteristic approaches constant volume operation. The new operating point of particular interest is at

$$\left.\begin{aligned} \phi' &= \phi + \Delta\phi \\ \psi' &= \psi \end{aligned}\right\} \delta = a \tag{2}$$

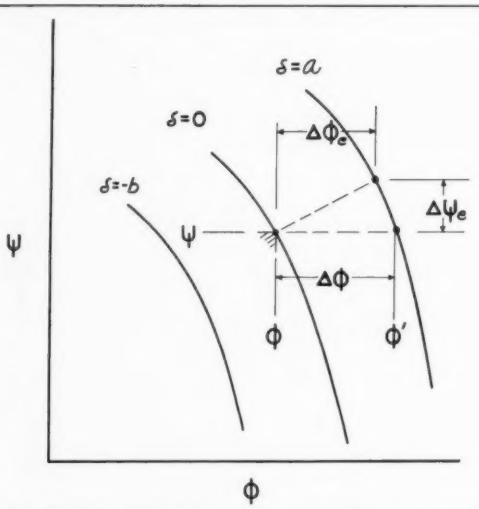

FIG. 2. Typical constant-speed characteristics with resetting of rotor or stator grid.

This latter condition, representing a change of flow at constant pressure rise, provides a criterion for defining the blade-control effectiveness.

Let the relative increase of flow be given by

$$n = \Delta\phi/\phi = (\phi' - \phi)/\phi \tag{3}$$

at $\psi' = \psi$. Then the rate of change of relative flow with respect to adjustment angle under these conditions is

$$(\partial n/\partial\delta)_\psi \approx n/\delta \tag{4}$$

which will depend upon the blade diagram design and the amount of grid adjustment angle. In order to compare different types of blading design, this derivative may be evaluated at the original design conditions —i.e., at $\delta = 0$. It then represents the initial slope of the $n - \delta$ function at constant stage pressure rise and provides a definition of the blade-control effectiveness. Thus,

$$E = (\partial n/\partial\delta)_{\psi,\ \text{at}\ \delta = 0} \tag{5}$$

(2) Assumptions

For any analysis of compressor blading, certain conditions must be imposed. The assumptions that are presently introduced are: (1) incompressible fluid; (2) radial flow components in the increased flow obtained by blade adjustment are similar to those existing at design conditions for each blade element; (3) constant fluid exit angles from grid elements; and (4) uniform radial distribution of stage pressure rise.

The assumption of incompressible fluid, while perhaps inconsistent with the term "compressor," is common to most blade theories for purposes of at least first approximations. Methods of compressibility correction for higher order approximations exist.

The second of the above assumptions is not intended to exclude any possibilities of any radial flow. It is intended to admit the existence of radial flow components at the design condition, determinable by radial equilibrium conditions,[2–4] but assumes that similar radial flows exist in the off-design flow obtained by blade adjustments. It is expected that this condition may be rather closely realized when the grid reset angles are small, and in this case the effectiveness of blade adjustment is evaluated at the design conditions with zero reset.

The assumption of constant fluid exit angles is necessarily introduced in view of the present inability to specify variations of deviation angles except in terms of a particular grid configuration. For more exact calculations, the known characteristics of the particular cascade considered may be substituted for this assumption.

While the assumption of uniform rotor work in a normal stage is common to most direct theories, it is strictly valid only at the stage design conditions. For off-design operating conditions, this assumption constitutes somewhat of an oversimplification and leads to

only first-order determination of the flow distributions at the larger departures from design flow. However, uniform energy addition is physically desirable for multistaging purposes. The flow distributions obtained by this assumption may be employed as the basis of further approximation by direct numerical methods with variable energy rise. The magnitude of induced effects and radial variation of pressure rise may be generally estimated as proportional to nonuniformity of blade-adjustment effectiveness, as determined by the present method.

(3) Stator Blade Adjustment

For a fixed position of the rotor grid, the change in volume flow may be determined in terms of the stator-blade adjustment angle, δ_S.

At a constant pressure rise, $\psi = \psi'$ and

$$\Delta\lambda = \Delta\lambda' = \psi/2\xi \tag{6}$$

where the primes denote values obtained at stator reset angle, δ_S. Radial equilibrium effects may cause the condition that

$$\phi_1 \neq \phi_2$$

at a particular radius.

Therefore, let the change of volume flow rate (axial velocity) at an arbitrary radius be given in terms of both the rotor inlet and exit conditions,

$$n_1 = \frac{\phi_1' - \phi_1}{\phi_1}, \qquad n_2 = \frac{\phi_2' - \phi_2}{\phi_2} \tag{7}$$

The condition that the relative flow exit angle remain constant may be written for the rotor as

$$(\xi - \lambda_2')/\phi_2' = (\xi - \lambda_2)/\phi_2 \tag{8}$$

and for the stator grid,

$$\tan\delta = \tan(\gamma_1' - \gamma_1) = \frac{(\phi_1'/\lambda_1') - (\phi_1/\lambda_1)}{1 + (\phi_1'/\lambda_1')(\phi_1/\lambda_1)} \tag{9}$$

Eq. (8) may be written in terms of the rotor inlet conditions as

$$\frac{\phi_2'}{\phi_2} = \frac{\xi - \lambda_1' - (\psi/2\xi)}{\xi - \lambda_1 - (\psi/2\xi)} \tag{8a}$$

From the assumption that the increased flow produces similar radial velocity components at each radial element, $n_1 = n_2 = n$, and

$$\phi_2'/\phi_2 = \phi_1'/\phi_1 \tag{10}$$

Introducing Eqs. (8a) and (10) into Eq. (9), the stator-adjustment angle is given by

$$\tan\delta = \frac{\phi_1}{\dfrac{n+1}{n}\dfrac{\lambda_1^2 + \phi_1^2}{\xi - (\psi/2\xi)} - \lambda_1} \tag{9a}$$

The relative flow variations may be obtained as

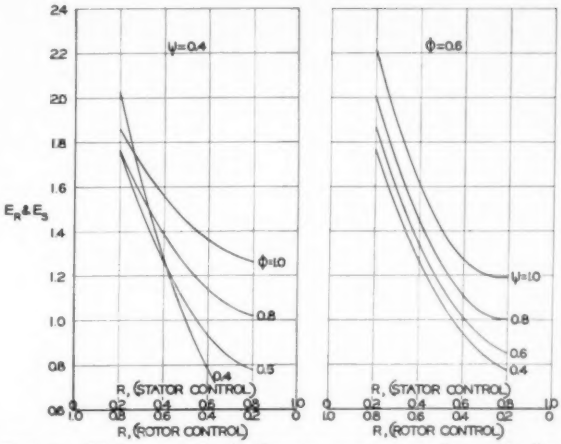

FIG. 3. Blade control effectiveness versus reaction ratio for grid element.

$$n = B/(A\cot\delta + 1 - B) \tag{11}$$

where

$$A = \frac{\phi_1}{\lambda_1}, \qquad B = \frac{\lambda_1 + (\phi_1^2/\lambda_1)}{\xi - (\psi/2\xi)}$$

Accordingly, the derivative of the $n - \delta$ functional relation is

$$\left(\frac{\partial n}{\partial\delta_S}\right)_\psi = \frac{B\sec^2\delta_S}{A + (1-B)\tan\delta_S} + \frac{B\tan\delta_S(1-B)\sec^2\delta_S}{[A + (1-B)\tan\delta_S]^2} \tag{12}$$

and the stator-blade-control effectiveness, by definition established in Eq. (5), is

$$E_S = \left(\frac{\partial n}{\partial\delta_S}\right)_{\psi,\,\delta=0} = \frac{B}{A} = \frac{\lambda_1^2 + \phi_1^2}{\phi_1[\xi - (\psi/2\xi)]} \tag{13}$$

(4) Rotor-Blade Adjustment

The effectiveness of rotor-blade control with a fixed position of the stator grid may be similarly determined. In this case, the constancy of the stator grid exit flow angle is

$$\lambda_1'/\phi_1' = \lambda_1/\phi_1 \tag{14}$$

and the corresponding condition for the rotor blades with adjustment angle, δ_R, may be expressed as

$$\tan\delta_R = \tan(\beta_2' - \beta_2) = \frac{(\phi_2'/\mu_2') - (\phi_2/\mu_2)}{1 + (\phi_2'/\mu_2')(\phi_2/\mu_2)} \tag{15}$$

where $\mu_2 = \xi - \lambda_2$.

By a procedure similar to that used in the case of stator-blade adjustment, the effectiveness of rotor-blade control may be obtained in the form

$$E_R = \left(\frac{\partial n}{\partial\delta_R}\right)_{\psi,\,\delta_R=0} = \frac{\mu_2^2 + \phi_2^2}{\phi_2[\xi - (\psi/2\xi)]} \tag{16}$$

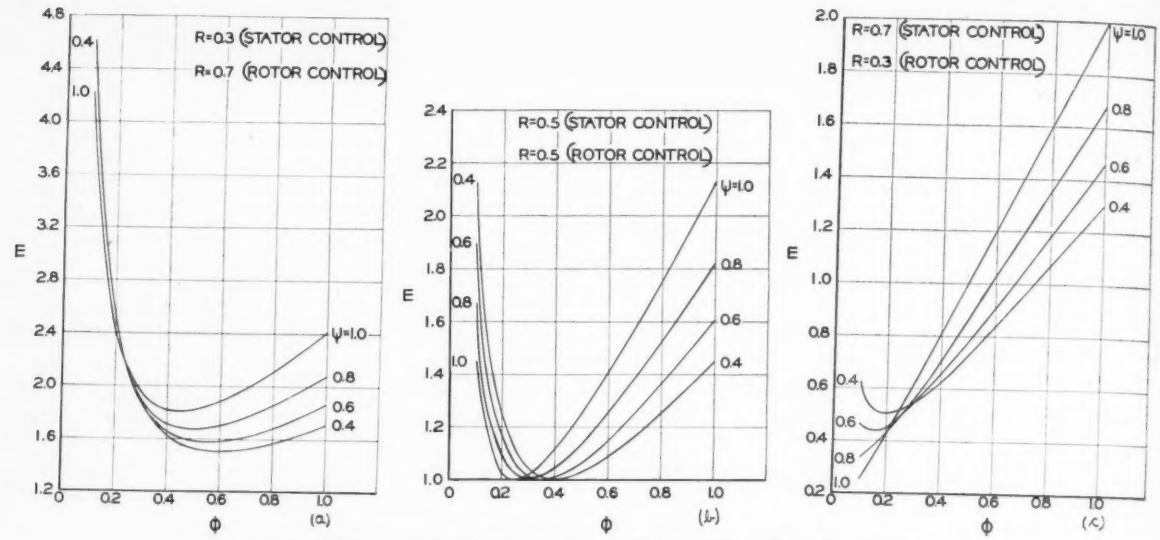

FIG. 4. Blade control effectiveness versus flow coefficient for grid element.

EFFECTIVENESS OF ELEMENT

To permit comparison of rotor and stator-blade control, it is desirable to consider the flow conditions at a particular radius. In this case, an arbitrary radius ratio, ξ^*, was selected in such a manner that

$$\phi_1 = \phi_2 = \phi \qquad (\text{at } \xi = \xi^*) \tag{17}$$

With radial equilibrium this condition is usually obtained at essentially mean radius, and the degree of reaction is defined simply as

$$R = 1 - (\lambda_m/\xi^*) \tag{18}$$

where $\lambda_m = \lambda_1 + (\Delta\lambda/2)$.

Since attention is now confined to this particular grid element, the reference velocity may be changed from the rotational speed at the rotor tip to that at the particular element. Thus, in terms of "local" values,

$$E_S = \frac{[1 - R - (\psi/4)]^2 + \phi^2}{\phi[1 - (\psi/2)]} \tag{19}$$

$$E_R = \frac{[R - (\psi/4)]^2 + \phi^2}{\phi[1 - (\psi/2)]} \tag{20}$$

By these equations, the effectiveness of both rotor and stator adjustment of a grid element is expressed in terms of the fundamental design parameters of reaction ratio and pressure and flow coefficients. The independent influence of these design parameters is shown in Figs. 3–5.

Reaction ratio effects are shown in Fig. 3 for particular values of flow and pressure coefficients. From Eqs. (19) and (20), it may be noted that the reaction ratio, R, is the only design parameter that gives rise to differences between rotor- and stator-blade-control effectiveness. Furthermore, both types of adjustment have equal effectiveness at 50 per cent reaction ratio. As indicated in Fig. 3, with increase of reaction ratio, the rotor-blade-control effectiveness is increased, whereas the corresponding effectiveness of stator-blade-control decreases.

The effect of flow coefficient on the effectiveness of rotor- or stator-blade adjustment is shown in Fig. 4. These curves indicate the general desirability of high flow and pressure coefficients in attaining high effectiveness of blade control. The difference between rotor- and stator-blade control is dependent only upon the reaction ratio, as noted previously.

The variation of effectiveness with pressure coefficient is seen to be dependent upon the values of the other design parameters. Certain further insight may be had by examining the conditions for the minimum effectiveness values shown in the $E - \phi$ plots of Fig. 4. Differentiating Eq. (19) for the stator-blade-control effectiveness with respect to the flow coefficient,

$$\frac{\partial E_S}{\partial \phi} = \frac{1}{1 - (\psi/2)} - \frac{\lambda_1^2}{\phi^2[1 - (\psi/2)]} \tag{21}$$

and the condition for minimum effectiveness of stator-blade control is that

$$\lambda_1 = \phi \tag{22}$$

which occurs at a rotor inlet flow angle of $\pi/4$. The resulting expression for the minimum stator-blade-control effectiveness is

$$E_{S_{min.}} = \frac{2\lambda_1}{1 - (\psi/2)} = 1 + \frac{1 - 2R}{1 - (\psi/2)} \tag{23}$$

The corresponding condition for minimum rotor-control effectiveness is

$$\mu_2 = \phi \tag{24}$$

and the minimum value is given by

$$E_{R_{min.}} = 1 - \{(1 - 2R)/[1 - (\psi/2)]\} \quad (25)$$

Again, these relations for rotor and stator control are symmetrical about 50 per cent reaction and are shown in Fig. 5. It is indicated that the advantages of increased pressure coefficient depend upon which control method is employed and whether the reaction ratio is greater or less than one-half. The minimum effectiveness of stator-blade control increases with pressure coefficient provided the reaction ratio is less than one-half. This condition for rotor-blade control requires reactions of greater than one-half.

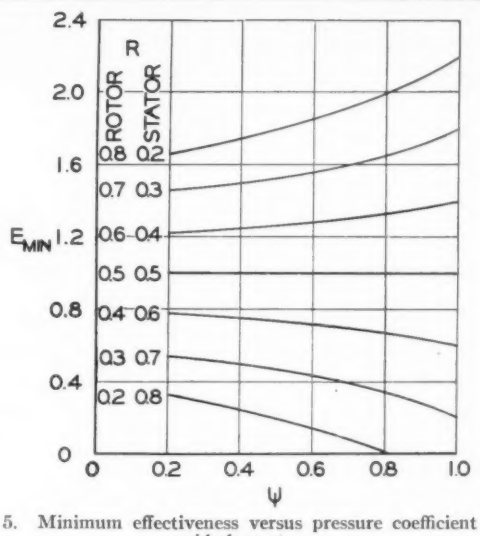

FIG. 5. Minimum effectiveness versus pressure coefficient for grid element.

BLADE CONTROL IN COMPLETE STAGES

The relations for blade-control effectiveness have been given in Eqs. (13) and (16) for stator- and rotor-blade adjustment and were expressed in terms of the relative rotor inlet and absolute rotor discharge conditions, respectively. By use of a simplifying assumption that

$$\phi_1 = \phi_2 = \phi \quad (26)$$

at all radii, it is possible to make immediate comparisons of various stage designs for application to blade control. For this comparison the equations for blade-control effectiveness are

$$E_S = (\lambda_1^2 + \phi^2)/\phi[\xi - (\psi/2\xi)] \quad (13a)$$

$$E_R = (\mu_2^2 + \phi^2)/\phi[\xi - (\psi/2\xi)] \quad (16a)$$

Several conventional compressor-stage types may be specified by writing the absolute compressor inlet spin velocity as

$$\lambda_1 = K\xi^X \quad (27)$$

and the flow types obtained with $X = -1$, 0, and $+1$ will be considered. The blade diagrams corresponding to these selections are of fundamental nature and are frequently discussed for other comparative purposes. By conventional reference they shall be called:

Free Vortex (FV), $X = -1$
Constant Inlet Spin (CIS), $X = 0$
Wheel Flow (WF), $X = 1$

The constant K may be selected according to the reaction ratio desired at a particular radius.

It is also considered desirable to include comparison of blading types that would offer uniform effectiveness distribution along the blade span. By definition, these uniform effectiveness distribution blading types would satisfy the relation

$$\partial E/\partial\xi = \partial^2 n/\partial\xi\partial\delta = 0 \quad (28)$$

Description of the flow in terms of the absolute rotor inlet spin velocity may be made for comparison with conventional blade types given by Eq. (27).

The velocity diagram for uniform distribution of stator blade adjustment effectiveness (USED) is given by

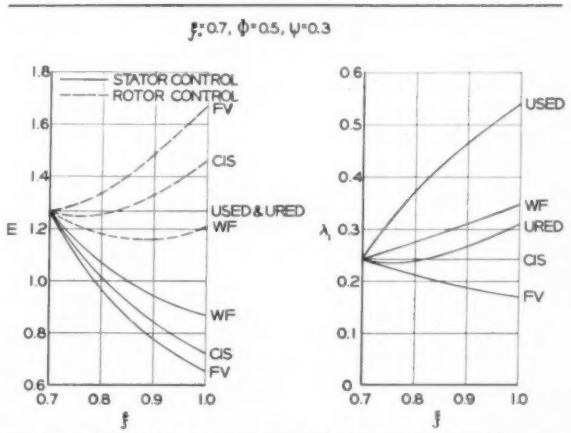

FIG. 6. Comparison of blade types with equal root conditions—$R_0 = 0.5$.

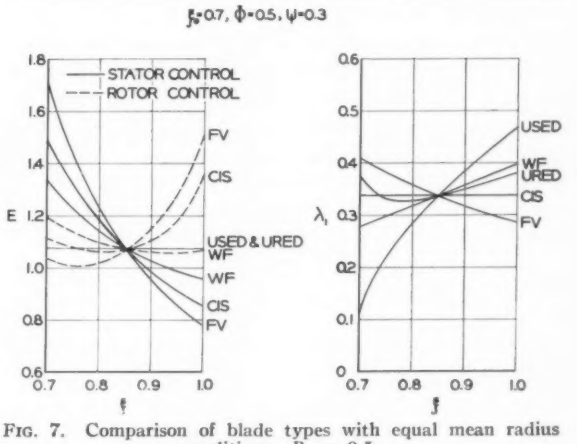

FIG. 7. Comparison of blade types with equal mean radius conditions—$R_m = 0.5$.

$$\lambda_1 = \{E_S\phi[\xi - (\psi/2\xi)] - \phi^2\}^{1/2} \quad (29)$$

and for uniform rotor control effectiveness distribution (URED) by

$$\lambda_1 = \xi - \frac{\psi}{4\xi} - \left[E_R\phi\left(\xi - \frac{\psi}{2\xi}\right) - \phi^2\right]^{1/2} \quad (30)$$

where E_S and E_R are selected constants.

Plots of the spanwise effectiveness distributions for both rotor- and stator-blade control with the stage types considered are shown in Figs. 6 and 7. The rotor inlet spin components are also indicated for comparisons. In Fig. 6, the appropriate constants have been selected such as to produce a symmetrical velocity diagram at the blade root section. The overall effectiveness of these stages is seen to vary appreciably, and a further comparison, with a symmetrical diagram at mean radius, is shown in Fig. 7.

The examples of blade control in conventional axial-flow compressor stages show that the control effectiveness is, in general, nonuniformly distributed over the blade span. For wide departure from design conditions, the flow pattern will be influenced by such conditions as radial unbalance and possible secondary flow development. These effects will be most predominant in blade types that exhibit highly nonuniform distribution of blade control effectiveness here. Certain additional qualitative information may be deduced from the investigations by application of simple radial unbalance considerations.

All cases of stator-blade control, shown in Fig. 7 for conventional diagrams, indicate an effectiveness distribution such that maximum values are obtained at the blade root sections. Thus, for an increase of flow, the axial velocity profiles will tend to peak at the hub and reduce the aerodynamic loading of these root elements. Consideration of radial equilibrium effects indicates that the flow will then readjust itself such that these excess axial velocities will be reduced somewhat and the stage energy addition will contain some positive radial gradient. This positive energy gradient is in the direction of increased flow stability.[5] Similar stator-blade adjustment for decreased flow will produce an opposite effect, leading to flow starvation at the hub elements, negative radial energy gradient, and possible instability. These effects may persist and result in reduction of the attainable pressure rise and operating range at less than design flow.

Rotor-blade adjustment is seen to produce a more nearly uniform distribution of blade-control effectiveness than corresponding stator-blade adjustment for the conventional-stage types considered. In some cases, stator and rotor control complement one another to some extent, and a method of combination control could be employed to provide an essentially uniform distribution of the combined blade-control effectiveness.

While both types of blading for uniform blade-control effectiveness differ from those in conventional use, the required flow patterns do not appear unduly radical. This is particularly true of the uniform rotor-control diagram, which appears to resemble a combination of free-vortex and wheel flow characteristics. Since radial unbalance and limit loading conditions were not considered, further comparison of stage types should include such effects.

Conclusions

From considerations of the blade-control effectiveness of a grid element, it is indicated that high effectiveness values may be attained by use of high values of flow and pressure coefficients. Volume control by either rotor- or stator-blade adjustment produces symmetrical behavior of the control effectiveness about a 50 per cent reaction ratio axis. Low reaction ratios should be used for stator-blade control and high values for corresponding rotor adjustment.

The radial distribution of blade-control effectiveness in several conventional-stage diagrams is shown to be generally nonuniform. In all cases of stator-blade control and in some instances with rotor-blade control, the effectiveness is a maximum at the blade roots. This spanwise distribution is somewhat more uniform in the case of rotor-blade control. Special stage types for uniform distribution of stator- or rotor-blade control effectiveness do not appear unduly extreme and further analysis to include radial unbalance and loading limitations is suggested.

References

[1] Wattendorf, F. L., *Simplified Design Comparisons of Axial Compressors*, Journal of the Aeronautical Sciences, Vol. 18, No. 7, p. 447, July, 1951.

[2] Bowen, John T., Saversky, Rolf H., and Rannie, W. D., *Theoretical and Experimental Investigation of Axial Flow Compressors*, USN Contract No. N6-OR-102, January, 1949.

[3] Wu, Chung Hua, and Wolfenstein, *Application of Radial Equilibrium Condition to Axial Flow Compressor and Turbine Design*, N.A.C.A. T.N. No. 1795, January, 1949.

[4] Weske, J. R., Rubin, B. F., and Gardiner, F. J., *Theory for Design of Axial Flow Compressors*, Chrysler Corporation Engineering Division, TR No. A-61805.57, 1945.

[5] Weske, J. R., *A Criterion of Radial Stability of Flow in Passages of Circular or Annular Cross Sections*, unpublished, 1946.

Generalized Theory of Convective Heat Transfer in a Free-Molecule Flow*

A. K. OPPENHEIM†

University of California at Berkeley

ABSTRACT

The theoretical analysis of convective heat transfer in a free-molecule flow with Maxwellian velocity distribution is generalized by reducing all relationships to a form common to all gases irrespective of their molecular structure. A simplified computing procedure is set up, and the heat-transfer characteristics of a flat plate, cylinder, and sphere are presented and correlated graphically. A method of applying these results to a cone and to compound shapes is described.

NOMENCLATURE

c_p = specific heat capacity at constant pressure, (ft.lbs.)/(lb.sec.²/ft.)°F.

c_v = specific heat capacity at constant volume, (ft.lbs.)/(lb.sec.²/ft.)°F.

D = reference diameter, (ft.)

E = molecular energy transport rate, (ft.lbs./sec.)

e = molecular energy transport rate per unit surface area, (ft.lbs./ft.²sec.)

e = base of natural logarithms 2.7183

$erfs$ = error function, $\frac{2}{\sqrt{\pi}}\int_0^s e^{-x^2}\,dx$, (dimensionless)

$erfcs$ = complementary error functions, $1 - erfs$, (dimensionless)

$\bar{F}$ = average surface integral defined by Eq. (2.13), $\frac{1}{S}\int_S f\,dS$, (see $\bar{Q}$)

$\bar{G}$ = average surface integral defined by Eq. (2.14), $\frac{1}{S}\int_S g\,dS$, (see $\bar{Q}$)

h = heat-transfer coefficient, $\bar{Q}/(T_w - T_{aw})$, (ft.lbs./ft.²sec. °F.)

$I_0(s)$ = modified Bessel function of first kind and zeroth order, $\frac{1}{\pi}\int_0^\pi e^{-s\cos\phi}\,d\phi$, (dimensionless)

$I_1(s)$ = modified Bessel function of first kind and first order, $-\frac{1}{\pi}\int_0^\pi e^{-s\cos\phi}\cos\phi\,d\phi$, (dimensionless)

$ierfcs$ = integral of the complementary error function, $\int_s^\infty erfcx\,dx$, (dimensionless)

j = number of degrees of freedom, (dimensionless)

k = Boltzman constant $5.66.10^{-24}$ (ft.lb./molecule°F.)

M = Mach Number (dimensionless)

N = number of molecules per unit volume (molecules/ft.³)

Nu = Nusset Number hD/κ (dimensionless)

n = number of molecules striking unit surface area per unit time, (molecules/ft.²sec.)

Pr = Prandtl Number, $c_p\mu/\kappa$ (dimensionless)

Q = heat-transfer rate (ft.lbs./sec.)

$\bar{Q}$ = average heat-transfer rate per unit area, $\frac{1}{S}\int_S q\,dS$ (e.g., for a cylinder $\bar{Q}_c = \frac{1}{\pi}\int_{-\pi/2}^{\pi/2} q\,d\theta$; for a sphere $\bar{Q}_s = \frac{1}{2}\int_{-\pi/2}^{\pi/2} q\cos\theta\,d\theta$), (ft. lbs./ft.² sec.)

q = local heat-transfer rate per unit area, (ft.lbs./ft.²sec.)

Re = Reynolds Number, $DU\rho/\mu$, (dimensionless)

r = recovery factor, $(T_{aw} - T_0)/(T_s - T_0)$, (dimensionless)

S = surface area, (sq. ft.)

St = Stanton Number, $h/c_pU = Nu/RePr$, (dimensionless)

s = molecular speed ratio, $U/V_m = \sqrt{\gamma/2}\,M$, (dimensionless)

T = temperature, °R.

U = mass velocity, (ft. per sec.)

u = internal energy, (ft lbs./molecule)

V_m = most probable molecular speed, (ft. per sec.,

α = accommodation coefficient, $(e_i - e_r)/(e_i - e_w)$, (dimensionless)

γ = c_p/c_v, (dimensionless)

η = $U/V_m = s\sin\theta$, (dimensionless)

θ = angle of incidence, (deg.)

κ = thermal conductivity, [ft.lbs./(ft.²sec. °F./ft.)]

μ = viscosity, (lb. sec./ft.²)

ρ = density, (lbs.sec.²/ft.⁴)

τ = $(T_{aw}/T_0) - 1$, (dimensionless)

Φ = $(NV_m/2\sqrt{\pi})(e^{-\eta^2}/2)$ (molecules/ft.² sec.)

ψ = $1 + \frac{e^{-\eta^2} + (3/2)\sqrt{\pi}\eta(1 + erf\eta)}{e^{-\eta^2} + \sqrt{\pi}\eta(1 + erf\eta)}$ (dimensionless)

Subscripts

aw = adiabatic wall (equilibrium) condition

F = front side of body with respect to flow direction

i = incident molecules

n = flat plate normal to flow direction

0 = free-stream condition

R = rear side of body with respect to flow direction

r = re-emitted molecules

s = stagnation condition

t = the translational energy

w = (incident) molecules at wall temperature condition

η = velocity component normal to surface

θ = flat plate at an angle of incidence

(1) INTRODUCTION

THE FREE-MOLECULE FLOW RÉGIME represents one of the few instances, besides some examples in laminar flow, where the convective heat-transfer

Received May 21, 1952.

* This work was done as part of an Office of Naval Research contract with the Department of Engineering, University of California at Berkeley.

† Assistant Professor of Mechanical Engineering.

characteristics can be deduced entirely from fundamental principles. To date, the expression for the heat-transfer rate to a plane surface exposed to a free-molecule stream with Maxwellian velocity distribution has been derived,[1] and the results integrated for, transverse flow past a circular cylinder[2] and for a sphere.[3] Furthermore, a satisfactory experimental check for the case of the cylinder has been demonstrated.[4]

In all the above-mentioned analyses, separate expressions were derived for a monatomic and a diatomic gas. While such a distinction is obviously necessary for practical applications, it does not have to be carried through in the analysis where the gas properties depending on the molecular structure can be represented by a suitable function of the number of degrees of freedom, j, or of the ratio of specific heats, γ. The results then become general as far as the molecular structure of the substance is concerned. Furthermore, by correlating the results for a few fundamental surface shapes, a basis is formed for a simple method of evaluating the heat-transfer characteristics for a great variety of surfaces. This is due to the fact that the results are functions of average values of integrals taken over the surface for which the heat-transfer characteristics are evaluated, and the integrands are the same for all surfaces. Consequently, the computation for any compound surface will consist in simply evaluating the average solution for the component fundamental shapes.

In this paper the theory of the convective heat transfer in a free-molecule flow in Maxwellian equilibrium is generalized and correlated in the sense indicated in the preceding paragraph. The results are applicable to a substance of any molecular structure and cover the range of all the extreme and simple surface shapes.

(2) Analysis

(2.1) *Energy Equation*

The convective heat transfer from a body in a free-molecular flow is governed by the energy balance,

$$q = e_r - e_i \tag{2.1}$$

where $q \equiv dQ/dS$ is the convective heat-transfer rate to the gas stream per unit surface area of the body, $e_i \equiv dE_i/dS$ is the energy transport rate of the incident molecules per unit surface area, and $e_r \equiv dE_r/dS$ is the energy transport rate of re-emitted molecules per unit surface area of the body.

Since the number of re-emitted molecules depends on the "accommodating" property of the surface, which can be determined only by experiment, the energy associated with these molecules is usually expressed by means of the accommodation coefficient defined as

$$\alpha \equiv (e_i - e_r)/(e_i - e_w) \tag{2.2}$$

where $e_w \equiv dE_w/dS$ and E_w is the flow rate of the energy that would be reflected from the surface if all the molecules were re-emitted with Maxwellian distribution at the body wall temperature. Eq. (2.1) then becomes

$$q/\alpha = e_w - e_i \tag{2.3}$$

Each of the energy terms appearing in the above equation consists of the translational energy plus that part of the internal energy which is due to other degrees of freedom than those associated with translational motion.

By the principle of equipartition, the internal energy of a gas molecule with j degrees of freedom in equilibrium at temperature T is $u = (j/2)kT$, where k is the Boltzman constant, and, since

$$\gamma \equiv \frac{c_p}{c_v} = \frac{(d/dT)(u+kT)}{(du/dT)} = 1 + \frac{2}{j}$$

one obtains

$$u = [1/(\gamma - 1)]kT.$$

Now, the translational energy of a molecule issuing from the wall at temperature T_w is $e_{tw} = 2nkT_w$—that is, 4/3 times as great as the mean translational energy of the gas in equilibrium at the same temperature.[5] Since the translational part of the internal energy of a gas in equilibrium is due to three degrees of freedom, it follows that

$$e_w = e_{tw} + \frac{j-3}{2} nkT_w = \frac{j+1}{2} nkT_w = \frac{\gamma+1}{2(\gamma-1)} nkT_w \tag{2.4}$$

where n is the number of molecules striking unit surface area of the wall per unit time.

Similarly, the energy transport rate of the incident molecules is

$$e_i = e_t + \frac{j-3}{2} nkT_0 = e_t + \frac{5-3\gamma}{2(\gamma-1)} nkT_0 \tag{2.5}$$

where $e_t \equiv dE_t/dS$ is the translational energy flow rate of the stream striking a unit surface area of the wall per unit time and T_0 is the free-stream temperature.

Introducing Eqs. (2.4) and (2.5) into Eq. (2.3) results in

$$\frac{1}{\alpha} q = \frac{j+1}{2} nkT_w - \left(e_t + \frac{j-3}{2} nkT_0\right) \tag{2.6}$$

or, in terms of γ,

$$\frac{1}{\alpha} q = \frac{\gamma+1}{2(\gamma-1)} nkT_w - \left[e_t + \frac{5-3\gamma}{2(\gamma-1)} nkT_0\right] \tag{2.7}$$

which, with the proper values of $j = 3$ or $\gamma = 5/3$ for a monatomic gas and $j = 5$ or $\gamma = 7/5$ for a diatomic gas, reduce readily to Eqs. (30) and (31) of reference 1 or Eqs. (1) and (2) of reference 3.

(2.2) *Average Heat-Transfer Rate*

In order to determine the heat-transfer rate from a given body, expressions for the number of molecules striking a unit surface area per unit time, n, and for the flow rate of translational energy, e_t, must be introduced into Eq. (2.6) and the equation integrated over the body surface. The expressions are as follows:

$$n = \frac{NV_m}{2\sqrt{\pi}} [e^{-\eta^2} + \sqrt{\pi}\,\eta(1 + erf\eta)] \tag{2.8}$$

$$e_t = \left\{[s^2 + (5/2)]n - \Phi\right\} kT_0 \tag{2.9}$$

where N is the number of molecules per unit volume; V_m is the most probable molecular speed; $\eta \equiv U_\eta/V_m$, U_η being the component normal to wall of the mass flow velocity U; $s \equiv U/V_m = \sqrt{\gamma/2}\,M$ is the so-called molecular speed ratio, which is related directly, as shown, to the Mach Number, M; and

$$\Phi \equiv (NV_m/4\sqrt{\pi})e^{-\eta^2} \tag{2.10}$$

The derivation of Eq. (2.8) is described in reference 6, while an equation equivalent to Eq. (2.9) was obtained by Stalder and Jukoff in reference 1. In the latter, e_t is expressed in terms of a function ψ (see nomenclature), which has been here replaced by a somewhat simpler function Φ, defined by Eq. (2.10).

By the substitution of Eqs. (2.8) and (2.9) for n and e_t, Eq. (2.7) becomes

$$\frac{1}{\alpha} q = \frac{\gamma + 1}{2(\gamma - 1)} nkT_w - \left[\left(s^2 + \frac{\gamma}{\gamma - 1}\right) n - \Phi\right] kT_0 \tag{2.11}$$

or, in a nondimensional form,

$$\frac{q}{\alpha nkT_0 U} = \frac{\gamma + 1}{2(\gamma - 1)} \frac{n}{NV_m s} \frac{T_w}{T_0} - \left(s^2 + \frac{\gamma}{\gamma - 1}\right) \frac{n}{NV_m s} + \frac{\Phi}{NV_m s} \tag{2.12}$$

The integration of the above equation is performed most conveniently by evaluating first the following average surface integrals:

$$\bar{G} \equiv \frac{1}{S}\int_S \frac{e^{-\eta^2}}{2\sqrt{\pi}s}\, dS \tag{2.13}$$

$$\bar{F} \equiv \frac{1}{S}\int_S \frac{\eta(1 + erf\eta)}{2s}\, dS \tag{2.14}$$

S denoting the surface area of the body under question. Then Eq. (2.12) yields

$$\frac{\bar{Q}}{\alpha NkT_0 U} = \frac{\gamma + 1}{2(\gamma - 1)} (\bar{G} + \bar{F}) \frac{T_w}{T_0} - \left(s^2 + \frac{\gamma}{\gamma - 1}\right) (\bar{G} + \bar{F}) + \frac{1}{2}\bar{G} \tag{2.15}$$

where

$$\bar{Q} \equiv \frac{1}{S}\int_S q\, dS$$

is the average heat-transfer rate by convection per unit surface area. It might be of interest here to note that $\bar{G}$ and $\bar{F}$ are related to the function χ, used in reference 1, as follows:

$$\bar{G} + \bar{F} = \frac{1}{S}\int_S \frac{\chi}{2\sqrt{\pi}s}\, dS$$

(2.3) *Heat Transfer Parameters*

All the essential results of the heat-transfer analysis in the free-molecule flow are most conveniently represented in terms of the Stanton Number, St, and the recovery factor, r. It is of interest to note that the relationships between these parameters and the Mach Number, M, can be again represented in a general manner for any gas independently of its molecular structure.

For $\bar{Q} = 0$, Eq. (2.15) yields the expression for the adiabatic wall (equilibrium) temperature to the free-stream temperature,

$$\frac{T_{aw}}{T_0} = 2\frac{\gamma - 1}{\gamma + 1}\left(\frac{\gamma}{\gamma - 1} + s^2 - \frac{1}{2}\frac{\bar{G}}{\bar{G} + \bar{F}}\right) \tag{2.16}$$ *

Introducing the above into Eq. (2.15) results in

$$\bar{Q} = \alpha \frac{\gamma + 1}{2(\gamma - 1)} (\bar{G} + \bar{F})(T_w - T_{aw}) NkU \tag{2.17}$$

and the Stanton Number

$$St \equiv \frac{h}{\rho c_p U} \equiv \frac{\bar{Q}}{(T_w - T_{aw})\rho c_p U} = \frac{\gamma + 1}{2\gamma}\, \alpha (\bar{G} + \bar{F}) \tag{2.18}$$

since

$$\frac{\gamma + 1}{2(\gamma - 1)} \frac{Nk}{\rho c_p} = \frac{\gamma + 1}{2(\gamma - 1)} \frac{c_p - c_v}{c_p} = \frac{\gamma + 1}{2\gamma}$$

It should also be noted that

$$St = \frac{Nu}{RePr} = \frac{9\gamma - 5}{4\gamma} \frac{Nu}{Re} \tag{2.19}$$

since, in the free-molecule régime, Eucken's expression for the Prandtl Number, Pr, in terms of γ is well justified. With Eq. (2.19), therefore, Eq. (2.18) can also be regarded as expressing the relationship between the Nusselt Number, Nu, the Reynolds Number, Re, and the Mach Number, M. The latter does not appear explicitly in Eq. (2.18), but, it should be remembered, the values of $\bar{G}$ and $\bar{F}$ are, for a given body geometry, only functions of the molecular speed ratio, s, or Mach Number.

Finally, by the use of Eq. (2.16), the recovery factor can be expressed as

* In integral form valid only, of course, if T_w is constant over the body surface—i.e., if the body conductivity is infinite.

TABLE 1

CONVECTIVE HEAT TRANSFER CHARACTERISTICS OF FREE MOLECULE FLOW PAST A FLAT PLATE, A SPHERE AND A TRANSVERSE CIRCULAR CYLINDER

FLOW SYSTEM	PARA-METER	FORMULA	$S = \sqrt{\frac{\gamma}{2}}\,M$												
			0	0.2	0.4	0.6	0.8	1.0	1.2	1.6	2	3	4	5	∞
	$\bar{G}$	$\frac{1}{2\sqrt{\pi}S}$ $(\bar{F}=0)$	∞	1.4105	0.7052	0.4702	0.3526	0.2821	0.2351	0.1763	0.1410	0.0940	0.0705	0.0564	0
	$\frac{1}{\alpha}\frac{\gamma}{\gamma+1}St$	$\frac{1}{4\sqrt{\pi}S}$ $(\frac{\gamma+1}{\gamma}r=2)$	∞	0.7052	0.3526	0.2351	0.1763	0.1411	0.1175	0.0882	0.0705	0.0470	0.0353	0.0282	0
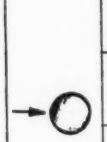	$\bar{G}$	$\frac{1}{4S^2}\,erfs$	∞	1.3919	0.6694	0.4193	0.2899	0.2107	0.1580	0.0953	0.0622	0.0278	0.0155	0.010	0
	$\bar{F}$	$\frac{1}{4}\left[1+\frac{1}{S}ierfcs-\frac{1}{2S^2}erfs\right]$	0	0.0373	0.0729	0.1053	0.1335	0.1572	0.1764	0.2032	0.2190	0.2361	0.243	0.246	0.2500
	$\frac{1}{\alpha}\frac{\gamma}{\gamma+1}St$	$\frac{1}{8}\left[1+\frac{1}{S}ierfcs+\frac{1}{2S^2}erfs\right]$	∞	0.7146	0.3711	0.2623	0.2117	0.1640	0.1672	0.1493	0.1406	0.1319	0.129	0.128	0.1250
	$\frac{\gamma+1}{\gamma}r$	$\frac{(2S^2+1)(1+\frac{1}{S}ierfcs)+(1-\frac{1}{2S^2})erfs}{S^2\left[1+\frac{1}{S}ierfcs+\frac{1}{2S^2}erfs\right]}$	2.6667	2.6551	2.6140	2.5575	2.4927	2.4273	2.3663	2.2659	2.1947	2.0994	2.059	2.038	2.0000
	$\bar{G}$	$\frac{1}{2\sqrt{\pi}S}e^{-\frac{S^2}{2}}\,I_0\left(\frac{S^2}{2}\right)$	∞	1.3827	0.6521	0.3959	0.2627	0.1820	0.1297	0.0713	0.0435	0.0183	0.0101	0.0064	0
	$\bar{F}$	$\frac{1}{2\sqrt{\pi}}Se^{-\frac{S^2}{2}}\left[I_0\left(\frac{S^2}{2}\right)+I_1\left(\frac{S^2}{2}\right)\right]$	0	0.0559	0.1085	0.1553	0.1947	0.2261	0.2501	0.2803	0.2955	0.3090	0.3132	0.3151	0.3183
	$\frac{1}{\alpha}\frac{\gamma}{\gamma+1}St$	$\frac{e^{-\frac{S^2}{2}}}{4\sqrt{\pi}}\left\{\frac{1}{S}I_0\left(\frac{S^2}{2}\right)+S\left[I_0\left(\frac{S^2}{2}\right)+I_1\left(\frac{S^2}{2}\right)\right]\right\}$	∞	0.7193	0.3745	0.2756	0.2287	0.2040	0.1899	0.1758	0.1695	0.1636	0.1617	0.1608	0.1592
	$\frac{\gamma+1}{\gamma}r$	$\frac{(2S^2+3)\,I_0\left(\frac{S^2}{2}\right)+(2S^2+1)\,I_1\left(\frac{S^2}{2}\right)}{(S^2+1)\,I_0\left(\frac{S^2}{2}\right)+S^2\,I_1\left(\frac{S^2}{2}\right)}$	3.0000	2.9708	2.8916	2.7826	2.6651	2.5541	2.4572	2.3115	2.2179	2.1049	2.0805	2.0392	2.0000
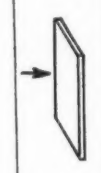	$\bar{G}$	$\frac{1}{4\sqrt{\pi}S}e^{-S^2}$	∞	1.3552	0.6010	0.3280	0.1859	0.1038	0.0557	0.0136	0.0026				0
	$\bar{F}$	$\frac{erfs}{2}$	0	0.1114	0.2142	0.3019	0.3711	0.4214	0.4552	0.4882	0.4977				0.5000
	$\frac{1}{\alpha}\frac{\gamma}{\gamma+1}St$	$\frac{1}{4\sqrt{\pi}S}\left[e^{-S^2}+\sqrt{\pi}S\,erfs\right]$	∞	0.7333	0.4076	0.3150	0.2785	0.2626	0.2554	0.2509	0.2501				0.2500
	$\frac{\gamma+1}{\gamma}r$	$\frac{2Se^{S^2}+(2S^2+1)\sqrt{\pi}\,erfs}{S(e^{-S^2}+\sqrt{\pi}S\,erfs)}$	4.0000	3.8982	3.6423	3.3314	3.0341	2.8024	2.6187	2.3600	2.2487	2.1111	2.06	2.04	2.0000

	$\frac{\gamma+1}{\gamma} r_F$	$\frac{s(e^{-S^2}+\sqrt{\pi}\,s\,\mathrm{erfs})}{s(e^{-S^2}+\sqrt{\pi}\,s\,\mathrm{erfs})}$	4.0000	3.8982	3.6423	3.3314	3.0341	2.8024	2.6187	2.3800	2.2487	2.1111	2.06	2.04	2.0000

TABLE 2

CONVECTIVE HEAT TRANSFER CHARACTERISTICS OF THE FRONT SIDE OF A SPHERE, A TRANSVERSE CIRCULAR CYLINDER AND A FLAT PLATE IN A FREE MOLECULE FLOW

FLOW SYSTEM	PARAMETER	FORMULA	$S=\sqrt{\frac{\gamma}{2}}\,M$												
			0	0.2	0.4	0.6	0.8	1.0	1.2	1.6	2	3	4	5	∞
	$\bar{F}_F$	$\bar{F}+\frac{1}{4}=\frac{1}{4}\left[2+\frac{1}{S}\,\mathrm{ierfc}\,s-\frac{1}{2S^2}\,\mathrm{erfs}\right]$	0.2500	0.2873	0.3229	0.3553	0.3835	0.4072	0.4264	0.4532	0.4690	0.4861	0.493	0.496	0.5000
	$\frac{1}{\alpha}\frac{\gamma}{\gamma+1}St_F$	$\frac{1}{\alpha}\frac{\gamma}{\gamma+1}St+\frac{1}{8}=\frac{1}{8}\left[2+\frac{1}{S}\,\mathrm{ierfc}\,s+\frac{1}{2S^2}\,\mathrm{erfs}\right]$	∞	0.8396	0.4961	0.3673	0.3367	0.3090	0.2922	0.2743	0.2656	0.2569	0.2543	0.253	0.2500
	$\frac{\gamma+1}{\gamma} r_F$	$\frac{(2S^2+1)(2+\frac{1}{S}\,\mathrm{ierfc}\,s)+(1-\frac{1}{2S^2})\,\mathrm{erfs}}{S^2+\frac{1}{S}\,\mathrm{ierfc}\,s+\frac{1}{2S^2}\,\mathrm{erfs}}$	∞	6.2773	4.0338	3.2741	2.8898	2.6590	2.5067	2.3228	2.2207	2.1051	2.0606	2.039	2.0000
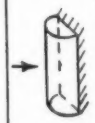	$\bar{F}_F$	$\bar{F}+\frac{1}{\pi}=\frac{e^{-\frac{S^2}{2}}}{2\sqrt{\pi}}\left\{\frac{2}{\sqrt{\pi}}e^{\frac{S^2}{2}}+S\left[I_0(\frac{S^2}{2})+I_1(\frac{S^2}{2})\right]\right\}$	0.3183	0.3742	0.4268	0.4736	0.5130	0.5444	0.5684	0.5986	0.6138	0.6273	0.6315	0.6334	0.6366
	$\frac{1}{\alpha}\frac{\gamma}{\gamma+1}St_F$	$\frac{1}{\alpha}\frac{\gamma}{\gamma+1}St+\frac{1}{2\pi}=\frac{e^{-\frac{S^2}{2}}}{4\sqrt{\pi}S}\left\{\frac{2S}{\sqrt{\pi}}e^{\frac{S^2}{2}}+(S^2+1)I_0(\frac{S^2}{2})+I_1(\frac{S^2}{2})\right\}$	∞	0.8765	0.5337	0.4348	0.3879	0.3632	0.3491	0.3350	0.3287	0.3228	0.3208	0.3200	0.3183
	$\frac{\gamma+1}{\gamma} r_F$	$\frac{(2S^2+1)\frac{2}{\sqrt{\pi}}\frac{e^{\frac{S^2}{2}}}{S}+(2S^2+3)I_0(\frac{S^2}{2})+(2S^2+1)I_1(\frac{S^2}{2})}{\frac{2}{\sqrt{\pi}}S\,e^{\frac{S^2}{2}}+(S^2+1)I_0(\frac{S^2}{2})+S^2I_1(\frac{S^2}{2})}$	∞	7.3250	4.4724	3.5130	3.0335	2.7496	2.5653	2.3491	2.2335	2.1080	2.0615	2.0396	2.0000
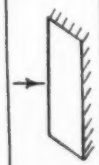	$\bar{F}_F$	$\bar{F}+\frac{1}{2}=\frac{1}{2}\left[1+\mathrm{erfs}\right]$	0.5000	0.6114	0.7142	0.8019	0.8711	0.9214	0.9552	0.9882	0.9977				1.0000
	$\frac{1}{\alpha}\frac{\gamma}{\gamma+1}St_F$	$\frac{1}{\alpha}\frac{\gamma}{\gamma+1}St+\frac{1}{4}=\frac{1}{4\sqrt{\pi}S}\left\{e^{-S^2}+\sqrt{\pi}S\left[1+\mathrm{erfs}\right]\right\}$	∞	0.9833	0.6576	0.5650	0.5285	0.5126	0.5054	0.5009	0.5001				0.5000
	$\frac{\gamma+1}{\gamma} r_F$	$\frac{2Se^{-S^2}+(2S^2+1)\sqrt{\pi}\,(1+\mathrm{erfs})}{S\left\{e^{-S^2}+\sqrt{\pi}S\left[1+\mathrm{erfs}\right]\right\}}$	∞	9.7720	5.3941	3.9714	3.2878	2.8988	2.6562	2.3853	2.2494	2.1111	2.06	2.04	2.0000

TABLE 3

CONVECTIVE HEAT TRANSFER CHARACTERISTICS OF THE REAR SIDE OF A SPHERE, A TRANSVERSE CIRCULAR CYLINDER AND A FLAT PLATE IN A FREE MOLECULE FLOW

FLOW SYSTEM	PARAMETER	FORMULA	$S = \sqrt{\frac{\gamma}{2}}\,M$ = 0	0.2	0.4	0.6	0.8	1.0	1.2	1.6	2	3	4	5	∞
	$\bar{F}_R$	$\bar{F}-\frac{1}{4}=\frac{1}{4}\left[\frac{1}{S}\,\mathrm{ierfcs}-\frac{1}{2S^2}\,\mathrm{erfs}\right]$	-0.2500	-0.2127	-0.1771	-0.1447	-0.1165	-0.0928	-0.0736	-0.0468	-0.0310	-0.0139	-0.007	-0.004	0
	$\frac{1}{\alpha}\frac{\gamma}{\gamma+1}St_R$	$\frac{1}{\alpha}\frac{\gamma}{\gamma+1}St-\frac{1}{\theta}=\frac{1}{\theta}\left[\frac{1}{S}\,\mathrm{ierfcs}+\frac{1}{2S^2}\,\mathrm{erfs}\right]$	∞	0.5896	0.2461	0.1373	0.0867	0.0590	0.0422	0.0243	0.0153	0.0069	0.0043	0.003	0
	$\frac{\gamma+1}{\gamma}r_R$	$\frac{(2S^2+1)\frac{\mathrm{ierfcs}}{S}+\left(1-\frac{1}{2S^2}\right)\mathrm{erfs}}{S^2+\frac{1}{S}\,\mathrm{ierfcs}+\frac{1}{2S^2}\,\mathrm{erfs}}$	-∞	-2.5095	-0.2483	-0.5362	0.9502	1.2129	1.3944	1.6231	1.7516	1.890	1.937	1.960	2
	$\bar{F}_R$	$\bar{F}-\frac{1}{\pi}=\frac{e^{-\frac{S^2}{2}}}{2\sqrt{\pi}}\left\{S\left[I_0\left(\frac{S^2}{2}\right)+\left(\frac{S}{S}\right)^2\right]-\frac{2}{\sqrt{\pi}}e^{\frac{S^2}{2}}\right\}$	-0.3183	-0.2624	-0.2098	-0.1630	-0.1236	-0.0922	-0.0682	-0.0380	-0.0228	-0.0093	-0.005i	-0.0032	0
	$\frac{1}{\alpha}\frac{\gamma}{\gamma+1}St_R$	$\frac{1}{\alpha}\frac{\gamma}{\gamma+1}St-\frac{1}{2\pi}=\frac{e^{-\frac{S^2}{2}}}{4\pi S}\left\{(S^2+1)I_0\left(\frac{S^2}{2}\right)+I_1\left(\frac{S^2}{2}\right)-\frac{2S}{\sqrt{\pi}}e^{\frac{S^2}{2}}\right\}$	∞	0.5601	0.2153	0.1164	0.0695	0.0446	0.0307	0.0166	0.0103	0.0044	0.0025	0.0016	0
	$\frac{\gamma+1}{\gamma}r_R$	$\frac{(2S^2+1)\frac{2}{2\sqrt{\pi}}\frac{e^{\frac{S^2}{2}}}{S}-(2S^2+3)I_0\left(\frac{S^2}{2}\right)-(2S^2+1)I_1\left(\frac{S^2}{2}\right)}{\frac{2}{\sqrt{\pi}}\frac{e^{\frac{S^2}{2}}}{S}-(S^2+1)I_0\left(\frac{S^2}{2}\right)-S^2I_1\left(\frac{S^2}{2}\right)}$	-∞	-3.8555	-0.9646	-0.0559	0.8116	0.9733	1.2299	1.5542	1.7246	1.8852	1.9362	1.960	2
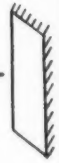	$\bar{F}_R$	$\bar{F}-\frac{1}{2}=-\frac{\mathrm{erfcs}}{2}$	-0.5000	-0.3887	-0.2858	-0.1981	-0.1290	-0.0787	-0.0448	-0.0118	-0.0024				0
	$\frac{1}{\alpha}\frac{\gamma}{\gamma+1}St_R$	$\frac{1}{\alpha}\frac{\gamma}{\gamma+1}St\frac{1}{4}=\frac{1}{4\sqrt{\pi}S}\left\{e^{-S^2}-\sqrt{\pi}S\,\mathrm{erfcs}\right\}$	∞	0.4833	0.1576	0.0650	0.0285	0.0126	0.0054	0.0009	0.0001				0
	$\frac{\gamma+1}{\gamma}r_R$	$\frac{2Se^{-S^2}-(2S^2+1)\sqrt{\pi}\,\mathrm{erfcs}}{S\left\{e^{-S^2}-\sqrt{\pi}S\,\mathrm{erfcs}\right\}}$	-∞	-8.0528	-3.6678	-2.2339	-1.5361	-1.1297	-0.8675	-0.5664	-0.3925	-0.197	-0.116	-0.078	0

$$r \equiv \frac{T_{aw} - T_0}{T_s - T_0} = \frac{\gamma}{\gamma + 1}\left(2 + \frac{1}{s^2}\frac{\bar{F}}{\bar{G} + \bar{F}}\right) \quad (2.20)^*$$

since the ratio of the stagnation temperature T_s to the free-stream temperature T_0 is

$$\frac{T_s}{T_0} = 1 + \frac{\gamma - 1}{2} M^2 = 1 + \frac{\gamma - 1}{\gamma} s^2$$

It is obvious from Eqs. (2.18) and (2.20) that, in order to represent the results of the analysis in a general form independent of the molecular structure of the substance, one should express the results in terms of $[\gamma/(\gamma + 1)]St$ instead of St and in terms of $[(\gamma + 1) \div \gamma]r$ instead of r. It is of some interest to note here that the product of the Stanton Number and the recovery factor is independent of the molecular structure of the substance.

(3) Discussion

(3.1) Results

According to the method developed in the preceding section, the analysis of the convective heat transfer in a free-molecular flow consists of computing first the values of $\bar{G}$ and $\bar{F}$ defined by Eqs. (2.13) and (2.14) and then determining

* In integral form valid only, of course, if T_w is constant over the body surface—i.e., if the body conductivity is infinite.

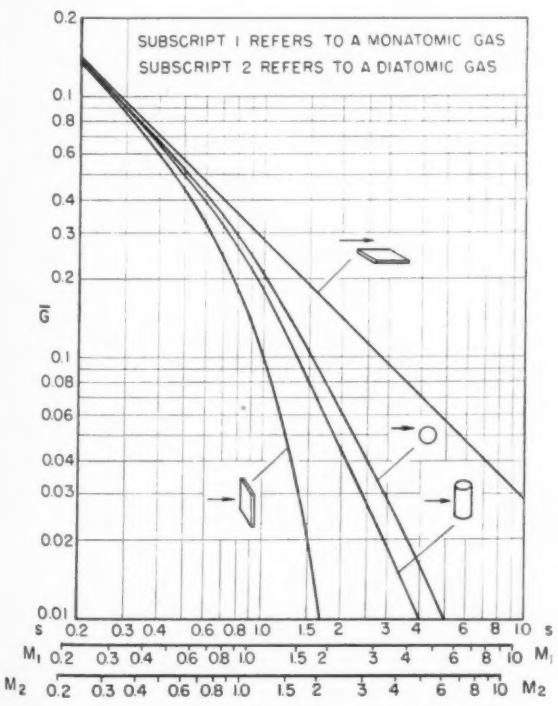

Fig. 1. Average surface integral $\bar{G}$ as a function of the molecular speed ratio (and the Mach Number) for a flat plate, a sphere, and a transverse circular cylinder.

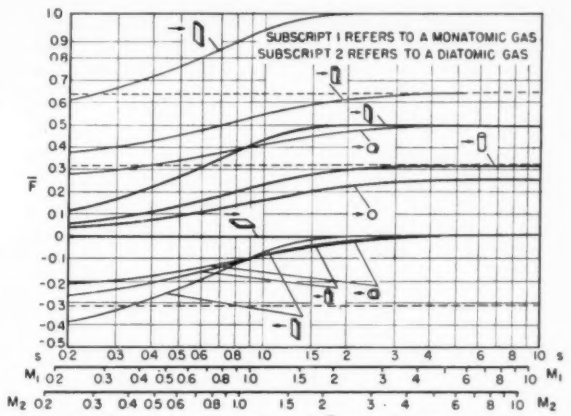

Fig. 2. Average surface integral $\bar{F}$ as a function of the molecular speed ratio (and the Mach Number) for a flat plate, a sphere, and a transverse circular cylinder.

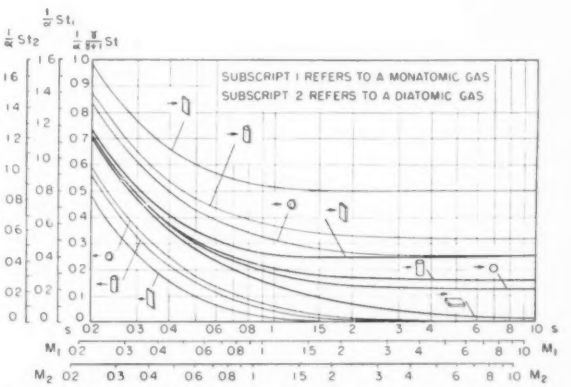

Fig. 3. Stanton Number for a flat plate, a sphere, and a transverse circular cylinder in a free-molecule flow.

$$\frac{1}{\alpha}\frac{\gamma}{\gamma + 1} St = \frac{1}{\alpha}\frac{9\gamma - 5}{4(\gamma + 1)}\frac{Nu}{Re} = \frac{\bar{G} + \bar{F}}{2} \quad (3.1)$$

$$\frac{\gamma + 1}{\gamma} r = 2 + \frac{1}{s^2}\frac{\bar{F}}{\bar{G} + \bar{F}} \quad (3.2)$$

This has been done for a flat plate, a sphere, and a transverse flow past a circular cylinder. The algebraic and numerical results are represented in tabular form and are plotted as a function of the molecular speed ratio and the free-stream Mach Number for a monatomic gas (subscript 1) and a diatomic gas (subscript 2).

Table 1 represents the results concerned with the flow around the objects under investigation, Table 2 represents the results referred to their front side only, and Table 3 represents those of their rear side with respect to the mass flow direction. Fig. 1 represents the plot of the average surface integral $\bar{G}$; Fig. 2, that of $\bar{F}$; Fig. 3, the Stanton Number; Fig. 4, the recovery factor; and Fig. 5, the ratio of the adiabatic wall (equilibrium) temperature, T_{aw}, to the free stream temperature, T_0. The abscissa of all the diagrams is the molecular speed ratio, s, with a superimposed scale for the Mach Number, M.

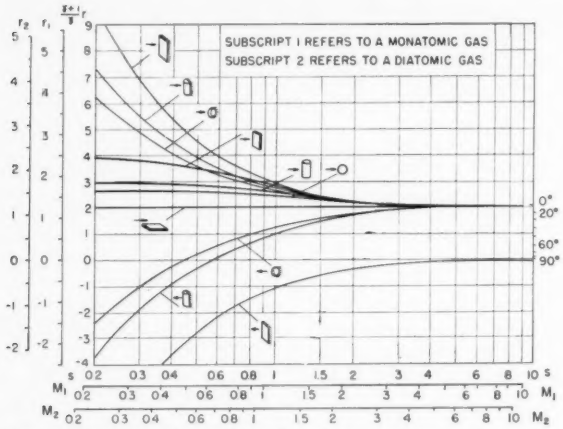

FIG. 4. Recovery factor for a flat plate, a sphere, and a transverse circular cylinder in a free-molecule flow.

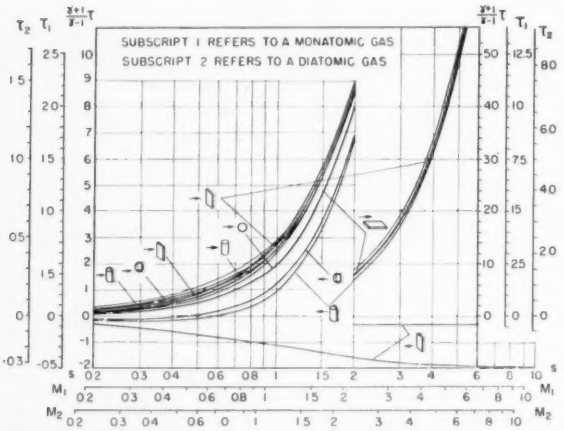

FIG. 5. Ratio of the adiabatic wall temperature and the free-stream temperature for a flat plate: a sphere, and a transverse circular cylinder in a free-molecule flow [$\tau \equiv (T_{aw}/T_0) - 1$].

The only odd function in the expressions for $\bar{G}$ and $\bar{F}$, Eqs. (2.13) and (2.14), is the first term of the $\bar{F}$ function—namely,

$$\frac{1}{S}\int_S \frac{\eta}{2s}\, dS = \frac{1}{2S}\int_S \sin\theta\, dS$$

where θ is the local angle of incidence. The value of the average integral $\bar{G}$ is therefore the same for the whole object as for its front or rear side only; consequently, the values of this parameter have not been repeated in Tables 2 and 3, and the four curves plotted in Fig. 1 apply to all the cases under consideration. For the case of the flat plate parallel to the flow direction, $\bar{F} = 0$, the heat-transfer characteristics are the same for both sides as for each side separately; consequently, this case has not been repeated in Tables 2 and 3. Furthermore, since the values of the odd term, as shown above, are independent of the molecular speed ratio, the value of $\bar{F}$ for one side of the object differs only by a constant from that for the whole object, for all values of s. By virtue of the same argument and from Eq. (2.18), it follows that the Stanton Number has the same property.

The effect of shape on the Stanton Number decreases with the decreasing values of the molecular speed ratio (or Mach Number), and, for small values of s, the Stanton Number approaches the value of $[(\gamma + 1)/\gamma] \div (\alpha/4\sqrt{\pi}s)$. Although, for large values of s, the shape effect is evident, for high enough values of this parameter (say $s > 2$) the variation of the Stanton Number for an object of any shape exposed to the free stream cannot exceed the value of $[(\gamma + 1)/4\gamma]\ \alpha$ [$(2/5)\ \alpha$ for a monatomic and $(3/7)\alpha$ for a diatomic gas], and the maximum possible local value of the Stanton Number at $s = \infty$ is $[(\gamma + 1)/2\gamma]\alpha$.

In contrast to the Stanton Number characteristics, the effect of shape on the recovery factor is most pronounced for small values of s. For large values of s the recovery factor for any surface shape, with the exception of the rear side of a flat plate, approaches rapidly the value of $2\gamma/(\gamma + 1)$ (5/4 for a monatomic and 7/6 for a diatomic gas), so that for $s \geqslant 5$ it is practically equal to this asymptote. The asymptotic value of r for the rear side of a flat plate normal to the flow direction is zero, while the corresponding asymptotes for the rear sides of plates at an angle of incidence lie between zero and $2\gamma/(\gamma + 1)$, as indicated on the right-hand side margin of Fig. 4.

The physical interpretation of this behavior of the recovery factor is not immediately clear. However, since the recovery factor serves only for the determination of the adiabatic wall temperature, T_{aw}, and is used only in conjunction with the Mach Number or the molecular speed ratio, the situation becomes clearer if one considers the ultimate result of the recovery factor application by observing the behavior of parameter τ, defined as

$$\tau \equiv \frac{T_{aw}}{T_0} - 1 = \frac{\gamma - 1}{\gamma} rs^2 \qquad (3.3)$$

which is plotted on Fig. 5. The ordinate of this diagram is expressed as $[(\gamma + 1)/(\gamma - 1)]\ \tau$ so that its value is simply equal to the product of corresponding ordinate of Fig. 4 and s^2 $\{$since $[(\gamma + 1)/(\gamma - 1)]\tau = [(\gamma + 1) \div \gamma]rs^2\}$. As evidenced by Fig. 5 and as should be expected, the effect of shape on the ratio of adiabatic wall temperature to free-stream temperature is small for low, as well as for high, values of the molecular speed ratio and is most pronounced in the vicinity of $s = 1$.

(3.2) *Applications*

Besides the shapes analyzed so far and indicated on the diagrams, the heat-transfer characteristics of a flat plate inclined at any angle of incidence, θ, to the flow direction can be easily found by extrapolating the results corresponding to the flat plate normal to flow, since, by Eqs. (2.13) and (2.14), respectively,

$$\bar{G}_\theta(s) = g_\theta(s) = \frac{e^{-\eta^2}}{2\sqrt{\pi}s} = \frac{\eta}{s}\frac{e^{-\eta^2}}{2\sqrt{\pi}\eta} = \sin\theta\,\bar{G}_n(\eta) \tag{3.4}$$

and, similarly,

$$\bar{F}_\theta(s) = f_\theta(s) = \sin\theta\,\bar{F}_n(\eta) \tag{3.5}$$

where $\eta = s\sin\theta$, subscript θ denotes the value of the parameter corresponding to the flat plate at an angle of incidence θ, and subscript n denotes that of the flat plate normal to flow direction.

From the above by virtue of Eqs. (3.1), (3.2), and (3.3), it follows that

$$St_\theta(s) = \sin\theta\,St_n(\eta) \tag{3.6}$$

$$r_\theta(s) = \frac{2\gamma}{\gamma+1}\cos^2\theta + \sin^2\theta\,r_n(\eta) \tag{3.7}$$

$$\tau_\theta(s) = \frac{2(\gamma-1)}{\gamma+1}s^2\cos^2\theta + \tau_n(\eta) \tag{3.8}$$

On the basis of these expressions and using the results presented here in tabular or graphical form, the heat-transfer characteristics for a flat plate at any angle of incidence can easily be computed. As an example for the front side of a flat plate at $\theta = 30°$ and $s = 2$,

$$\frac{1}{\alpha}\frac{\gamma}{\gamma+1}St = 0.5 \times 0.5126 = 0.2563$$

$$\frac{\gamma+1}{\gamma}r = 1.5 + 0.25 \times 2.8988 = 2.2247$$

since, from Table 2, for $\eta = 2 \times 0.5 = 1$,

$$\frac{1}{\alpha}\frac{\gamma}{\gamma+1}St_n(1) = 0.5126$$

$$\frac{\gamma+1}{\gamma}r_n(1) = 2.8988$$

Furthermore, it should be noted that the flat plate results apply to any surface with a constant angle of incidence—that is, the heat-transfer characteristics of a flat plate at an angle of incidence θ are the same as those corresponding to the axial flow past a wedge or a cone with θ as the semiapex angle—and the heat-transfer data of a flat plate tangent to the flow direction are the same as those for axial flow past a cylinder of any shape exposed to the free-molecular stream.

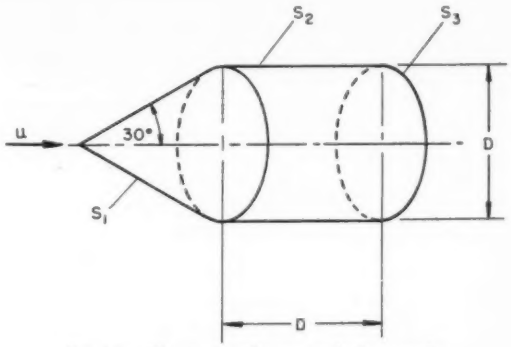

FIG. 6. Illustration for numerical example.

Finally, the results of the analysis can also be extrapolated to other surfaces by noting that, by virtue of Eqs. (2.13), (2.14), and (3.1),

$$St = (1/S)\sum St_i S_i \tag{3.9}$$

$$\frac{\gamma+1}{\gamma}r = 2 + \frac{1}{s^2}\frac{\sum\bar{F}_i S_i}{\sum\bar{G}_i S_i + \sum\bar{F}_i S_i} \tag{3.10}$$

where subscript i denotes the fundamental components of a given surface.

As an illustration, the preceding example is continued in order to find the heat-transfer characteristics of a simple body shown on Fig. 6 at $s = 2$. Basic values for computations are presented in Table 4, and the results are as follows:

$$\frac{1}{\alpha}\frac{\gamma}{\gamma+1}St = \frac{0.1987}{1.75} = 0.1135$$

$$\frac{\gamma+1}{\gamma}r = 2 + \frac{1}{2^2}\frac{0.22975}{0.1676+0.22975} = 2.1446$$

SUMMARY

The analysis of the convective heat transfer in a free-molecule flow with Maxwellian velocity distribution has been generalized by reducing all the relationships to a form common to all gases irrespective of their molecular structure. The heat-transfer characteristics of a number of simple surfaces consisting of a flat plate in the direction of flow, a flat plate normal to flow, a transverse cylinder, and a sphere have been computed and correlated. A simple method has been outlined for

TABLE 4

		1	2	3	4	5	6	7
		$S/(\pi)D^2$	$\bar{G}$	$\bar{F}$	St	$S\cdot\bar{G}$	$S\cdot\bar{F}$	$S\cdot St$
Symbol	Source:	Fig. 6	Table 1	Tables 2, 1, 3	Table 3, previous example	1·2	1·3	1·4
S_1	Front cone	0.5	0.0519	0.4607	0.2563	0.02595	0.23035	0.1282
S_2	Cylinder	1	0.1410	0	0.0705	0.1410	0	0.0705
S_3	Back plate	0.25	0.0026	−0.0024	0.0001	0.00065	−0.0006	0.0000
		Σ: 1.75				0.1676	0.22975	0.1987

extrapolation of the results to a flat plate at any angle of incidence, a wedge, or a cone and for the evaluation of heat transfer parameters for a compound surface.

The effect of shape on convective heat-transfer characteristics has been found to be small. At low Mach Numbers, the Stanton Number of all shapes approaches the value of

$$[(\gamma + 1)/\gamma] \cdot (\alpha/4\sqrt{\pi s})$$

The difference between various shapes becomes more distinct at high Mach Numbers. For $M > 2$, the magnitude of the Stanton Number cannot exceed the value of $[(\gamma + 1)/2\gamma]\alpha$. The effect of shape on the recovery factor is more distinct at low Mach Numbers and becomes hardly noticeable for Mach Numbers higher than 5. For the temperature ratio, T_{aw}/T_0, this effect is small for both low and high Mach Numbers and is most noticeable in the vicinity of Mach Number unity.

References

[1] Stalder, J. R., and Jukoff, D., *Heat Transfer to Bodies Traveling at High Speed in the Upper Atmosphere*, Journal of the Aeronautical Sciences, Vol. 15, No. 7, pp. 381–391, July, 1948 (N.A.C.A. Report No. 944, 1949).

[2] Stalder, J. R., Goodwin, G. C., and Creager, M. O., *A Comparison of Theory and Experiment for High-Speed Free-Molecule Flow*, N.A.C.A. T.N. No. 2244, December, 1950.

[3] Sauer, F. M., *Convective Heat Transfer from Spheres in a Free-Molecule Flow*, University of Calif., Engineering Projects Report HE-150-77, January 29, 1951. Also published in Journal of the Aeronautical Sciences, Vol. 18, No. 5, pp. 353–354, May, 1951.

[4] Stalder, J. R., Goodwin, G. C., and Creager, M. O., *Heat Transfer to Bodies in a High-Speed Rarefied-Gas Stream*, London Conference on Heat Transfer, A.S.M.E. Preprints, Section II, September, 1951. Also published as N.A.C.A. T.N. No. 2438 August, 1951.

[5] Kennard, E. H., *Kinetic Theory of Gases*, 1st Ed., p. 64; McGraw-Hill Book Company, Inc., New York, 1938.

[6] Tsien, H. S., *Superaerodynamics, Mechanics of Rarefied Gases*, Journal of the Aeronautical Sciences, Vol. 13, No. 1, pp. 653–664, December, 1946.

Proceedings

Third Anglo-American Aeronautical Conference

Now Available

Proceedings of the Joint Conference between The Royal Aeronautical Society and the Institute, held in Brighton in September, 1951, are now ready for distribution. These volumes contain all of the full-length papers and discussions presented at the Conference. Only a limited supply is available for distribution.

Order Direct from

The Royal Aeronautical Society

4 Hamilton Place — London, W. 1, England

Send remittance with order:
£5.5.0 ($14.80), postage prepaid.

(10% U.S. Customs Duty
Payable upon Receipt.)

Readers' Forum

BRIEF REPORTS of investigations in the aeronautical sciences and discussions of papers published in the JOURNAL are presented in this special department. Publication will be completed as soon as possible after receipt of the material. The Editorial Committee does not hold itself responsible for the opinions expressed by the correspondents. Contributions should not exceed 800 words in length.

A Rational Discussion of the Hydraulic Analogy

E. V. Laitone
Associate Professor, University of California at Berkeley
September 5, 1952

THIS NOTE IS AN ANSWER to reference 1, a comment on my paper[2] on the application of the hydraulic analogy to transonic flow studies. Reference 1 doubts my statement that the analogy is restricted to $^1/_4$-in. water depths since the group velocity, which is given by[3]

$$a = c - \lambda(dc/d\lambda) \tag{1}$$

approaches the wave velocity c as $\lambda \to \infty$. However, who can build an infinite model, much less move it?

For the analogy to hold, the group velocity must be equal to the wave velocity, as shown in reference 2. Now for ordinary finite wave lengths λ, we have $c > a$ for all $h > {}^1/_4$ in., as may be shown by neglecting the surface tension. Then the so-called wave velocity (which is actually only a phase, not a true propagation, velocity) is given approximately by

$$c = [(g\lambda/2\pi)\tanh(2\pi h/\lambda)]^{1/2} \tag{2}$$

Then, combining Eqs. (1) and (2) we have the ratio of the group velocity (a) to the wave velocity (c) given by

$$\frac{a}{c} = 1 - \frac{\lambda}{c}\left(\frac{dc}{d\lambda}\right) = \frac{1}{2}\left(1 + \frac{4\pi h/\lambda}{\sinh 4\pi h/\lambda}\right) \tag{3}$$

so that

$$a/c \to 1/2$$

for $h/\lambda \gg 1$ and

$$\left(\frac{a}{c}\right) \to \left[1 - \frac{1}{12}\left(\frac{4\pi h}{\lambda}\right)^2\right]$$

for $h/\lambda \ll 1$.

This proves that all $\lambda < 10h$ have a varying group velocity ranging from 50 to 80 per cent of the wave velocity. For example, a water depth of 1 in. requires that all the wave lengths less than 1 ft. be practically eliminated by using a sufficiently large model. However, making a *finite* wedge, no matter how sharp the nose angle, 1 ft. wide does not mean that only wave lengths over 1 ft. long have a significant influence on the flow pattern, *especially in the transonic case*. Consequently, the model would have to be enormous in size before the analogy became valid.

Comparing the effect of water depths over $^1/_4$ in. for the case of an attached oblique shock wave at the nose of a wedge does not even enter into a discussion of the effect of group velocity. This finite discontinuity is a hydraulic jump having a momentum discontinuity that has no direct relation to the group velocity defined by Eqs. (1) and (2). The group velocity is a potential-flow relationship that gives the analogy to a potential gas flow with $\gamma = 2$, while the hydraulic jump is an irreversible (nonpotential) finite discontinuity that does not have a direct analogy with a shock wave in a perfect gas. However, weak shock waves approach the potential-flow solution; consequently, the analogy is valid for weak discontinuities as occur in transonic flow or for very slender wedges. This again means that the water depth must be of the order of $^1/_4$ in.

It is interesting to note that reference 4, the same report as referred to in reference 1, shows that even the experimental data corresponding to finite oblique shocks are in much better agreement with a perfect gas having $\gamma = 2$ when the water depth is about $^1/_4$ in. (Fig. 8, reference 4). As a matter of fact, the author states on page 19 of reference 4 that the oblique shock angles measured in water compared most favorably with that for a perfect gas having $\gamma = 2$ when the water depth was 0.225 in.

References

[1] Randels, W. C., *Comments on "A Study of Transonic Gas Dynamics by the Hydraulic Analogy,"* Readers' Forum, Journal of the Aeronautical Sciences, Vol. 19, No. 8, p. 572, August, 1952.

[2] Laitone, E. V., *A Study of Transonic Gas Dynamics by the Hydraulic Analogy*, Journal of the Aeronautical Sciences, Vol. 19, No. 4, pp. 265–272, April, 1952.

[3] Lamb, H., *Hydrodynamics*, 6th Ed., p. 381; University Press, Cambridge, England, 1932.

[4] Bruman, J. R., *Application of the Water Channel-Compressible Gas Analogy*, North American Aviation, Inc., Report No. NA-47-87, March 3, 1947.

A Heat Cycle Low Reynolds Number Transonic Tunnel

Raymond L. Chuan
Graduate Student, Guggenheim Aeronautical Laboratory, California Institute of Technology, Pasadena, Calif.
August 11, 1952

A TRANSONIC WIND TUNNEL with low Reynolds Number flow designed to aid the study of viscous effects has been built at GALCIT. Using water vapor as the working fluid, the tunnel operates at Mach Numbers up to 1.8 and at Reynolds Numbers of about 5,000 per cm. The continuous operating closed return circuit tunnel has no mechanical compressor. The superheated vapor in the diffuser is condensed; the liquid flows under the influence of gravity to the stagnation chamber where it is evaporated and superheated. The pressure differential between diffuser and stagnation chamber ordinarily supplied by a mechanical compressor is maintained in the new tunnel by a simple difference in liquid level between these two chambers. The low stagnation chamber pressure (20 to 35 mm. Hg) and density (10^{-6} Gm. per cu.cm.) necessary to produce the desired Reynolds Number

would have necessitated operation at extremely low efficiency had a mechanical compressor been used.

For a tunnel with fixed Mach Number, test-section dimensions, and stagnation temperature, the mass flow decreases with the Reynolds Number, while the volume flow remains constant. Hence, if mechanical compressors are used, the physical size of the compressors remains about constant, and the power consumption of the compressors decreases more slowly than the mass flow. On the other hand, if the compression is done by a phase-change system, as in the new tunnel, the power consumption decreases with the mass flow. One advantage of a phase-change compression system for a low Reynolds Number transonic wind tunnel is then obvious: low power consumption.

This principle of using phase changes in the compression process was suggested to the author by Prof. H. W. Liepmann in the summer of 1950. The present water-vapor tunnel has accordingly been built, and the initial success indicates that the feasibility of wider application of the principle warrants further study. For instance, the application of the phase-change compression principle to hypersonic tunnels appears especially attractive since the extremely high compression ratio necessary for hypersonic Mach Numbers can be accomplished at nearly 100 per cent efficiency with leakproof, unlubricated liquid pumps.

Fig. 1 shows the complete tunnel. The stagnation pressure and temperature are regulated by two autotransformers controlling the power input to the electrical immersion heaters and superheaters. The nozzle has flexible walls controlled by two pairs of jacks and provisions for model mounts and traversing mechanisms. The condenser is driven by a refrigerator that rejects heat into cooling water, although power consumption could be reduced by rejecting part of the heat into the boiler. In addition to the conventional pressure switches on the refrigerator, a by-pass evaporator is provided for regulating the heat removal in the condenser. The difference in water levels between the condenser and the boiler makes up the pressure difference between the diffuser and the stagnation chamber.

Instrumentation consists of the following: silicone fluid manometers to measure pressure referred to the stagnation pressure; absolute pressure gage to measure stagnation pressure; dial-type thermometers to measure temperatures of the boiler, superheater, and condenser; and gage glasses for observing liquid levels. A two-mirror schlieren system, arranged with symmetry to minimze distortions, is used to detect shock waves with density gradients of the order of 10^{-4} Gm./cm.^{4}, which are about five orders of magnitude below those in corresponding shock waves in more conventional supersonic tunnels.

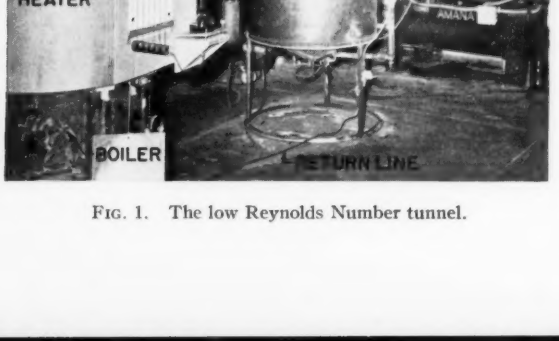

FIG. 1. The low Reynolds Number tunnel.

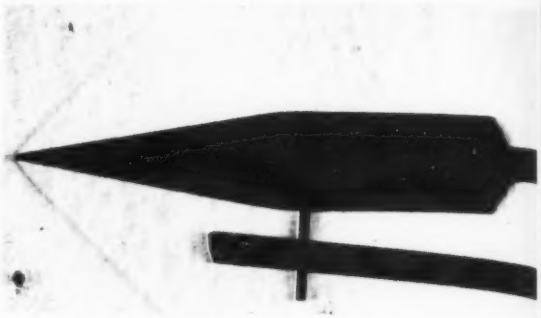

FIG. 2. Flow at $M = 1.7$ over a 20° wedge.

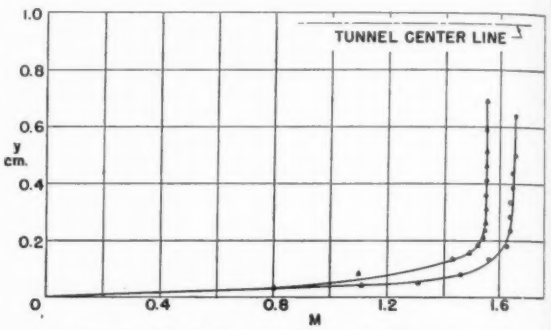

FIG. 3. Mach Number profiles in test section.

Typical operating data are as follows:

p_0 = stagnation pressure = 30 mm. Hg
T_0 = stagnation temperature = 180°C.
ρ_0 = stagnation density = 2×10^{-5} Gm. per cu.cm.
p = static pressure in test section = 6 mm. Hg
M = Mach Number = 1.7
ρ = static density = 5×10^{-6} Gm. per cu.cm.
λ = mean free path $\simeq 10^{-3}$ cm.
R_e = Reynolds Number = 4,500 per cm.
W = total power consumption = 7 kw.
A = test-section cross-sectional area = 3.9 sq.cm.

Fig. 2 shows a schlieren photograph of the flow over a 20° wedge at $M = 1.7$. Fig. 3 shows two Mach Number profiles across the test section.

At present, two problems are being investigated using this tunnel: One is the curvature of an attached shock wave in the close neighborhood of the nose of a wedge, with the intention of deducing some knowledge of the boundary-layer structure there; the other is a study of heat transfer from a heated flat ribbon, which would be difficult to carry out in a tunnel at higher density because of the greater possibility of vibration difficulty at high dynamic pressure.

The initial success of this low-density tunnel has not only provided an instrument for the study of flow in the lower part of the continuum gas dynamics régime but has pointed the way to wider applications of the vapor cycle to other wind tunnels. Further study of the latter aspect is proceeding.

On Second-Order Supersonic Flow Past a Slowly Oscillating Airfoil

Milton D. Van Dyke
Ames Aeronautical Laboratory, N.A.C.A., Moffett Field, Calif.
October 15, 1952

THE WRITER HAS RECENTLY CALCULATED the second-order effects of thickness upon a slowly oscillating airfoil in supersonic flow. Because the results disagree with those of other treatments of the problem, [1, 2] it seems worth while to summarize them here.

Consider a sharp-nosed airfoil whose upper surface is described at zero angle of attack by $y = Y(x)$. Let the airfoil pivot about a point lying a distance b downstream from the leading edge and oscillate with small angle of attack $\alpha(t)$ (for example, $\alpha = \alpha_0 \sin \omega t$ for sinusoidal oscillations). A solution in terms of elementary functions is obtained by restricting consideration to slow oscillations so that, for example, in the case of sinusoidal motion only linear terms in frequency are retained. Then, to second order in thickness (but only first order in angle of attack, which is sufficient for investigating stability), the pressure coefficient on the upper surface is found to be

$$C_p = \frac{2}{\beta}(Y' - \alpha) + \frac{2\dot{\alpha}}{\beta U}\left(\frac{2 - M^2}{\beta^2}\,x + b\right) + \frac{M^2N - 2}{\beta^2}(Y'^2 - 2Y'\alpha) + \frac{2\dot{\alpha}}{U}\left\{2M^2\frac{N-1}{\beta^4}\,Y + \left[\frac{(2 - M^2)(M^2N - 1)}{\beta^4}\,x + \frac{M^2N - 2}{\beta^2}\,b\right]Y'\right\} \quad (1)$$

Here, U and M are free-stream speed and Mach Number, $\beta = (M^2 - 1)^{1/2}$, and $N = (1/2)(\gamma + 1)M^2/\beta^2$, where γ is the adiabatic exponent. The prime and dot indicate differentiation with respect to x and time t, respectively.

The first two terms in Eq. (1) are the usual result of linearized theory. The third term is the second-order "quasi-steady" term, which would result from using the instantaneous slope in Busemann's formula. The fourth term is the new result of this analysis.

Consider now the stability of pitching oscillations for a symmetrical airfoil with sharp trailing edge. The pressure on the lower surface is obtained by reversing the sign of α in Eq. (1). Thus, the pitching moment coefficient (about the pivot) is found to contain, in addition to a restoring term, a damping term given by

$$\frac{4c\dot{\alpha}}{U}\left[\frac{2 - M^2}{3\beta^3}\left(1 - \frac{3}{2}\frac{b}{c}\right) + \frac{b}{2\beta c}\left(1 - 2\frac{b}{c}\right) - \frac{M^2(N-1)}{\beta^4} \times \frac{b}{c^3}\int_0^c Y\,dx + \frac{2(M^2N - 2)}{\beta^2}\frac{1}{c^3}\int_0^c (x - b)Y\,dx\right] \quad (2)$$

where c is the airfoil chord. The moment is stabilizing or destabilizing according as this term is negative or positive. It is well known that linearized theory, represented by the first two terms in brackets, indicates the possibility of instability for certain combinations of Mach Numbers less than $(5/2)^{1/2}$ and pivot points ahead of two-thirds of the chord. The effect of thickness is to shift this range of possible instability toward higher Mach Numbers and more forward pivot points, as shown in Fig. 1 for a 6 per cent thick double-wedge airfoil or 4 1/2 per cent thick biconvex airfoil. (The dotted portion of the curve corresponds to subsonic flow behind the bow wave for either airfoil, so that the theory is inapplicable.)

The second-order effects of thickness are small, as would be expected, and ordinarily tend to destabilize. These results differ from those of reference 1 and are in sharp disagreement with the results of reference 2, which predict strong stabilizing effects of thickness. The details of the theory of reference 1 are not available for discussion. The analysis of reference 2 appears to contain a basic error. The author avoided the difficulties associated with kinked streamlines by the strategem of considering a general "smoothed" problem and then passing to the limit of sharp corners in the solution. This artifice is justified because to second-order a shock wave is the limit of a rapid continuous isentropic compression. However, it appears that the author failed to solve the actual smoothed problem before passing to the limit.

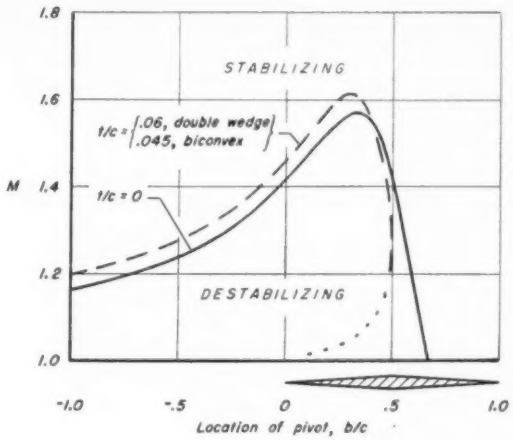

FIG. 1.

A simple test can be applied to these solutions. Just at the nose of an oscillating airfoil (so long as the shock wave remains attached), the pressure depends only upon the instantaneous local velocity (see reference 3). Therefore, at the nose the pressure must equal that on the same airfoil in steady flow with the instantaneous angle of attack increased by the apparent downwash angle, $\dot{\alpha}b/U$. The present result [Eq. (1)] passes this test, whereas the result of reference 2 fails to do so.

The writer expects to publish soon the details of his analysis.

REFERENCES

[1] Beavan, M. A., and Holder, D. W., *Recent Developments in High-Speed Research in the Aerodynamics Division of the N.P.L.*, Jour. Roy. Aero. Soc., Vol. 54, No. 477, pp. 571–572, September, 1950.

[2] Wylly, Alexander, *A Second-Order Solution for an Oscillating Two-Dimensional Supersonic Airfoil*, Ph.D. Thesis, Caltech, 1950; Published in abridged form, Journal of the Aeronautical Sciences, Vol. 19, No. 10, p. 685, October, 1952.

[3] Courant, R., and Friedrichs, K. O., *Supersonic Flow and Shockwaves*, 1st Ed., p. 297: Interscience, New York, 1948.

A Method for Location of Detached Shock Waves Ahead of Plane Bodies

Robert Wesley Truitt
Professor of Aeronautical Engineering, Virginia Polytechnic Institute, Blacksburg, Va.
September 8, 1952

DISCUSSION

RECENT EXPERIMENTS ON WEDGE PROFILES, reported in reference 1, reveal that in transonic flow the shock detachment distance is affected considerably by the opening angle of the profile at the leading edge. It is the purpose of this paper to derive an expression for the shock detachment distance which is an explicit function of the opening angle of the wedge.

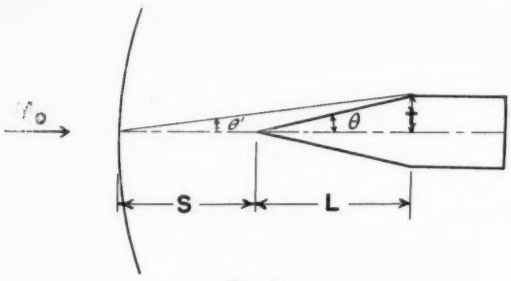

FIG. 1.

The pertinent limiting conditions for transonic flow are particularly well defined for the present study and occur at $M_0 = 1$ and at minimum shock attachment Mach Number, M_a, for a given profile. Considering the fact that sonic velocity occurs at the shoulder of a wedge (see reference 2) and using the limiting conditions for shock detachment at $M_0 = 1$ and M_a, the shock detachment distance, S, for any transonic Mach Number may be found (see Fig. 1).

Consider the angle θ' in Fig. 1, where the first limiting condition is such that $\theta' \to 0$ as $M_0 \to 1$ (i.e., $S \to \infty$). The other limiting condition is such that $\theta' \to \theta$ as $M_0 \to M_a$ (i.e., $S \to 0$). An expression that satisfies these limiting conditions may be written as (see Fig. 1).

$$\tan \theta' = t/(S + L) \backsimeq \theta'$$

or

$$\theta' = (t/L)/[(S/L) + 1] \tag{1}$$

where θ' may now be identified as the angle corresponding to the minimum free-stream Mach Number, M_0, $(1 \leq M_0 \leq M_a)$, which will still produce an attached shock wave at the nose of a wedge having a nose angle of $2\theta'$. In other words, exact shock theory gives for every transonic Mach Number, M_0, the maximum nose angle θ' which will still allow shock attachment.

From Fig. 1, $t/L \backsimeq \theta$ (the semiangle of the wedge), and Eq. (1) may be written in terms of the shock detachment parameter, S/L, as

$$S/L = (\theta/\theta') - 1 \tag{2}$$

Again, when $M_0 = M_a$, $\theta' = \theta$ and $S = 0$; when $M_0 = 1$, $\theta' = 0$ and $S = \infty$. From the above consideration it appears that Eq. (2) should give reasonably accurate values of S/L in the entire transonic range.

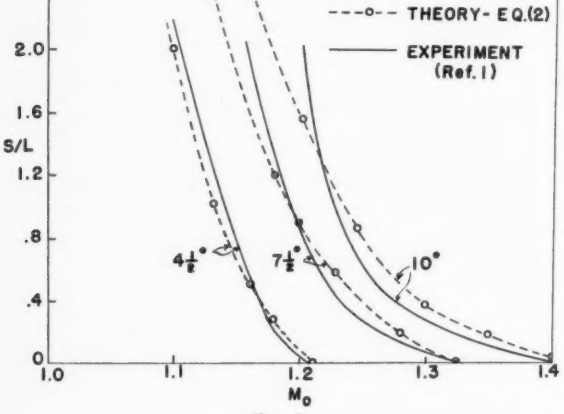

FIG. 2.

COMPARISON WITH EXPERIMENT

Eq. (2) has been used to calculate S/L values in the transonic range for $4^1/_2°$, $7^1/_2°$ and 10° two-dimensional semiangle wedges. The calculated values of S/L have been compared with the experimental results of reference 1 and are presented in Fig. 2. The agreement of Eq. (2) with these experiments is evident.

CONCLUSIONS

Other simple expressions have been derived for shock detachment distance which predict no direct effect due to the nose shape or varying nose angle.[3] This prediction is not true, as is borne out by experimental evidence, for thin wedges where the detached shock location is considerably affected by the nose angle. Eq. (2) predicts a considerable effect due to nose angle, as is evident from Fig. 2. The present analysis has been made only for the two-dimensional case of thin wedges with well-defined shoulders and had not been attempted for bodies of revolution at the time of writing.

REFERENCES

[1] Bryson, A. E., Jr., *An Experimental Investigation of Transonic Flow Past Two-Dimensional Wedge and Circular-Arc Sections Using a Mach-Zehnder Interferometer*, N.A.C.A. T.N. No. 2560, November, 1951.

[2] Cole, J. D., *Drag of a Finite Wedge at High Subsonic Speeds*, Jour. Math. and Phys., Vol. 30, No. 2, July, 1951.

[3] Moeckel, W. E., *Approximate Method For Predicting Form and Location of Detached Shock Waves Ahead of Plane or Axial Symmetric Bodies*, N.A.C.A. T.N. No. 1921, July, 1949.

A Note on Tabular Methods for Flexural Vibrations

William T. Thomson
Department of Engineering, University of California at Los Angeles
September 24, 1952

TABULAR METHODS OFFER a practical approach to problems of beam vibrations where the stiffness and mass distribution are nonuniform. These methods are all based on the fact that, in forced harmonic oscillations, the deflection, slope, moment, and shear are linearly related along the beam. It appears that such problems can be formulated in many different ways, and the presentation here offers an advantage of algebraic simplicity which retains the physical concepts of the beam.

UNCOUPLED FLEXURAL VIBRATION

The beam section is chosen as in Fig. 1. The influence coefficients are defined differently from those of previous papers as follows: The coefficients α_S, α_M, d_S, and d_M are the slope or deflection at station $i + 1$ measured from a tangent at station i due to a unit shear or moment at i.

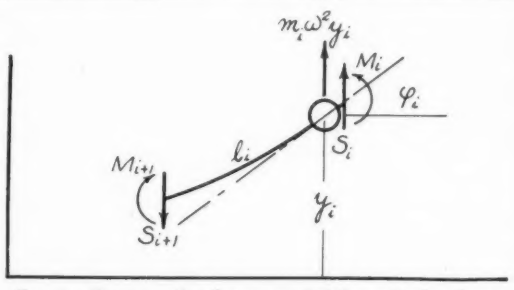

FIG. 1. Beam section for uncoupled flexural vibrations.

With the influence coefficients so defined, the computational equations for the uncoupled flexural vibrations can be obtained directly from Fig. 1 as

$$S_{i+1} = S_i + m_i\omega^2 y_i \quad (1)$$
$$M_{i+1} = M_i + S_{i+1}l_i \quad (2)$$
$$\varphi_{i+1} = \varphi_i - S_{i+1}\alpha_{Si} - M_i\alpha_{Mi} \quad (3)$$
$$y_{i+1} = y_i - \varphi_i l_i + S_{i+1}d_{Si} + M_i d_{Mi} \quad (4)$$

where the first two equations are deduced from equilibrium considerations and the last two are from the geometric configuration.

For a chosen value of ω, these equations enable one to calculate S, M, φ, and y at any point in terms of the corresponding quantities at some starting point. For instance, for a free-ended beam, the computations are started with the following boundary values at the free end:

$$S_1 = M_1 = 0, \quad \varphi_1 = \varphi_1, \quad y_1 = 1.0$$

Progressing to the other end, the quantities obtained are in the form

$$S_n = a_1 + b_1\varphi_1 \quad (5)$$
$$M_n = a_2 + b_2\varphi_1 \quad (6)$$
$$\varphi_n = a_3 + b_3\varphi_1 \quad (7)$$
$$y_n = a_4 + b_4\varphi_1 \quad (8)$$

where the a's and b's are numbers. Specifying the boundary conditions at n, φ_1 is determined, after which all other quantities at n are established. Procedures for the various boundary conditions are well known and are not repeated here.

Eqs. (5) to (8) indicate that the a's and b's independently satisfy the computational equations, Eqs. (1) to (4), thereby suggesting a tabular form in two parts.

Rotating Beams

The forces acting on a section of a rotating beam are shown in Fig. 2, where the vibration is assumed to take place in a direction perpendicular to the plane of rotation. The computational equations, including the effect of rotation are established from this diagram to be

$$S_{i+1} = S_i + m_i\omega^2 y_i - m_i\Omega^2 r_i\varphi_i \quad (9)$$
$$M_{i+1} = M_i + (S_i + m_i\omega^2 y_i)l_i - m_i\Omega^2 r_i(y_i - y_{i+1})$$
$$= M_i(1 + m_i\Omega^2 r_i d_{Mi}) + S_{i+1}(l_i + m_i\Omega^2 r_i d_{Si}) \quad (10)$$
$$\varphi_{i+1} = \varphi_i - S_{i+1}\alpha_{Si} - M_i\alpha_{Mi} \quad (11)$$
$$y_{i+1} = y_i - \varphi_i l_i + S_{i+1}d_{Si} + M_i d_{Mi} \quad (12)$$

It is evident here that only the shear and moment equations are altered in form by rotation and that the computational procedure and tabular form for the uncoupled flexural case apply.

Coupled Flexure-Torsion Vibration

Natural modes of vibration of airplane wings are always coupled flexure-torsion modes, which for higher modes may differ considerably from those of uncoupled modes. It is necessary here to introduce one additional influence coefficient h_i, defined as the angle of twist at station $i + 1$ with respect to station i due to a unit torque at station i. Referring to the beam section shown in Fig. 3, the following equations can be written:

$$S_{i+1} = S_i + m_i\omega^2(y_i + c_i\theta_i) \quad (13)$$
$$M_{i+1} = M_i + S_{i+1}\,l_i \quad (14)$$
$$T_{i+1} = T_i + J_i\omega^2\theta_i + m_i c_i\omega^2 y_i \quad (15)$$
$$\varphi_{i+1} = \varphi_i - S_{i+1}\,\alpha_{Si} - M_i\alpha_{Mi} \quad (16)$$
$$y_{i+1} = y_i - \varphi_i l_i + S_{i+1}\,d_{Si} + M_i d_{Mi} \quad (17)$$
$$\theta_{i+1} = \theta_i + T_i h_i \quad (18)$$

For free-ended beams we have the following boundary conditions to start with:

$$\varphi_1 = \varphi_1, \quad y_1 = 1.0, \quad \theta_1 = \theta_1$$

Here, again, the quantities of interest at any station are linearly related to φ_1 and θ_1 and can be expressed in the form

$$a + b\varphi_1 + c\theta_1$$

This suggests a tabular form where each quantity S, M, T, etc., would be divided into three parts—namely, a, b, and c.

Influence Coefficients

The influence coefficients α_S, α_M, d_S, and d_M are determined from the actual stiffness curve of the beam by the area-moment procedure. Letting the ordinates at i and $i + 1$ be aEI_0 and $(a + b)EI_0$, where EI_0 is a reference stiffness, the curve between the two stations is replaced by a straight line, which results in the following equations:

$$\alpha_{Mi} = \int_0^{l_i} \frac{d\xi}{EI} = \frac{1}{EI_0}\int_0^{l_i} \frac{d\xi}{(a + b) - (b/l_i)\xi} =$$
$$\frac{l_i}{bEI_0}\ln\left(\frac{a + b}{a}\right) \quad (19)$$

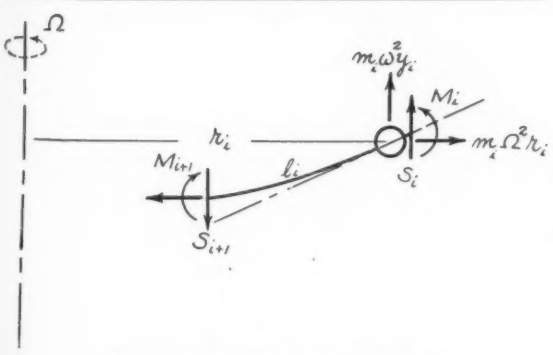

Fig. 2. Beam section under rotation.

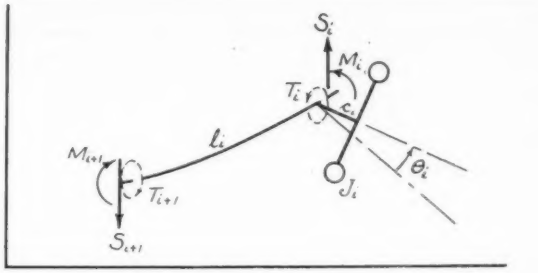

Fig. 3. Beam section for coupled flexure-torsion vibrations.

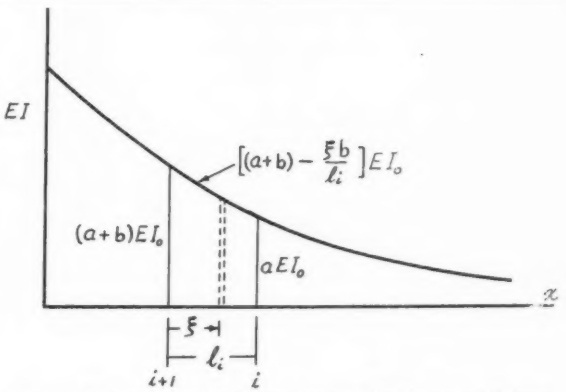

Fig. 4. Stiffness curve for determination of influence coefficients.

$$\alpha_{Si} = \int_0^{l_i} \frac{(l_i - \xi)\,d\xi}{EI} = \frac{l_i^2}{b^2 EI_0}\left[b - a \ln\left(\frac{a+b}{a}\right)\right] \quad (20)$$

$$d_{Mi} = \int_0^{l_i} \frac{\xi\,d\xi}{EI} = \frac{l_i^2}{b^2 EI_0}\left[(a+b)\ln\left(\frac{a+b}{a}\right) - b\right] \quad (21)$$

$$d_{Si} = \int_0^{l_i} \frac{(l_i - \xi)\xi\,d\xi}{EI} = \frac{l_i^3}{b^3 EI_0}\left[\frac{1}{2}b^2 + ab - a(a+b)\ln\left(\frac{a+b}{a}\right)\right] \quad (22)$$

It is of interest to compare the influence coefficient as defined here to those of Myklestad—i.e., slope and deflection at station i measured from a tangent at $i+1$ due to a shear or moment at i. Using the bar notation for the latter, the relationship between the two are

$$\begin{aligned} \alpha_{Mi} &= \bar{\alpha}_{Mi} \\ \alpha_{Si} &= \bar{\alpha}_{Si} = \bar{d}_{Mi} \\ d_{Mi} &= \bar{d}_{Si} - l_i\bar{\alpha}_{Mi} \\ d_{Si} &= \bar{d}_{Si} - l_i\bar{d}_{Mi} \end{aligned}$$

The above relationships indicate that the influence coefficients as used here can be checked experimentally in the usual manner.

References

[1] Myklestad, N. O., *A New Method of Calculating Natural Modes of Uncoupled Bending Vibration of Airplane Wings and Other Types of Beams*, Journal of the Aeronautical Sciences, Vol. 11, No. 2, p. 153, April, 1944.

[2] Myklestad, N. O., *Vibration Analysis;* McGraw-Hill Book Company, Inc., New York, 1944.

[3] Prohl, M. A., *A General Method for Calculating Critical Speeds of Flexible Rotors*, Trans. A.S.M.E., September, 1945.

On Linearized Theory

John W. Miles

Department of Engineering, University of California at Los Angeles

September 8, 1952

THE NECESSARY CONDITIONS for the linearization of the equations of irrotational compressible flow past a thin two-dimensional body have been set forth by Lin, Reissner, and Tsien.[1] An extension of their analysis to flow past three-dimensional wings of thickness ratio δ and aspect ratio A.R. shows that necessary conditions for linearization *in the neighborhood of the wing* are that all of the conditions

$$\delta,\ M\delta,\ k\delta,\ kM\delta \ll 1 \quad (1)$$

be satisfied and that any one or more of the conditions

$$|M - 1| \gg \delta^{2/3} \quad (2a)$$

$$k \gg \delta^{2/3} \quad (2b)$$

$$1/\text{A.R.} \gg \delta^{1/3} \quad (2c)$$

be satisfied. M is the free-stream Mach Number, and k is the reduced frequency (or, more generally, a dimensionless measure of time ratio of change). In the case of a slender body of revolution,[2] we may set A.R. $= \delta$, so that Eq. (2c) is included in Eq. (1).

Conditions equivalent to Eq. (2) may be obtained by introducing the transonic similarity parameters

$$c_M = [(\gamma+1)\delta]^{-2/3}|M - 1| \quad (3a)$$

$$c_k = [(\gamma+1)\delta]^{-2/3}k \quad (3b)$$

$$c_{\text{A.R.}} = [(\gamma+1)\delta]^{-2/3}(\text{A.R.})^{-2} \quad (3c)$$

and requiring one or more to be large (relative to unity). On the other hand, if all three parameters are 0(1) we obtain the dimensionless nonlinear transonic equation [cf. Eqs. (21) and (25), reference 1]

$$(2c_M + f_\xi)f_{\xi\xi} + 2c_k f_{\xi\tau} - c_{\text{A.R.}} f_{\eta\eta} - f_{\xi\xi} = 0 \quad (4)$$

for the dimensionless perturbation potential f. Previous special cases of this equation have been given by Oswatitsch and Wieghardt[3] ($c_M = c_k = c_{\text{A.R.}} = 0$), von Kármán[4] ($c_k = c_{\text{A.R.}} = 0$), and Garrick[5] ($c_{\text{A.R.}} = 0$).

The similarity parameter $c_{\text{A.R.}}$ was introduced first by Berndt,[6] but he implied that the potential equation may be linearized only in the limit A.R. $= 0$, whereas $c_{\text{A.R.}}$ can be large for only moderately small values of A.R. (For $\delta = 0.05$ and A.R. $= 1$, we have $c_{\text{A.R.}} = 4.1$.) If $c_{\text{A.R.}}$ is large and both c_M and c_k are 0(1), we have Jones' slender wing theory.[7] It should be remarked that $c_{\text{A.R.}} \gg 1$ is a *necessary* condition for slender wing theory in the transonic régime, whereas $M = 1$ (so $c_M = 0$) is neither necessary nor sufficient. Similarly, while $(M^2 - 1)^{1/2}$A.R. is a valid transonic similarity parameter [$= (c_M/c_{\text{A.R.}})^{1/2}$], it is neither necessary nor sufficient that it be small for the linearization of Eq. (4).

It is not possible to assert that the foregoing conditions are *sufficient* without (a) imposing restrictions on the curvature of the wing surface and (b) investigating the boundary conditions at infinity. In general, the linearized approximation will not be uniformly valid in the neighborhood of the wing edges, but this difficulty can be circumvented by the method of Poincaré and Lighthill.[8] At infinity the solution must behave as an outgoing disturbance of finite energy, and in transonic flow past an airfoil at zero incidence, this can be ensured only by requiring the asymptotic solution to satisfy Eq. (4), even though Eq. (2c) may permit linearization in the neighborhood of the wing.

References

[1] Lin, C. C., Reissner, E., and Tsien, H. S., *On Two-Dimensional Nonsteady Motion of a Slender Body in a Compressible Fluid*, J. Math. Phys., Vol. 27, No. 3, pp. 220–231, October, 1948.

[2] Miles, J. W., *Slender Body Theory for Supersonic Unsteady Flow*, Journal of the Aeronautical Sciences, Vol. 19, No. 4, p. 280, April, 1952.

[3] Oswatitsch, K., and Wieghardt, K., *Theoretische Untersuchungen über stationare Potentialstromongen und Grenzschichten bei hohen Geschwindigkeiten*, Lilienthal-Gesselschaft für Luftfahrhtforschung Bericht S 13/1, Teil, pp. 7–24.

[4] von Kármán, Th., *The Similarity Law of Transonic Flow*, J. Math. Phys., Vol. 26, pp. 182–190, 1947.

[5] Garrick, I. E., *A Survey of Flutter*, N.A.C.A. University Conference in Aerodynamics, pp. 182–190, 1947.

[6] Berndt, S. B., *Similarity Laws for Transonic Flow Around Wings of Finite Aspect Ratio*, Aero. T.N. 14, Division of Aeronautics, Royal Inst. of Tech., Stockholm, February 20, 1950.

[7] Jones, R. T., *Properties of Low-Aspect-Ratio Pointed Wings at Speeds Below and Above the Speed of Sound*, N.A.C.A. T.N. No. 1032, 1946.

[8] Lighthill, M. J., *A Technique for Rendering Approximate Solutions to Physical Problems Uniformly Valid*, Phil. Mag. (7), Vol. 40, pp. 1179–1201, December, 1949.

Interaction Between Stalled and Unstalled Flow

Peter F. Jordan

Now Royal Aircraft Establishment, Farnborough, Hants., England

October 1, 1952

WICK[1], IN A PAPER recently referred to by Bird[2] discussing experimental lift distributions over a Δ-wing in partly stalled flow, writes: "The spanwise variation of $c_{n_{max.}}$ is not explainable . . . . since $c_{n_{max.}}$ reached a maximum at 39.6 per cent semispan rather than at the center of the wing . . . . . It can be concluded that there exist as yet undefined effects of the boundary-layer flow on the wing stalling characteristics."

The writer[3] investigated the mutual influence of stalled and unstalled flow (AVA-Göttingen, 1937 and early 1938). He found that excessive sectional c_l-values were due to periodical occurrences. Let y be the spanwise coordinate and let y_0 be the border between stalled and unstalled flow; let $y > y_0$ be the stalled region. Then the flow will suddenly attach itself at a point $y_1 > y_0$, thus

forming an island of unstalled flow; this island will immediately move toward y_0, making room for a new island to be formed at y_1, and so on. The start of this process is explained partly by a minimum of induced downwash that exists near y_1 and partly by a spanwise boundary-layer flow near L.E.; the process as a whole produces, between y_0 and y_1, an effective camber of the wing profile, thus leading to excessive c_l-values.

The above observations were made on wings with constant chord; of course they are not sufficient to explain fully the more complicated occurrences on Δ-wings, but they seem to explain why $c_{n_{max.}}$ will occur neither at mid-span nor at the wing tips. Indeed, the c_l-value belonging to $c_{n_{max.}}$ as measured by Wick[1] was far in excess of the two-dimensional $c_{l_{max.}}$-value for his wing profile in two-dimensional flow (1.7 against 0.9). Such excessive lift coefficients require interaction between unstalled flow and stalled flow.

It should perhaps be mentioned that a boundary-layer fence was used—for the first time to the writer's knowledge—to determine the part played by the boundary-layer flow; it was shown to effectively fence in the stalled region. The Reynolds Number of the test was $Re = 0.2 \times 10^6$, a rather low value; however, the flow observations were repeated and confirmed on an aircraft in flight by Liebe.[4]

References

[1] Wick, B. H., N.A.C.A. T.N. No. 1650, June, 1948.

[2] Bird, J. D., *Visualization of Flow Fields by Use of a Tuft Grid Technique*, Journal of the Aeronautical Sciences, Vol. 19, No. 7, p. 481, July. 1952.

[3] Jordan, P., *Lilienthal Gesellschaft Prize-Competition 1937/8;* Printed Lufo 16, p. 184, 1939.

[4] Liebe, W., *D.V.L. Flight Experiments (from Mid 1938 Onwards)*, Interavia VII, p. 215, 1952.

Physical Explanation of Singular Integrals at Supersonic Speeds

Lee S. Wasserman

September 19, 1952

Chief, Aerodynamics Research Branch, Flight Research Laboratory, Wright Air Development Center, Wright-Patterson Air Force Base, Ohio

THIS NOTE PRESENTS a physical explanation of a type of singular integral appearing in linearized supersonic theory. We consider a pressure source at the origin expressed by Eq. (1).

$$p(x,y,z) = \epsilon/2\pi \sqrt{x^2 - (M^2 - 1)(y^2 + z^2)} \qquad (1)$$

The vertical acceleration of an air particle at x, y, z, due to the pressure source is given by Newton's Law.

$$\rho \frac{dw}{dt} = -\frac{\partial p}{\partial z} = -\frac{\epsilon(M^2 - 1)z}{2\pi[x^2 - (M^2 - 1)(y^2 + z^2)]^{3/2}} \qquad (2)$$

For steady flow $dW/dt = U(dw/dx)$, so that integration yields for w

$$w = \frac{\epsilon}{2\pi\rho U} \Bigg|_{x^*}^{x} \frac{xz}{(y^2 + z^2)\,[x^2 - (M^2 - 1)(y^2 + z^2)]^{1/2}} \qquad (3)$$

where x^* is the value of x which makes the denominator vanish so that the velocity is infinite.

The trouble here comes from the fact that the derivative taken in Eq. (2) does not include the positive pressure jump that occurs just ahead of the Mach cone. It is possible to show that the velocity induced by this jump cancels out the infinity in Eq. (3). From acoustic theory, the velocity normal to a plane sound wave is given by the expression $p/\rho c$. The wave front on the Mach cone appears plane to particles very close, so that w due to the jump is given by the expression

$$w = \frac{p}{\rho c} \frac{z \cos \beta}{\sqrt{y^2 + z^2}} = \frac{\epsilon z \cos \beta}{2\pi\rho c \sqrt{y^2 + z^2}\sqrt{x^{*2} - (M^2 - 1)(y^2 + z^2)}} \qquad (4)$$

where $z \cos \beta/\sqrt{y^2 + z^2}$ gives the component of the axially symmetric induced velocity in the vertical direction. Now

$$\cos \beta/c = \sqrt{M^2 - 1}/U$$

$$x^*/\sqrt{y^2 + z^2}(U) = \sqrt{M^2 - 1}/U$$

so that the velocity induced by the pressure jump in Eq. (4) exactly cancels the infinite velocity given by Eq. (3).

Frequency Response and the Transfer Functions of the Human Pilot Measured in Flight

G. M. Andrew

Air Force Flight Test Center, Edwards, Calif.

August 11, 1952

Introduction

THE IMPORTANCE OF determining experimentally the transfer function of the human pilot was recognized only in the recent years. Some attempts of measurements along the line were made.[1, 2] In these tests flight simulators were used.

The method proposed in this note is based on the actual flight tests. The pilot reacts thus under actual flying conditions, and such factors as altitude, accelerations, fatigue, speed, etc., are not neglected.

The theoretical background of the method, based on the theory of servomechanism, is given in detail in reference 3.

The transfer functions of the human pilot should be determined about all three axes. For purpose of illustration, only pitching axis is discussed below.

Instruments and Flying Technique

A simple angle of attack indicator can be used if gyro equipment is not available.

The time history of angle of attack α must be recorded. Thus, an oscillograph or some other recording device is required. The time history of elevator deflection δ_e must also be recorded.

The method requires little flying time. Two flight-test records are needed for each configuration.

(1) During the first flight test the pilot puts a step or, still better, a single pulse elevator motion. The recorded elevator motion and the aircraft response are shown in Fig. 1.

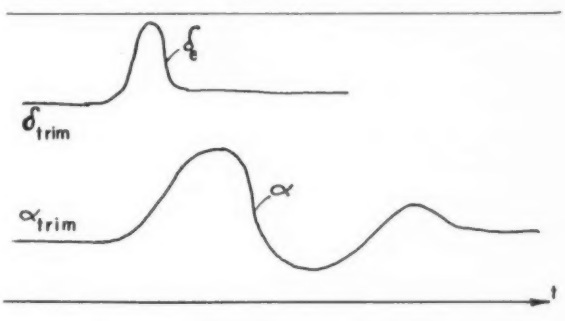

FIG. 1

(2) The panel instrument used by the pilot for observation of the airplane response should have a visible mark for the trim position of the angle of attack α trim. Immediately after the first flight test is finished, the second flight test can be started. Different flying techniques can be used, such as starting from initial steady state and trying to reach another selected steady state marked on the instrument.

Or a dynamic method can be used, as one described below. The pilot puts a considerable elevator step disturbance (Fig. 2). At time t_M, when the airplane response reaches its maximum value α_M, the pilot intervenes with elevator motion, trying to get back as fast as possible to the marked trim position α_{trim}. The motion of the elevator and of the airplane response are, of course, recorded. Both flight tests (for one configuration) take only few minutes. It is important to tabulate gross weight, c.g. position, altitude, speed, and other pertinent data describing the configuration.

Data Reducing

Fig. 3 represents the block diagram of the system. The dotted rectangle (1) refers to first flight test. In the language of block algebra, it represents the open loop of the airplane alone. The dotted rectangle (2) refers to the second flight test and represents the closed loop of the combination (aircraft plus pilot). The dotted rectangle (3) represents the open loop of the (aircraft plus pilot) combination.

The record of the first flight test (Fig. 1) provides data necessary to compute the open loop transfer function of the airplane alone:

$$F(j\omega) \tag{1}$$

The record of the second flight test (Fig. 2, starting from time t_N) gives the data for computation of the transfer function:

$$Y(j\omega) \tag{2}$$

which refers to the closed loop of the (aircraft plus pilot) combination.

The data reduction that leads to the transfer function is a laborious process. Where IBM machines are available, the method given in reference 4 is recommended. Otherwise, the methods outlined in references 5 and 6 can be used.

The block algebra (Fig. 3) as given in the theory of servomechanisms[7,8] gives the open loop of the (aircraft plus pilot) combination [see dotted rectangle (3)]:

$$H(j\omega) = F(j\omega) \times G(j\omega) = \alpha_0/(\alpha_{trim} - \alpha_0) \tag{3}$$

thus,

$$G(j\omega) = \alpha_0/(\alpha_{trim} - \alpha_0)F(j\omega) \tag{3a}$$

Also, by the rules of the block algebra, the transfer function of the closed loop is

$$Y(j\omega) = H(j\omega)/[1 + H(j\omega)] \tag{4}$$

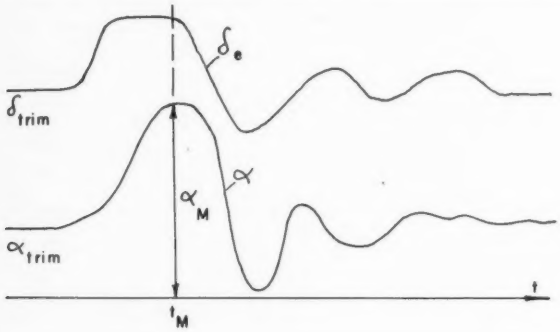

FIG. 2

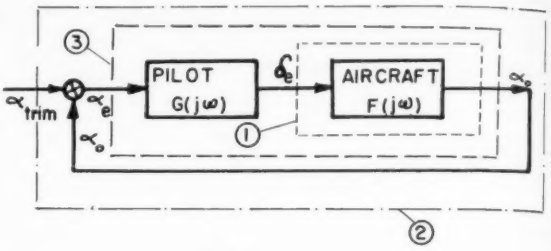

FIG. 3

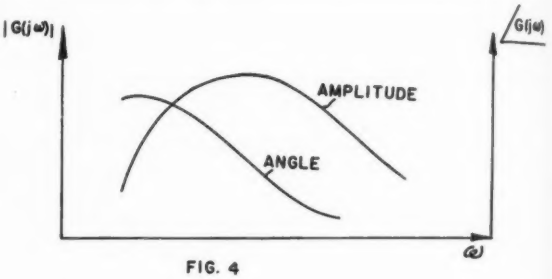

FIG. 4

From Eq. (4)

$$H(j\omega) = Y(j\omega)/[1 - Y(j\omega)] \tag{5}$$

Eq. (5) substituted into Eq. (3) gives the transfer function of the human pilot as

$$G(j\omega) = Y(j\omega)/F(j\omega)[1 - Y(j\omega)] \tag{6}$$

Eq. (3a) or (6) can be used to compute the frequency response of the human pilot. By determining the real and imaginary part of $G(j\omega)$, the amplitude and the angle of this transfer function can be obtained and tabulated for different values of the angular frequency ω.

Next, the amplitude and angle of $G(j\omega)$ can be plotted versus ω (Fig. 4). Also, a polar plot can be used.

No doubt a statistical approach is needed to arrive at some statistical conclusions or to get average data for a great number of pilots examined or for an average fighter or bomber type of airplane.

The flight-test data can be supplemented using as a simulator a modern Link trainer, having provision for changing the damping and sensitivity of the system.

The above method gives, in the hand of the medical profession, an exact tool to measure the behavior of the human pilot. Cooperation with some engineering outfit in data reduction and program planning is, of course, desirable.

References

[1] Philips, H. W., *Ability of Pilots to Control Simulated Short Period Yawing Oscillations*, N.A.C.A. T.M. No. L50D06.

[2] Cheatham, D. C., *A Study of the Characteristics of Human Pilot Control Response to Simulated Lateral Motions*, N.A.C.A. R.M. No. L52C17, 1952.

[3] Andrew, G. M., *The Dynamics of the Automatically Controlled Aircraft*, paper presented at the VIIIth International Congress of Applied Mechanics, 1952. Also Tech. Rep. No. AFFTC 52-24 Air Force Flight Test Center, Edwards, Calif.

[4] Shumacher, L., *Method of Analyzing Transient Flight Test Data to Obtain Aircraft Frequency Response*, U.S.A.F. Report Serial No. 2268.

[5] Andrew, G. M., and Polve, J. H., *Frequency Response of an Airplane from Flight-Test Data*, Readers' Forum, Journal of the Aeronautical Sciences, Vol. 19, No. 4, p. 285, April, 1952.

[6] Andrew, G. M., *End Correction for Frequency Response by Laplace Transform*, Readers' Forum, Journal of the Aeronautical Sciences, Vol. 19, No. 8, p. 569, August, 1952.

[7] Brown, G. S., and Campbell, D. P., *Principle of Servomechanisms;* John Wiley & Sons, Inc., New York, 1948.

[8] Chestnut, H., and Mayer, R. W., *Servomechanisms and Regulating System Design;* John Wiley & Sons, Inc., New York, 1951.

[9] Breaux, G. P., and Zeiler, E. L., *Presentation and Theoretical Consideration of the Transient Analysis Method Employed for Obtaining Frequency Response Function from Flight Data*, Rep. FZA-36-195, Consolidated Vultee Aircraft Corporation, Fort Worth Division, 1952.

[10] Ellson, D. C., and Gilbard, D., *The Application of Operational Analysis for Human Pilot Behavior*, Indiana University, Memorandum Rep. MC REXD-694-2J, A.M.C., Dayton, Ohio, 1948.

[11] Fitts, Paul M., *Psychological Aspects of Equipment Design*, U.S.A.F. Tech. Rep. 5820, A.M.C., Dayton, Ohio, 1949.

[12] Andrew, G. M., *Frequency Response of the Human Pilot*, Tech. Rep. No. AFFTC 52-28, Air Force Flight Test Center, Edwards, Calif.

Compressible Laminar Boundary Layer on a Heat-Insulated Body*

N. Rott
Associate Professor of Aeronautical Engineering, Cornell University, Ithaca, N.Y.

September 5, 1952

CONSIDER A HEAT-INSULATED BODY submerged in a two-dimensional compressible gas flow. Suppose the isentropic flow outside the boundary layer is known—i.e., the velocity U and Mach Number M are given along the body contour. The isentropic temperature T_1 outside the layer is

$$T_0/T_1 = 1 + [(\gamma - 1)/2]\, M^2 \tag{1}$$

(T_0 = stagnation temperature). The wall temperature T_w over the surface portion where the boundary layer is laminar is given to a good approximation by the formula

$$\frac{T_w}{T_1} = 1 + r(\sigma)\, [(\gamma - 1)/2]\, M^2 \tag{2}$$

where $r(\sigma)$ is the "recovery factor," which is a function of the Prandtl number σ alone. For σ not too far from unity,

$$r = \sqrt{\sigma} \tag{3}$$

and the connection between σ and the adiabatic exponent γ may be taken from Eucken's approximate formula—viz.,

$$\sigma = 4\gamma/(9\gamma - 5) \tag{4}$$

Theoretical support for Eq. (2) (originally derived by Pohlhausen for the flat plate only) was given by calculations of Eckert and Drewitz[1] and Tifford,[2] carried out for velocity distributions $U \sim x^k$. Experimental evidence was provided by Eckert and Weise[3] and by Ryan[4] through measurements on heat-insulated circular cylinders.

For the temperature T inside the boundary layer, at a point with local velocity u, an interpolation formula may be used which fulfills the boundary conditions—namely,

$$\frac{T}{T_1} = 1 + r(\sigma)\, \frac{\gamma - 1}{2}\, M^2 \left(1 - \frac{u^2}{U^2}\right) \tag{5}$$

Eq. (5) is exact for $\sigma = r = 1$, but for $\sigma \neq 1$ it gives a somewhat less accurate result in general than for the special value at the wall. Here, it is proposed to accept Eq. (5) as an approximate solution for the "thermal" part of the boundary-layer problem with the purpose of computing the density ρ and viscosity μ by Eq. (5), so that subsequently the "momentum" part of the problem may be attacked.

The density variation across the boundary layer is given by the law

$$\rho T = \rho_1 T_1 = \rho_w T_w \tag{6}$$

As to the variation of the viscosity, a further simplification will be needed, introduced first by Chapman and Rubesin.[5] Let us assume a variation of μ proportional to T across the boundary layer,

$$\mu/\mu_w = T/T_w \tag{7}$$

but let the wall value μ_w (T_w) be computed by any more accurate formula—e.g.,

$$\mu_w/\mu_0 = (T_w/T_0)^\omega \tag{8}$$

with $0.5 \leq \omega \leq 1.5$—or by Sutherland's law. Naturally, some inconsistency is introduced by evaluating μ according to different laws along and across the boundary layer, but it is felt that it is more important to calculate μ_w accurately, whereas the variation across the layer is less significant, especially for the heat-insulated body with vanishing normal temperature gradient on the surface.

The purpose of the present note is to point out that, once the approximations stated above are accepted, the remaining problem may be reduced exactly to an incompressible laminar boundary-layer problem by a slight extension of a transformation given previously by Illingworth[6] and Stewartson.[7] The extended transformation will be given without proof, since its verification closely follows the derivation of the original transformation. The problem is reduced to the incompressible case by introduction of new coordinates x_i, z_i, parallel and perpendicular to the surface, which are connected with the actual coordinates x, z by the equations

$$x_i = \int_0^x \left(\frac{T_1}{T_0}\right)^{[\gamma/(\gamma - 1)] + (r/2)} \frac{T_0\mu_w}{T_w\mu_0}\, dx \tag{9}$$

$$z_i = \left(\frac{T_1}{T_0}\right)^{[1/(\gamma - 1)] + (r/2)} \int_0^z \frac{\rho}{\rho_1}\, dz \tag{10}$$

and in the incompressible case, a velocity U_i has to be taken outside the layer which is connected with U by the formula

$$U_i = (T_0/T_1)^{r/2}\, U \tag{11}$$

The original Illingworth-Stewartson transformation, which was derived for $\sigma = r = \omega = 1$, is included; in this special case, the equations for the "thermal" part of the solution are exact, and the whole solution is also exact. The present extension allows one to eliminate the restrictions concerning the material properties of the gas, naturally at the price of the approximations discussed above.

It is possible to apply the transformation, Eqs. (9) to (11), to the "quadrature" formulas of incompressible boundary-layer theory, which are simplified versions of the Pohlhausen method. This was carried through for the original Illingworth-Stewartson transformation in a recent paper by Rott and Crabtree,[8] so that, here again, only the results will be presented.

The momentum thickness θ of the compressible boundary layer is given by the formula

$$\theta^2 = 0.45\, \nu_0 \left(\frac{T_0}{T_1}\right)^{[2/(\gamma - 1)] - 2r} U^{-6} \times \int_0^x \left(\frac{T_1}{T_0}\right)^{[\gamma/(\gamma - 1)] - 2r} \frac{T_0\mu_w}{T_w\mu_0}\, U^5\, dx \tag{12}$$

or, for $\gamma = 1.4$ and $\sigma = 0.737$ from Eq. (4), and from Eq. (8)

$$\theta^2 = 0.45\nu_0 \left(\frac{T_0}{T_1}\right)^{3.32} U^{-6} \times \int_0^x \left(\frac{T_1}{T_0}\right)^{1.82} \left(\frac{T_0}{T_w}\right)^{1\,-\,\omega} U^5\, dx \tag{12a}$$

Here, ν_0 is the kinematic viscosity at the stagnation point.

The (modified) Pohlhausen parameter m_i (see reference 8) for the corresponding incompressible flow is

$$m_i = -\frac{dU}{dx}\frac{\theta^2}{\nu_0} \left(\frac{T_1}{T_0}\right)^{(3\,-\,2\gamma)/(\gamma\,-\,1)} \frac{T_w^2\mu_0}{T_0^2\mu_w} \tag{13}$$

which becomes, with the numerical values as before,

$$m_i = -\frac{dU}{dx}\frac{\theta^2}{\nu_0} \left(\frac{T_1}{T_0}\right)^{0.5} \left(\frac{T_w}{T_0}\right)^{2\,-\,\omega} \tag{13a}$$

* This research was supported by the U.S.A.F. under Contract No. AF33(038)-21406, A.R.D.C., Office of Scientific Research.

The shape parameter H_i and the non-dimensional shearing stress l_i are known functions of m_i (see reference 8). In the compressible flow, H follows from the relation

$$H = (T_w/T_1)H_i + (T_w/T_1) - 1 \tag{14}$$

and the shearing stress is given by the formula

$$\tau_w = l_i \mu_w (T_1/T_w)(U/\theta) \tag{15}$$

As a simple check, consider the flat plate, U = constant. For the coefficient of friction, c_f, it is easily found from Eqs. (12), (15), and (8) that

$$c_f = c_{f_1}(T_1/T_w)^{(1-\omega)/2} \tag{16}$$

where c_{f_1} is the skin friction coefficient calculated with values ρ_1 and μ_1 outside the boundary layer by the formula for incompressible flow. Eq. (16) contains the exact result that, for $\omega = 1$ and arbitrary σ, $c_f = c_{f_1}$.

If $\omega \neq 1$ but $\sigma = 1$, comparison with exact calculations of Hantzsche and Wendt[9] shows that Eq. (16) still reproduces the main part of the compressibility effect on c_f, although it is not exact. However, even for moderately supersonic Mach Numbers, the difference is completely negligible. In the limiting case $M \to \infty$, Eq. (16) gives c_f-values that are 6 and 15 per cent too low for $\omega = 0.8$ and $\omega = 0.5$, respectively. In the general case, when $\omega \neq 1$ and $\sigma \neq 1$, comparison with Crocco's calculations[10] shows differences of similar character.

It is believed that for not too high Mach Numbers and for a heat-insulated body (which is an idealized case anyway) the present simple approach is sufficiently accurate. Extension for bodies of revolution is easily obtained, as was shown in reference 8.

References

[1] Eckert, E., and Drewitz, O., *Die Berechnung des Temperaturfeldes in der laminaren Grenzschicht schnell angeströmter unbeheizter Körper*, Luftfahrtforschung, Vol. 19, pp. 189–196, 1942.

[2] Tifford, A. N., *The Thermodynamics of the Laminar Boundary Layer of a Heated Body in a High-Speed Gas Flow Field*, Journal of the Aeronautical Sciences, Vol. 12, No. 2, pp. 241–251, April, 1945.

[3] Eckert, E., and Weise, W., *Messungen der Temperaturverteilung auf der oberfläche schnell angeströmter unbeheizter Körper*, Forschung Ing. Wes., Vol. 12, pp. 246–254, 1942.

[4] Ryan, L. F., *"Experiments on Aerodynamic Cooling,"* Mitt. Inst. f. A erod. ETH Zurich, No. 18, 1951.

[5] Chapman, D. R., and Rubesin, M. W., *Temperature and Velocity Profiles in the Compressible Laminar Boundary Layer with Arbitrary Distribution of Surface Temperature*, Journal of the Aeronautical Sciences, Vol. 16, No. 9, pp. 547–565, September, 1949.

[6] Illingworth, C. R., *Steady Flow in the Laminar Boundary Layer of a Gas*, Proc. Roy. Soc. London, Vol. 199, pp. 533–558, 1949.

[7] Stewartson, K., *Correlated Incompressible and Compressible Boundary Layers*, Proc. Roy. Soc. London, Vol. 200, pp. 84–100, 1949.

[8] Rott, N., and Crabtree, L. F., *Simplified Laminar Boundary-Layer Calculations for Bodies of Revolution and for Yawed Wings*, Journal of the Aeronautical Sciences, Vol. 19, No. 8, pp. 553–565, August, 1952.

[9] Hantzsche, W., and Wendt, H., *Die laminare Grenzschicht der ebenen Platte mit und ohne Wärmeübertragung unter Berücksichtigung der Kompressibilität*, Jahrbuch d.d. Luftfahrt-Forschung, pp. 40–50, 1942.

[10] Crocco, L., *Lo strato limite laminare nei gas*, Mon. Scient. di Aeronautica, No. 3, 1946.

Potential Limit in Transonic Flow

Pei Chi Chou
Aerodynamicist, Republic Aviation Corporation, New York

September 4, 1952

In reference 1, a criterion of collapse of potential flow is formulated for flow with a local supersonic region bounded by the airfoil and the line of transition from subsonic to supersonic velocity. This criterion is in terms of the local velocity and local airfoil curvature. Nothing is mentioned about the free-stream velocity and overall airfoil configuration. In this note, following the method given in reference 2, numerical solutions are found for flow past different families of airfoils. The relations among the limiting free-stream Mach Number, limiting maximum local Mach Number, the airfoil thickness ratio, and the local airfoil curvature are plotted explicitly. The result shows agreement with reference 1.

In reference 2, an example has been worked out for a Kaplan section by a simplified iteration process. For comparison, two modified Kaplan sections are solved by the same method here. The parametric representation of these modified sections are:

Modified Section I

$$x = \cos t$$
$$y = (\tau/5)(4 \sin t - \sin 3t)$$

Modified Section II

$$x = \cos t$$
$$y = (\tau/6)(5 \sin t - \sin 3t)$$

The configuration of these sections is shown in Fig. 1. The curvatures C at midchord are 3τ, 2.6τ, and 2.33τ for Kaplan section, the modified section I, and the modified section II, respectively, where τ is the thickness ratio. The general forms of the three are alike, except that the last two differ from the first in that C is not zero at leading edge and, hence, introduces stagnation points. The simplified equation used here, however, is valid only within a rectangle of a length of about 0.3 chord at the midchord. Therefore the effect of stagnation point can be neglected.

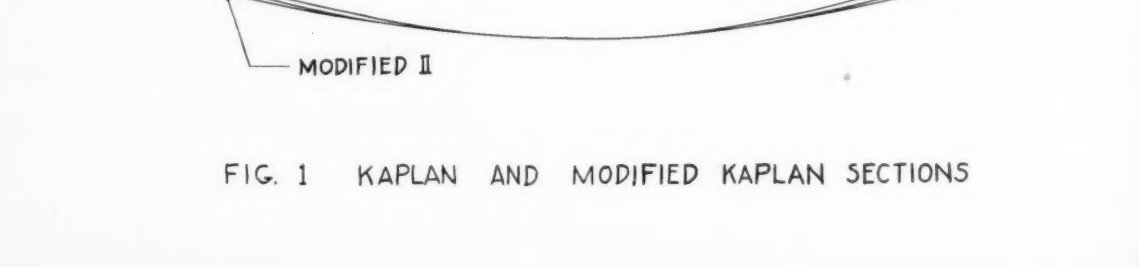

FIG. 1 KAPLAN AND MODIFIED KAPLAN SECTIONS

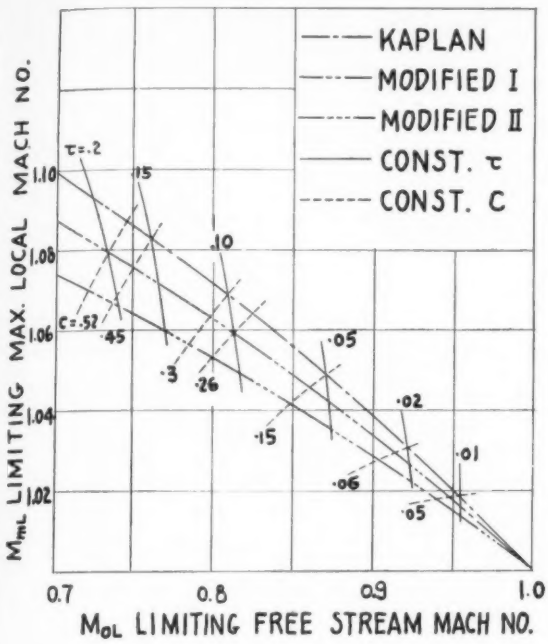

FIG. 2 M_{mL} VS M_{0L} CURVES

The resulting maximum velocity increments for the first three approximations are:

Modified Section I

$$(\phi_x)_{max.} = (\tau/\beta)\,(1.4000 + 0.7153K + 1.0273K^2 + \dots)$$

Modified Section II

$$(\phi_x)_{max.} = (\tau/\beta)\,(1.3333 + 0.6517K + 0.9220K^2 + \dots)$$

Let the subscript "L" denote the limiting value corresponding to the breakdown of potential flow or the occurrence of shock waves. The estimated K_L are 0.375 and 0.38 for modified section I and modified section II. The corresponding values of limiting free-stream Mach Number M_{0L} and limiting maximum local Mach Number M_{mL} are plotted in Fig. 2. Adding the M_{mL} vs. M_{0L} curve of Kaplan section to Fig. 2 and connecting the equal thickness ratio lines and equal curvature lines, the following conclusions are drawn:

(1) For the same family of airfoil sections, an increase in thickness ratio (hence, local curvature) results in an increase of M_{mL} and decrease of M_{0L}. In other words, a thicker airfoil in a family can sustain a higher local Mach Number but at a lower free-stream Mach number without introducing shock waves. Considering M_{mL} and local airfoil curvature alone, this agrees with reference 1.

(2) If the thickness ratio is kept constant, an increase in the airfoil midchord curvature raises the M_{mL} considerably at a cost of some decrease of M_{0L}.

(3) Both M_{0L} and M_{mL} increase with a decrease in thickness ratio if the midchord curvature can be kept unchanged.

The values of M_{mL} from these curves are considerably lower than the actual values, since only three approximations are employed. However, the above conclusions give a good qualitative description.

References

[1] Nikolskii, A. A., and Taganov, G. I., *Gas Motion in a Local Supersonic Region and Conditions of Potential-Flow Breakdown*, N.A.C.A. T.M. No. 1213, May, 1949.

[2] Braun, W. H., and Klein, M. M., *Calculation of Higher Approximations for Two-Dimensional Compressible Flow by a Simplified Iteration Process*, N.A.C.A. T.N. No. 2511, October, 1951.

Note on the Dynamic Stability of a Missile in Rolling Flight

Arthur E. Bryson, Jr.
Guided Missile Laboratories, Hughes Aircraft Company, Culver City, Calif.
September 26, 1952

In Ray E. Bolz's paper "Dynamic Stability of a Missile in Rolling Flight" (Journal of the Aeronautical Sciences, June, 1952), we believe there are several errors that should be corrected. They are enumerated below in the order in which they appeared in the subject paper.

(1) In Eqs. (3e) and (3f) the quantity called P_1 can *only* be the instantaneous roll rate of the missile. Eq. (4) is confusing, since it implies that P_1 is made up of the instantaneous roll rate *plus* "an angular velocity ω_x about the X axis due to precessional motion."

(2) The inclusion of forces and moments due to misaligned and canted surfaces and jet misalignment in a linearized stability analysis is obviously unnecessary, since their effect is simply to change the trim attitude of the missile.

(3) If one considers the small forces due to pitching and yawing angular velocities, as Mr. Bolz does, to be consistent one should also include the Magnus forces and moments due to pitching and yawing angular velocities. Since none of these quantities affects the stability to any important degree, they can be neglected.

(4) In Table II, item 4, it is stated that $K_{m_{\dot\alpha}}$ is always positive. We believe it is almost always negative for the manner in which it is defined in the paper.

(5) In Table I, item 7, K_D should be equal to $C_D\,(S/2d^2)$. Also, the term $\bar K_{z_\alpha} - 2\bar K_D$, which occurs in Eq. (22), should read $\bar K_{z_\alpha} - K_D$. This is the lift coefficient curve slope, which is always positive near $\alpha = 0$. Likewise, the term $2\bar K$ in Eq. (22) should read $\bar K$.

(6) The third stability criterion (III) on p. 400 is already implied by the other two stability conditions and, hence, is unnecessary.

(7) The transformation from time to distance along the flight path in Eqs. (15) is just as valid for subsonic as supersonic velocities. Thus the conclusion under (H) on p. 401—that dynamic stability is independent of velocity (except for variation of the coefficients with Mach Number)—applies equally well to subsonic velocities as it does to supersonic velocities.

(8) If reference axes are used which pitch and yaw with the missile but do not roll with it, the stability analysis is simplified and clarified (e.g., see reference 3 of Mr. Bolz's paper). If $\bar\varphi$ and $\bar\eta$ are the complex angular and linear velocities instantaneously resolved on this nonrolling reference system, then

$$\bar\varphi = \varphi e^{iPt}; \qquad \bar\eta = \eta e^{iPt}$$

where φ and η are Mr. Bolz's quantities. Taking the derivative with respect to time,

$$\dot{\bar\varphi} = e^{iPt}(\dot\varphi + iP\varphi); \quad \dot{\bar\eta} = e^{iPt}(\dot\eta + iP\eta)$$

Thus several terms could be eliminated from Eqs. (8a) and (8b) of Mr. Bolz's paper.

(9) In Tables I and II, item 3, reference is made to forces and moments "due to rolling combined with pitching and yawing angular velocities." Apparently it was intended to read "... combined with angles of attack and yaw." These forces and mo-

ments are actually the same as those under item 4; in nonrolling coordinates, one would write the complex moment due to accelerated motion as

$$K_{m_{\dot\alpha}}\,\rho d^3\ddot{\bar\eta}$$

Making the change to the rolling coordinates of Bolz, $\ddot{\bar\eta}$ is replaced by

$$e^{-iPt}(d/dt)\,(\eta e^{iPt}) = \ddot\eta + iP\eta$$

and, hence, the complex moment due to accelerated motion in Bolz's rolling coordinates is given by

$$K_{m_{\dot\alpha}}\rho d^3(\ddot\eta + iP\eta)$$

Therefore, $K_{s_p} = -K_{s_{\dot\alpha}}$ and $K_{m_p} = -K_{m_{\dot\alpha}}$ in Bolz's notation. Since $K_{s_{\dot\alpha}}$ has been neglected, K_{s_p} should also be neglected.

(10) We find the "discussion of Stability" rather unenlightening and in some cases misleading. For example, a missile that is dynamically stable (and, hence, also statically stable) for zero roll rate cannot be made dynamically unstable by the presence of a roll rate except under rather unusual conditions. This is shown in the following analysis, which is similar to that of Bolz except that we believe all errors have been eliminated, unessential forces and moments have been neglected, a simpler reference system has been used, and dimensionless quantities have been used throughout.

Symbols

α = $-i[(v + iw)/V]$, complex angle of attack
ω = $q + ir$, complex pitching velocity
l = $2m/\rho S$, ballistic length
r_A = $\sqrt{A/m}$, radius of gyration in roll
r_B = $\sqrt{B/m}$, radius of gyration in pitch (yaw)
C_{L_α} = $C_{s_\alpha} - C_D$, lift coefficient curve slope
$C_{L_{p\alpha}}$ = Magnus lift due to angle of attack $\div$ $[(\rho V^2/2)S(Pd/V)\alpha]$
C_{M_α} = moment coefficient curve slope
$C_{M_{\dot\alpha}}$ = $\partial C_M/\partial(\dot\alpha d/V)$, damping in plunge
$C_{M_{p\alpha}}$ = Magnus moment due to angle of attack $\div$ $[(\rho V^2/2) \times Sd(Pd/V)\alpha]$
C_{M_q} = $\partial C_M/\partial(qd/V)$, damping in pitch

and all other symbols not defined here are the same as Bolz's symbols or are defined in the text. All lift coefficient curve slopes are always positive; the moment coefficient curve slopes are positive if the point of action of the force creating the moment is ahead of the center of gravity.

Analysis

The two complex equations of motion of a coasting missile (zero thrust) referred to axes that pitch and yaw with the missile but do *not* roll with it are

$$\left.\begin{aligned} \omega - \dot\alpha - \frac{V}{l}\left(C_{L_\alpha} - iC_{L_{p\alpha}}\frac{Pd}{V}\right)\alpha = 0 \\ \dot\omega - i\frac{A}{B}P\omega - \frac{V^2d}{lr_B^2}\left[C_{M_q}\frac{\omega d}{V} + C_{M_{\dot\alpha}}\frac{\dot\alpha d}{V} + \left(C_{M_\alpha} - iC_{M_{p\alpha}}\frac{Pd}{V}\right)\alpha\right] = 0 \end{aligned}\right\} \quad (1)$$

Let

$$z = \int_0^t \frac{V(\tau)}{d}\,d\tau$$

distance along the flight path in diameters, $(\,)'$ = derivative with respect to z, and

$\bar C_L$ = $(d/l)C_L$
$\bar C_M$ = $(d/l)\,(d/r_B)^2\,C_M$
$\bar C_{M_{p\alpha}}$ = $d/l(d/r_A)^2 C_{M_{p\alpha}}$
P_0 = $(A/B)\,(Pd/V)$

Then Eqs. (1) become

$$\left.\begin{aligned} \frac{d}{V}\omega - \alpha' - (\bar C_{L_\alpha} - i\bar C_{L_{p\alpha}}P_0)\alpha = 0 \\ \frac{d}{V}[\omega' - (\bar C_{M_q} + iP_0)\omega] - \bar C_{M_{\dot\alpha}}\alpha' - (\bar C_{M_\alpha} - i\bar C_{M_{p\alpha}}P_0)\alpha = 0 \end{aligned}\right\} \quad (2)$$

It will be noticed that all imaginary terms (the Magnus force and moment and the gyroscopic torque) are proportional to the roll rate.

The characteristic equation of Eqs. (2), divided by d/V, is

$$\begin{vmatrix} 1 & \lambda + \bar C_{L_\alpha} - iC_{L_{p\alpha}}P_0 \\ \lambda - (\bar C_{M_q} + iP_0) & \bar C_{M_{\dot\alpha}}\lambda + \bar C_{M_\alpha} - i\bar C_{M_{p\alpha}}P_0 \end{vmatrix} = 0$$

or

$$\lambda^2 + (a_1 + iP_0a_2)\lambda + b_1 + iP_0b_2 = 0 \quad (3)$$

where

a_1 = $\bar C_{L_\alpha} - (\bar C_{M_q} + \bar C_{M_{\dot\alpha}})$
a_2 = $-1 + \bar C_{L_{p\alpha}}$
b_1 = $-\bar C_{M_\alpha} - \bar C_{M_q}\bar C_{L_\alpha} - P_0^2\bar C_{L_{p\alpha}}$
b_2 = $\bar C_{M_{p\alpha}} + \bar C_{L_{p\alpha}} - \bar C_{L_\alpha}$

The conjugate of Eq. (3) is, of course, also a characteristic equation. The product of Eq. (3) with its conjugate yields the stability quartic with real coefficients, which would have been obtained by the usual analysis (i.e., not using complex notation).

For stability, the real part of the roots of Eq. (3) must be negative. Writing down this condition in a manner similar to Bolz, the two stability conditions become

$$a_1 > 0$$

$$b_1 > b_2/a_1\,(b_2/a_1 - a)P_0^2$$

Substituting in the expressions for a_1, a_2, b_1, and b_2, the stability conditions become

$$\bar C_{L_\alpha} - (\bar C_{Mq} + \bar C_{M_{\dot\alpha}}) > 0$$

$$-\bar C_{M_\alpha} > \frac{(\bar C_{L_\alpha} - \bar C_{L_{p\alpha}} - \bar C_{M_{p\alpha}})\,(\bar C_{Mq} + \bar C_{M_{\dot\alpha}} - \bar C_{L_{p\alpha}} - \bar C_{M_{p\alpha}})}{[\bar C_{L_\alpha} - (\bar C_{M_q} + \bar C_{M_{\dot\alpha}})]^2}\,P_0^2$$

where products and squares of the barred coefficients have been neglected with respect to the barred coefficients themselves (which, in magnitude, are all very much less than unity).

If we let

$$s_1 = -(\bar C_{M_q} + \bar C_{M_{\dot\alpha}})/\bar C_{L_\alpha}$$

$$s_2 = -(\bar C_{Lp\alpha} + \bar C_{M_{p\alpha}})/\bar C_{L_\alpha}$$

then, finally, the stability conditions read

$$s_1 > -1 \quad (4a)$$

$$BM_\alpha < \frac{(1 + s_2)\,(s_1 - s_2)}{(1 + s_1)^2}\,(AP)^2 \quad (4b)$$

where $M_\alpha = C_{M_\alpha}(\rho V^2/2)Sd$ = pitching moment curve slope.

Eq. (4a) states that there must be positive aerodynamic damping. Eq. (4b) is a condition on the static stability; if $P = 0$, it says that the pitching moment curve slope must be negative. Now the only possibility that a statically stable missile ($M_\alpha <$

0) with positive aerodynamic damping ($s_1 > -1$) could be made dynamically unstable by the presence of a roll rate is for

$$(1 + s_2)(s_1 - s_2) < 0$$

For this to take place either $s_2 < -1$ or $s_2 > s_1$. Under these conditions a statically unstable missile ($M_\alpha > 0$) with positive aerodynamic damping ($s_1 > -1$) could *not* be spin-stabilized by increasing the roll rate. Upon examining these conditions it would appear to us that the missile would have to be of a peculiar design for them to be satisfied, since the Magnus force and moment are usually so small that $|s_2| \ll 1$ and for almost all missiles and projectiles $s_1 \approx 1$.

Incidentally, if we let $s = [(1 + s_2)/(1 + s_1)] - (1/2)$, we may rewrite Eq. (4b) as

$$BM_\alpha/(AP)^2 < (1/4) - s^2 \tag{5}$$

showing that the right-hand side has a stationary value in the neighborhood of $s = 0$ which is a maximum. Eq. (5) with $s = 0$ is precisely the condition for stability of a heavy symmetrical top with one point fixed; it is also the approximate stability condition that is often used for spin-stabilized projectiles, and it can be seen from Eq. (5) that this is a very good approximation, since usually $|s| \ll 1$.

Library Facilities of the
Institute of the Aeronautical Sciences

To serve Institute members and others in the aeronautical industry, the Institute of the Aeronautical Sciences offers the facilities of:

The W. A. M. Burden Library

2 East 64th Street
New York 21, N.Y.

The facilities of this library are available for reference study at the Institute.

The Paul Kollsman Lending Library

2 East 64th Street
New York 21, N.Y.

This library loans books without charge to members and others in the United States over eighteen years of age. Full information will be sent on request.

The Pacific Aeronautical Library

7660 Beverly Boulevard
Los Angeles 36, Calif.

This is a service and reference library for West Coast members and organizations. Full information as to its facilities will be sent on request.

INSTITUTE *of the* AERONAUTICAL SCIENCES

1932—1953

Since its incorporation in October, 1932, as a scientific membership society to advance the art and science of aeronautics, the Institute of the Aeronautical Sciences, in over twenty years of service to aviation, has become the representative technical society for the aviation industry and profession. It is the only organization in the United States which brings together all of the sciences and branches of engineering and technology which are applied to aeronautics.

Publications

Papers presented at meetings or submitted to the Editorial Board are published in the JOURNAL OF THE AERONAUTICAL SCIENCES or the AERONAUTICAL ENGINEERING REVIEW. The JOURNAL prints in each issue several full-length scientific papers on new research and developments in various fields applied to aviation. The REVIEW keeps members and subscribers up to date on aeronautical news and literature through reviews of new books and periodical articles, government publications and trade literature and publishes papers on applied engineering and aircraft production.

The AERONAUTICAL ENGINEERING CATALOG, published yearly, is a guide to sources and specifications of materials, parts, and accessories used in the design and production of aircraft, aircraft engines, and parts.

Research Facilities

Through the Aeronautical Archives of the Institute, members have for their use the most complete aeronautical library and reference research facilities maintained by any technical society. At the New York building of the Institute, The W. A. M. Burden Library of books, reports and periodicals, the Aeronautical Index of subject files, biographic files and bibliography, and the historical and art collections in the Archives are available for study. The Pacific Aeronautical Library at 7660 Beverly Boulevard, Los Angeles, maintains a reference collection and reading room for members and loans books to company libraries in the area. Through The Paul Kollsman Lending Library, aeronautical books are lent by mail without charge to members anywhere in the continental United States. In addition to a complete collection of standard aeronautical reference works, the Kollsman Lending Library has available for loan new aviation books as they are reviewed in the AERONAUTICAL ENGINEERING REVIEW.

Membership

In addition to membership in professional societies representing their particular fields, specialists applying their knowledge and experience to aeronautics find membership in the Institute of great value in the contacts made with others engaged in aeronautical work and in the broad coverage of all aeronautical problems furnished through its meetings and publications. All applications for membership are carefully reviewed by the Membership Committee, which recommends the grade of membership for which the applicant is found eligible. There are advanced grades of membership—Fellow and Honorary Fellow—to which members may be elected as their experience warrants. Thus, a member receives due recognition—more valuable because it is given by his colleagues—for his contributions to the progress of aeronautics. New applicants may be elected by the Membership Committee to the grade of Associate Fellow if they have been engaged for not less than ten years in the practice of the aeronautical sciences and shall have been in responsible charge of important scientific or engineering work, or shall have otherwise made outstanding contributions to the aeronautical sciences; to the grade of MEMBER if they have been engaged in professional work for at least eight years and have acquired a recognized standing in engineering, design, or other special work applied to aeronautics; to the grade of Associate Member if they have acquired a recognized standing in an administrative capacity in the aviation industry; to the grade of Technical Member if they are recent engineering school graduates or are engaged in technical aeronautical work. Student Members are admitted by application through Student Branches organized at their schools. Aeronautical companies, as well as individuals, are affiliated with, and participate in, the support of the Institute through Corporate Membership.

Dues

An entrance fee of $10 is required of all new members who apply for admission to a grade of membership to be specified by the Membership Committee (Corporate Members, Foreign Members, and Student Members being excepted).

Annual membership dues include a subscription to the AERONAUTICAL ENGINEERING REVIEW. Dues for the various grades of membership are as follows: Fellows—$16.50; Associate Fellows—$16.50; MEMBERS—$13.50; Associate Members—$13.50; Technical Members—(26 years of age and over) $13.50, (under 26) $6.50.

The regular subscription price for the JOURNAL OF THE AERONAUTICAL SCIENCES and the AERONAUTICAL ENGINEERING REVIEW is $12 and $3.00 per year, respectively. Members may subscribe to the JOURNAL at $4.00 per year.

Those who are engaged in aeronautical work or who have an interest in any technical phase of aviation will find the services of the Institute to be a necessary aid in keeping abreast of developments in these times of such rapid progress. An application form and further information about membership can be obtained from an Institute member or by writing to the Secretary.

INSTITUTE OF THE AERONAUTICAL SCIENCES, INC.

2 EAST 64TH STREET

NEW YORK 21, N.Y.